RADIOACTIVE ^{26}Al IN THE GALAXY: OBSERVATIONS VERSUS THEORY

Nikos PRANTZOS[a], **Roland DIEHL**[b]

[a]*Institut d'Astrophysique de Paris and Service d'Astrophysique, DAPNIA, CE Saclay, France*
[b]*Max Planck Institut für extraterrestrische Physik, Garching, Germany*

ELSEVIER

AMSTERDAM – LAUSANNE – NEW YORK – OXFORD – SHANNON – TOKYO

ELSEVIER

Physics Reports 267 (1996) 1–69

PHYSICS REPORTS

Radioactive ^{26}Al in the galaxy: observations versus theory

Nikos Prantzos[a], Roland Diehl[b]

[a] *Institut d'Astrophysique de Paris and Service d'Astrophysique, DAPNIA, CE Saclay, France*
[b] *Max Planck Institut für extraterrestrische Physik, Garching, Germany*

Received May 1995; editor: D.N. Schramm

Contents:

Elsevier Science B.V.
SSDI 0370-1573(95)00055-0

Abstract

^{26}Al is the first cosmic radioactivity ever detected, more than ten years ago, through its characteristic 1.8 MeV gamma-ray line. Its $\sim 10^6$ yr lifetime, much shorter than the $\sim 10^{10}$ yr of galactic evolution, convincingly demonstrates that nucleosynthesis is currently active in our Galaxy. Current models of nucleosynthesis are still too uncertain to allow identification of the sites of that nucleosynthetic activity, despite their continuous improvement in the past ten years. The recent results of the Compton Gamma-Ray Observatory shed, for the first time, some light on the origin of galactic ^{26}Al, favoring massive stars as the main sources. The various measurements of 1.8 MeV emission and the theoretical models of ^{26}Al sources are presented in this review, along with the implications of the latest results for nuclear, stellar and galactic astrophysics.

1. Introduction

Nuclear Astrophysics emerged in the 40ies from the marriage of the old science of astronomy with the young discipline of nuclear physics. The purpose of this marriage was, essentially, twofold: to understand the energetics of stars in their various evolutionary stages and to explain the origin of the chemical elements and their isotopes in the Universe. Since the epochal paper of B^2FH [16], it has been established that the majority of the chemical elements are produced by nuclear reactions in the hot stellar interiors, either during the long, quiescent phases of stellar evolution, or in the violent supernova explosion that marks the death of some stars. The material ejected from the dying stars is mixed in the interstellar medium from which new stellar generations are formed. The cycle then starts again, progressively enriching the Galaxy with heavy elements.

This scheme of stellar nucleosynthesis is supported by a large body of observational data, concerning the abundances of the chemical elements in the solar system, in stars of different ages, in the interstellar medium of our Galaxy and in external galaxies as well [160]. In the vast majority of cases observations reveal only elemental abundances, through electromagnetic transitions in the atomic shells. However, it is individual isotopes, not elements, that participate in nuclear reactions. This is not necessarily a big problem, since many elements have only one dominant isotope. Still, from a strictly empirical point of view, the situation is not quite satisfactory.

Enter *radioactivity*. Stellar nucleosynthesis produces not only stable, but also unstable nuclei with lifetimes ranging from seconds to billions of years. Their radioactive transitions may give rise to γ-ray photons which, under certain conditions, may be detected by sufficiently sensitive instruments. This possibility, first suggested by D. Clayton and collaborators in the sixties [30,32], would unambiguously allow to detect isotopes, through their characteristic γ-ray signature. Moreover, detection of species with lifetimes considerably shorter than the age of the Galaxy would clearly show that nucleosynthesis is still active today.

Unfortunately, gamma-ray photons rarely arrive on Earth; they are absorbed by the atmosphere, as is the largest part of the electromagnetic spectrum. Thus, observations of stellar radioactivity had to wait the advent of gamma-ray detectors on stratospheric balloons and aboard spacecrafts, in the late 70ies and the 80ies. The first cosmic radioactivity ever detected in γ-rays is ^{26}Al, unstable to positron emission (82%) or to electron capture (15%), with a mean life of $\tau_{26} = 1.05 \times 10^6$ yr. Its decay feeds the first excited state of ^{26}Mg at 1.809 MeV, which de-excites by emitting a γ-ray photon of that energy. The epochal detection of 1.809 MeV emission by the HEAO-3 satellite in 1982 [93] is a discovery of paramount importance [27,55]: it clearly demonstrates that nucleosynthesis is currently active in the Galaxy and offers an unprecedented opportunity to identify the sites of that activity, as discussed in this article. [Actually, the discovery of radioactive Tc at the surface of S stars by Merrill in 1952 is the very first indication of currently active stellar nucleosynthesis; however, we cannot have information on galaxywide activity from this observable, since the Galaxy is not transparent to optical photons.]

The HEAO-3 discovery came hardly as a surprise. Indeed, calculations in the late 60ies of explosive carbon burning in supernovae [2] had shown that substantial amounts of ^{26}Al may be produced in that environment. On the basis of those estimates it has been suggested in 1977 by Ramaty and Lingenfelter [126] and, independently, by Arnett [3] that the 1.8 MeV line of ^{26}Al would be an interesting target for γ-ray line astronomy. Due to its relatively long lifetime, ^{26}Al from several thousand supernovae should accumulate in the Galaxy, giving rise to a diffuse emission in the galactic plane. The flux

on Earth was estimated to $\sim 10^{-4}$ cm^{-2} s^{-1} from the galactic centre direction, making ^{26}Al a prime target for the HEAO-3 detectors. Moreover it was pointed out that, because of its long mean life, ^{26}Al would have enough time to be thermalised in the interstellar medium; therefore, it would de-excite essentially at rest and emit a narrow line, making easier its detection and identification with such a high-resolution instrument.

All those predictions were brilliantly confirmed by HEAO-3. However, the detected emission of $\sim 4 \times 10^{-4}$ cm^{-2} s^{-1} rad^{-1} from the galactic centre direction was even more intense than originally estimated (a rather rare case in astronomy); it required a large ratio of ^{26}Al/^{27}Al from supernovae, larger than what was obtained from supernova models in the early 80ies. Based on galactic chemical evolution arguments, Clayton [27] pointed out that supernovae, the main producers of the stable isotope ^{27}Al in the Galaxy, could not be at the origin of such an intense ^{26}Al emission, because in that case they would overproduce ^{27}Al by a large factor. This argument seems now less powerful than originally thought (see Section 4.3); nevertheless, it pushed theoreticians to look for other sources of ^{26}Al, like novae, red giants and Wolf-Rayet stars. The theoretical ^{26}Al yields of all those candidate sources in the 80ies seemed rather low to justify the observed flux, but because of considerable uncertainties in the modelling of all the sources no definite conclusions could be drawn.

In view of that difficulty, it has been suggested that help could be expected from a combination of improved spatial source distribution models and observations with good angular resolution [86]. Indeed, a detailed map of the spatial distribution of the 1.809 MeV emission in the Galaxy would reveal the nature of the underlying sources [86,120]. Much theoretical effort in the late 80ies went into finding plausible galactocentric distributions for the various candidate sources and calculating the corresponding flux profile as a function of galactic longitude, under the assumption of radial symmetry. Because of large uncertainties in the distributions of all the sources, it turned out that the resulting axisymmetric profiles could not really help to discriminate between the various candidates, as pointed out in [115]. In that paper it was argued instead that an asymmetric flux profile, resulting from the spiral pattern of our Galaxy, would be a clear test for a young population of massive stars at the origin of ^{26}Al. However, detectors during that period had too poor angular resolution and sensitivity to perform such a mapping, being only capable to detect the 1.809 MeV signal from the general direction of the Galactic centre. Those observational results lead even to arguments for a point source of ^{26}Al from that direction, located either in the galactic centre itself [69,170] or in a nearby supernova remnant [33,12,105].

The situation changed dramatically after the launch of NASA's Compton Gamma-Ray Observatory (CGRO), in April 1991. The COMPTEL instrument aboard CGRO performed the first mapping of the Galaxy in the light of 1.8 MeV photons [46,50]. The data exclude a point source in the galactic centre and show a diffuse, irregular emission along the galactic plane, favoring a massive star origin. These results shed, for the first time, some light on the origin of interstellar ^{26}Al and justify a review on that topic.

It should be reminded at this point that ^{26}Al was discussed in the astrophysical community long before the detectability of its γ-ray line drew the attention. Analyses of meteoritic samples suggested considerable melting of large asteroidal bodies in the early solar system, and the radioactivity of ^{26}Al made this nucleus an excellent heat source for such a melting, provided that it was present in relatively large amounts (see [31] for a historical introduction and references). This scenario leads to isotopic anomalies (i.e. an excess of ^{26}Mg) that were searched for and finally detected in the Allende meteorite [82]. If ^{26}Al decayed *in situ* (i.e. within the minerals, as found in the meteorite today),

the observations indicate a ratio $X_{26}/X_{27} \sim 5 \times 10^{-5}$ in the early solar system, enough for ^{26}Al to be the melting agent. Moreover, it has been suggested that the nucleosynthetic source of that ^{26}Al could not have preceeded the formation of the solar system by more than a few τ_{26} and could even have triggered it [18]. However, the assumption of in situ decay is not necessarily correct, as pointed out many years ago [28]; indeed, observations of grains in primitive meteorites show that ^{26}Al has been produced far away and the excess ^{26}Mg transported in the solar nebula inside those grains [1].

A previous review on ^{26}Al [31] discussed both its meteoritic implications and its status in γ-ray line astronomy. We do not attempt such a combined study here and we focus instead on the γ-ray aspects only, since it is not certain if a correlation between interstellar and meteoritic ^{26}Al exists at all. Indeed, even if meteoritic ^{26}Al were produced away from the early solar system, its source need not be the same as the one of the 1.8 MeV emission.

The outline of this review is as follows: In Section 2 are presented all balloon and satellite detections of 1.8 MeV emission prior to CGRO, mostly of historical interest now. Section 3 reviews the nucleosynthesis of ^{26}Al in the various proposed sources, with particular emphasis on the underlying uncertainties. In Section 4 the galactic ^{26}Al yield of each class of those sources in the last $\tau_{26} \sim 10^6$ yr is evaluated; the corresponding spatial distributions of the 1.8 MeV emission are also calculated and discussed. In Section 5 the results of COMPTEL and OSSE aboard CGRO are presented, after a brief introduction in the data analysis methods. Conclusions and future prospects are discussed in Section 6.

2. Measurement history of the galactic 1.809 MeV line

Instruments for the MeV regime of γ-ray lines differ from telescopes at longer wavelengths, mainly for two reasons:

(1) the *penetrating nature of gamma-ray photons* demands detection devices that record individual photon interaction processes within the detector itself, rather than being able to focus the photons to produce an image;

(2) the *cosmic ray environment* in near-Earth space *produces* a bombardment of the instrument with high-energy protons and neutrons, which results in *activation of the instrument* itself; therefore gamma-ray line detectors have to include special precautions to discriminate locally produced gamma-radiation from the targetted celestial gamma-rays.

Additionally, *the Earth's atmosphere* is turned into a *bright source of γ-rays and neutrons* by the same process. Gamma-ray measurements of the sky with large field-of-view instruments must account in the data analysis for this additional "source" and its mostly varying aspects.

All types of instruments detect the celestial γ-rays basically through the *conversion of the photon's momentum into fast electrons*. These can be measured either directly, through their ionization tracks or charge, or through their scintillation light. At MeV energies, the *Compton scattering* on atomic shell electrons is the prime interaction of photons with matter. Compton telescopes directly make use of the characteristics of this process, through a coincidence measurement of an event in two detector planes. Less sophisticated devices are scintillation detectors with a specified aperture defined by shields of material. In many cases active shield detectors that surround the prime γ-ray detector are operated in anti-coincidence with it and serve as precaution against the intense local radion. Optimization of the sensitivity of each detector for either local radiation (electromagnetic showers or many coincident

photons) or celestial gamma-rays (interacting just in the main detector in the ideal case) allows some suppression of background. Nevertheless, all instruments operate at *signal-to-background ratios in the percent regime* or below and need to determine residual background by dedicated measurements of 'non-source' regions simultaneously (or nearly so) with the source observation. This allows to identify instrumental γ-ray line features and separate them from celestial γ-ray lines (see e.g. [57] or [132]).

The development of detection devices for nuclear γ-ray lines followed the rapid boost of nuclear reactor and weapon technology after the second world war. Instruments were flown on stratospheric balloons for periods of a few hours to days, which helped to understand the instrumental challenges for measurements in an environment with high local activation. The early results and prospects were sufficient to set out for space-borne instruments, such as the HEAO and SMM spacecrafts, with several instruments on board and mission times of years, to cope with the low flux of celestial γ-rays. Indeed, typical effective areas of instruments are tens to hundreds of cm^2, while typical fluxes of celestial γ-ray sources are 10^{-4} ph cm^{-2} s^{-1} or less. The implied long accumulation times present additional challenges for maintaining stable instrument characteristics such as electronic gains; precautions have to be taken also to monitor any changes in the local background conditions over the time of the measurement.

Analysis of MeV γ-ray data generally is far from straightforward. The primary measurement still includes substantial *background*, preventing vizualisation of source features in the raw data. Additionally, the *complex responses of detectors*, due to incomplete absorption of the photon energy and multi-detector arrangements in coincidence, spread the signal over many measurement channels. Typical analysis steps are: (i) time-dependent background modelling and (ii) convolution of the assumed source intensity pattern through the instrumental response function. Statistical tests in the (sometimes rather weird) instrument data spaces allows then to iterate and constrain the assumed source intensity pattern. It is clear that for poor angular resolution and/or large field-of-view instruments the source model constraints will be rather weak. In order to reduce the free parameters of such analysis, a plausible source distribution for galactic ^{26}Al, such as the high-energy γ-ray map obtained with the COS-B satellite, was often assumed.

In spite of these difficulties, the 1.809 MeV study of the γ-ray sky presents a good case for a new astrophysical field that emerged in the past 15 years, and is now entering a stage of lively synergetic interaction between nuclear physicists and astrophysicists.

2.1. The discovery (HEAO-C)

It was the team of the HEAO-C1 instrument that shared the privilege of the pioneering detection of cosmic radioactivity in γ-rays. This instrument aboard the third High Energy Astronomy Observatory (HEAO-3) spacecraft consisted of four coaxial high-purity Ge detectors surrounded by an anticoincidence detector of CsI scintillation material. The instrument aperture was defined by holes in this anticoincidence to be effectively 42° wide (FWHM) at 1.8 MeV, with remaining plateau shield leakage of about 10%, even far from the aperture. The high energy resolution of 3.3 keV (FWHM) at 1.8 MeV was adequate to resolve the detected line at 1.809 MeV, thus providing a clear identification with radioactive ^{26}Al decay in the interstellar medium (Fig. 2.1). Two two-week observations of the Galactic plane in fall 1979 and spring 1980 provided the data base for this discovery of Galactic ^{26}Al [93]. Careful analysis of the individual 20 min rotation period scans along the Galactic plane for this

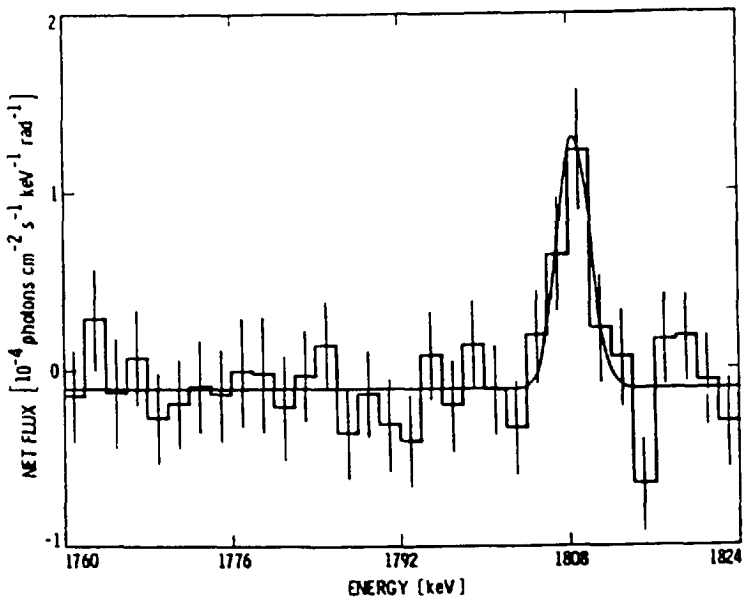

Fig. 2.1. The discovery measurement of the energy spectrum from the general direction of the inner Galaxy by HEAO-C [93]. Here the background has been subtracted, and the vicinity of the ^{26}Al line at 1.809 MeV is shown. The instrumental energy resolution of $\simeq$3 keV allowed identification of the measured feature with radioactive ^{26}Al in interstellar space.

spinning satellite enabled a comparison of the background corrected data with models of emissivity along the plane [94].

Because of the poor angular resolution and sensitivity of the instrument, no spatial information on the source of 1.8 MeV emission could be obtained. If supernovae are at the origin of the emission, its spatial distribution can be expected to follow the one of >100 MeV γ-rays, as mapped by the COS-B satellite [98]. The reason is that those high-energy gamma rays are thought to result from the interaction of cosmic ray protons, accelerated by supernovae, with the interstellar medium. Under this plausible assumption the HEAO-C team determined a line flux $F \sim 4.8 \times 10^{-4}$ cm^{-2} s^{-1} rad^{-1} from the galactic centre direction, at the 5 σ level.

For such a distribution the relationship between the observed flux and the total galactic emissivity Q (in photons s^{-1}) is: $F \sim 1 \times 10^{-46}\, Q$ [65], which leads to $Q \sim 4.8 \times 10^{42}$ photons s^{-1}. Assuming a steady state situation in the Galaxy, i.e. that the production rate of ^{26}Al just balances its decay rate, ($\mathrm{d}N/\mathrm{d}t \sim Q \sim N/\tau_{26}$) this emissivity leads to $N \sim 1.6 \times 10^{56}$ ^{26}Al nuclei currently present in the ISM, or to a galactic production rate $\dot{M}_{26} \sim 3\ M_{\odot}$ Myr^{-1}. Notice that assuming a distribution different from the one of COS-B leads to somewhat different numbers, but always in the range of a few $M_{\odot}$ (provided the distribution is relatively symmetric w.r.t. the galactic centre).

The HEAO-C team later re-analyzed their data, using each 10-minute dataset with separate background subtraction to constrain normalization parameters of plausible source distribution models, like novae and supernovae [95]. Using the supernova model as a template, they determined the 1.809 MeV line significance for different centroid positions of this distribution, in order to derive some imaging information. The result of this analysis (see Fig. 2.2) determines the best-fit centroid of the emission to be at galactic longitude $l = -6° \pm 22°$ and galactic latitude $b = -4° \pm 20°$. No distinction

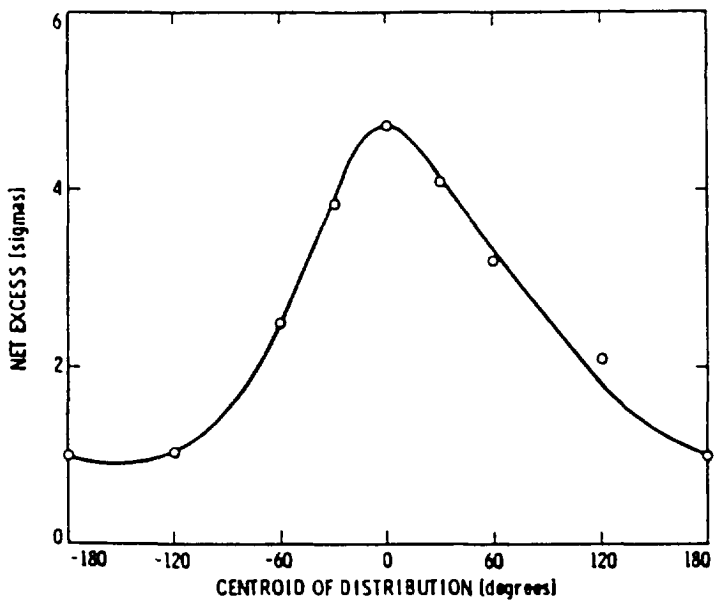

Fig. 2.2. Display of the HEAO-C measured ^{26}Al line significance as a function of Galactic longitude [95]. In this analysis, the centroid of the asumed distribution model (taken from the high-energy gamma-ray measurements of the COS-B satellite) was varied along the plane of the Galaxy. This allows to get some idea on the 'center of gravity' of the measured signal.

between nova and supernova models could be made from these results, however.

2.2. *The consolidation (SMM)*

The Solar Maximum Mission's (SMM) Gamma Ray Spectrometer operated from 1981 onwards for 9 years; although the instruments were pointed at the Sun as the main target of this mission, the opportunity of a sensitive γ-ray detector observing the sky from above the Earth atmosphere resulted in numerous unanticipated explorations of this instrument's data with respect to celestial γ-ray sources (such as detection of SN1987A supernova γ-rays, and sensitive limits to ^{22}Na, ^{44}Ti, and ^{60}Fe production in the Galaxy). SMM's spectrometer consisted of seven 7.5 cm $\times$ 7.5 cm NaI scintillation detectors with a CsI anticoincidence shield system. It thus had a modest energy resolution of 95 keV (FWHM) at 1.8 MeV, so that only on the basis of the HEAO-3 measurement the association of the SMM 1.8 MeV line with ^{26}Al could be made. The annual Galactic centre region transits over at least 5 years provided a high-precision confirmation of 1.8 MeV emission from the general region of the Galactic centre (Fig. 2.3). Instrumental lines in the vicinity of 1.8 MeV were demonstrated to show temporal signatures not related to transits of celestial regions, unlike the 1.8 MeV time profile; therefore this measurement had an excellent signal-to-background ratio of >20%, clearly establishing the detection of Galactic ^{26}Al. The aperture of this instrument of 160° (FWHM) at 1.8 MeV did not allow to derive any spatial information on the emission from these time profiles directly; see however the discussion of Earth occultation imaging analysis in Section 2.7 below.

The SMM measurement provided convincing proof that the HEAO-C discovery was truly the signature of Galactic ^{26}Al production. Now the stage was set for many experimental groups throughout

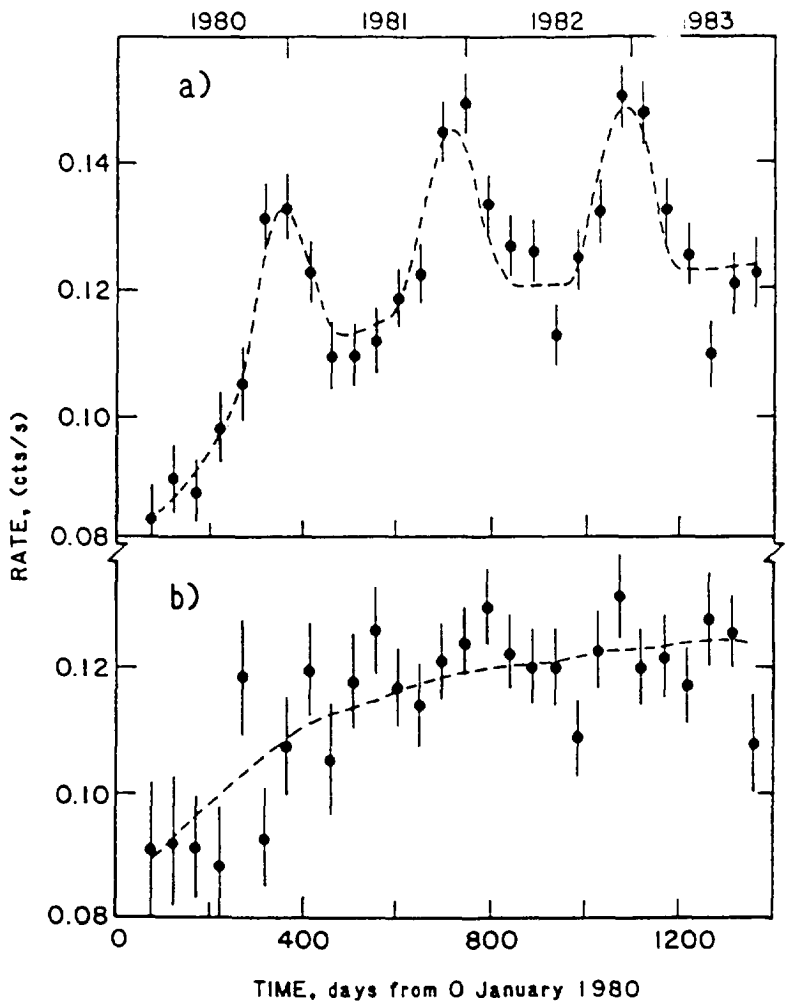

Fig. 2.3. Comparison of intensity variations in a 1.81 MeV line fit to the SMM measurement over four years of data, for sky viewing (above) and Earth-occulted (below) data [139,140]. The time span corresponds to three transits of the Galactic centre region through the instrument field-of-view, which was pointed towards the Sun at all times. The ^{26}Al line emission from the inner Galaxy is clearly confirmed.

the world in the young field of γ-ray line astronomy. A number of instruments were set up, aiming to improve the spatial information on Galactic 1.809 MeV emissivity. In the following sections we review the instrumental results from these various efforts. We reemphasize that the γ-ray instrumentation for the MeV regime is plagued with a very low signal-to- background ratio and the presence of rapidly variable local activation background, so that substantial systematic uncertainties remain for each type of instrument; therefore, comparison of results from different instrumental techniques are difficult but vital for the astrophysical interpretations.

2.3. Sandia/AT&T

The collaboration of the Sandia National Laboratories and AT&T Bell Laboratories set up an instrument based on a single large Ge detector surrounded by a massive (200 kg) NaI active anticoincidence shield. The opening aperture defined by the shield design was ~15° FWHM. This detector was originally designed to measure the 511 keV emission from the Galactic plane and centre, the variability of which was the hot topic of gamma-ray line astronomy in the 70ies and early 80ies. The data from four balloon flights of the instrument were used to derive constraints on the 1.809 MeV emission [90].

The longest of these flights (17.3 hours in November 1977) yielded only a 1.3σ detection of the line from the Galactic centre direction, with a reported flux of $1.6(^{+1.1}_{-1.2}) \times 10^{-4}$ ph cm^{-2} s^{-1}; the presence of a nearby instrumental line introduced additional uncertainty. For two subsequent flights a larger detector was used (200 cm^3 instead of 130 cm^3), but shorter flight durations resulted in insignificant 1.809 MeV fluxes. In the last flight (in 1984), the instrument pointing system was out of use, and although the aperture had been widened to ~87° FWHM for a Galactic plane transit observation, the 1.809 MeV signal was insignificant. In addition, no contemporaneous background measurements were possible in this flight and the background had to be extrapolated from previous flights.

The Sandia/AT&T team [90] combined the data from all four flights to derive a 1.809 MeV flux value of $1.3 \pm 0.9 \times 10^{-4}$ ph cm^{-2} s^{-1} for an assumed point source in the Galactic centre and $3.9(^{+2.0}_{-1.7}) \times 10^{-4}$ ph cm^{-2} s^{-1} rad^{-1} for an extended source assumed to be distributed like the observed high-energy gamma rays (> 100 MeV), taken from the COS-B measurement of [98]. They argued that a pointlike source at the Galactic centre was less likely than an extended source (at the 90% confidence level), as the large aperture version of the instrument gave a larger 1.809 MeV flux value. Note however that the total significance from all combined flights is 2σ only, under the favourable assumptions of an extended ^{26}Al source and absence of instrument-systematic effects.

2.4. GRIS

The Gamma Ray Imaging Spectrometer (GRIS) was set up by a collaboration of NASA/GSFC, the AT&T/Bell Laboratories and the University of New Mexico. Compared to the Bell Labs instrument, GRIS had a better definition of the aperture, and multiple detectors with better resolution. It consisted of 7 high-purity n-type coaxial Ge detector units in a dense package surrounded by a heavy active shielding based on NaI scintillator. The instrument operated in the 20 keV to 8 MeV energy range and its nominal spectral resolution was 2.8 keV at 1.809 MeV. The total geometrical area of the detectors was 1530 cm^2, at 1.809 MeV. Holes drilled into the anticoincidence defined the instrument aperture of nominally 24° FWHM; at 1.8 MeV the effective field of view was rather larger, ~40° for a triangular response. For the 1992 campaigns the instrument had been revised, with somewhat larger detector areas (on the average), and one of the detectors replaced by a ^{70}Ge enriched device. During these flights one of the seven detectors failed. These data have not been investigated for ^{26}Al signal yet.

Results from analysis at 1.809 MeV have been reported from the second 1988 balloon flight only [153,154]. In this flight two pointings of the instrument have been made, one at galactic longitude $l = 0°$ (i.e the galactic centre direction) and one at $l = 335°$. Background was determined through

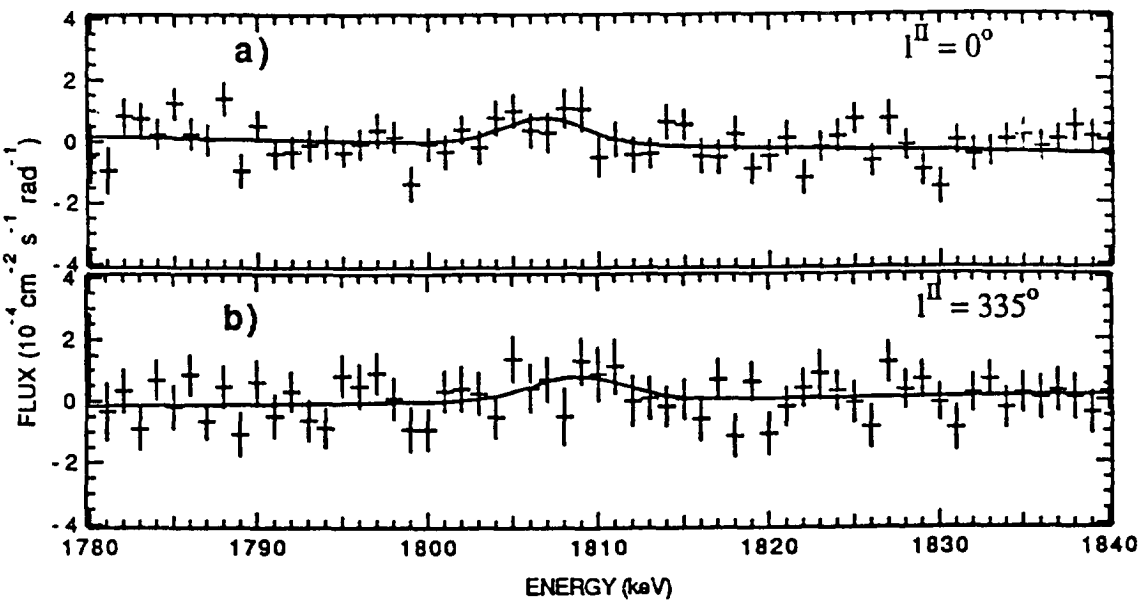

Fig. 2.4. Measurements of the energy spectrum in the vicinity of the ^{26}Al gamma-ray line by the balloon-borne GRIS instrument with its high-resolution Ge detector, pointed at Galactic longitudes 0° and 355° [153]. Limited exposure times and substantial instrumental background allow only a marginal detection, insufficient to provide a consistency check on the line identification from HEAO-C satellite instrument data.

"20 minute on / 10 minute off" pointing cycles, where the off pointing direction was defined by the same elevation as the "on" direction, but the azimuth angle chosen to achieve the largest Galactic latitude value. Both source pointings resulted in rather marginal detections (2.5σ for the $l = 0°$ pointing, 1.7σ for the $l = 335°$ pointing) of the 1.809 MeV line. In fact, the Galactic centre pointing data yielded a line energy 1.7 σ below the ^{26}Al decay line energy. Any measured line width above instrumental could in principle be interpreted as a hint for broadening due to Galactic rotation. The GRIS data actually are consistent with a narrow line (zero broadening). The GRIS team interpret the ratio of the measured fluxes at $l = 0°$ and $l = 335°$ ($\sim$0.90 for a point source and $\sim$0.78 for a COS-B-like distribution), as evidence for a diffuse source. They argue that their measurements, combined with the flux values from the Bell Labs instrument, HEXAGONE, SMM, and the MPE Compton telescope, do not support a single point source at the Galactic centre, the corresponding probability being 8×10^{-3} only. From Fig. 2.5 it is obvious that the results from these two pointings are not sensitive to distributions of candidate sources.

2.5. *The MPE Compton telescope*

The Compton telescope of the Max Planck Institute in Garching (MPE) introduced another type of instrument with intrinsic imaging capability within a large field of view [133]. This instrument records photons through successive interactions in its two detector planes, namely a Compton scatter in the upper liquid scintillator detector, and the interaction and absorption of the scattered photon in its lower NaI scintillation detector. Time-of-flight measurement between detector planes supports this coincidence measurement principle and discriminates against false coincidences from atmospheric

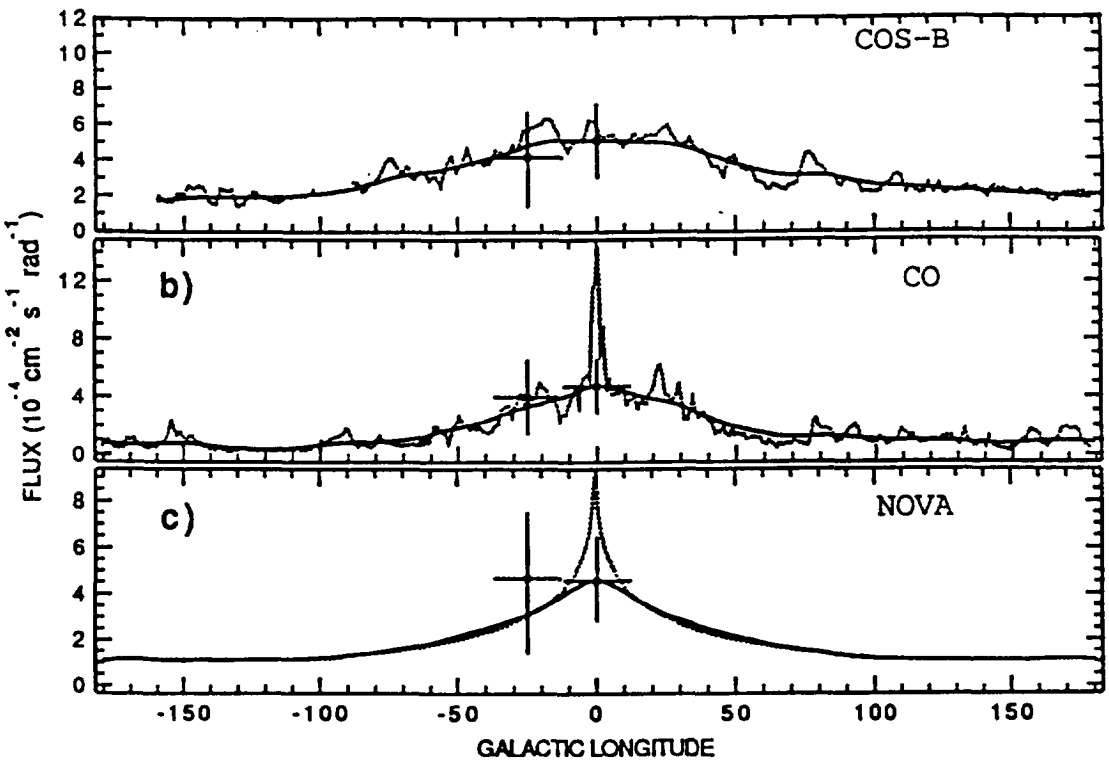

Fig. 2.5. Comparison of the GRIS balloon measurement to expected emission distributions for first-order models of the ^{26}Al source distribution [153]. Here the high-energy gamma-ray emission from COS-B measurements were used as a tracer of the total interstellar gas (top), the CO measurements as a tracer of molecular gas (centre), and nova models based on our and M31 galaxy measurements (below). Clearly the marginal detections cannot distinguish among these models, yet do not favour a model of a pointlike source at the Galactic centre dominating the emission.

and local background. The upper detector thickness of 15 cm maximizes the efficiency for a single Compton scatter interaction in the MeV regime, while the 7.5 cm thick layer of NaI detectors in the lower plane has a ~50% probability for total absorption of MeV scattered photons. An active shield of thin plastic scintillator surrounds both detector planes to discriminate against charged particle background; pulse shape measurement in the liquid scintillator of the upper detector plane suppresses background from atmospheric neutrons. Segmentation of the detector planes into 15cm × 15cm sized blocks provides a coarse location of the photon interaction and thus a determination of the direction of the scattered photon; on the other hand the energy measurements in the upper and lower detector planes determine the Compton scatter angle in the primary interaction. These measurements hold information on the arrival direction of the detected photon; however, decoding this information requires complex analysis techniques.

The revised version of this instrument observed the Galactic centre region in 1982 in the southern hemisphere from Uberaba/Brazil in a short balloon flight (~4.5 hrs at float altitude). Background was determined from the flight data by a method similar to the on/off techniques used by the non-imaging instruments: data selections on scattered photon directions allow to define events that have identical instrumental response, yet most likely originate from a direction that is opposite to the source

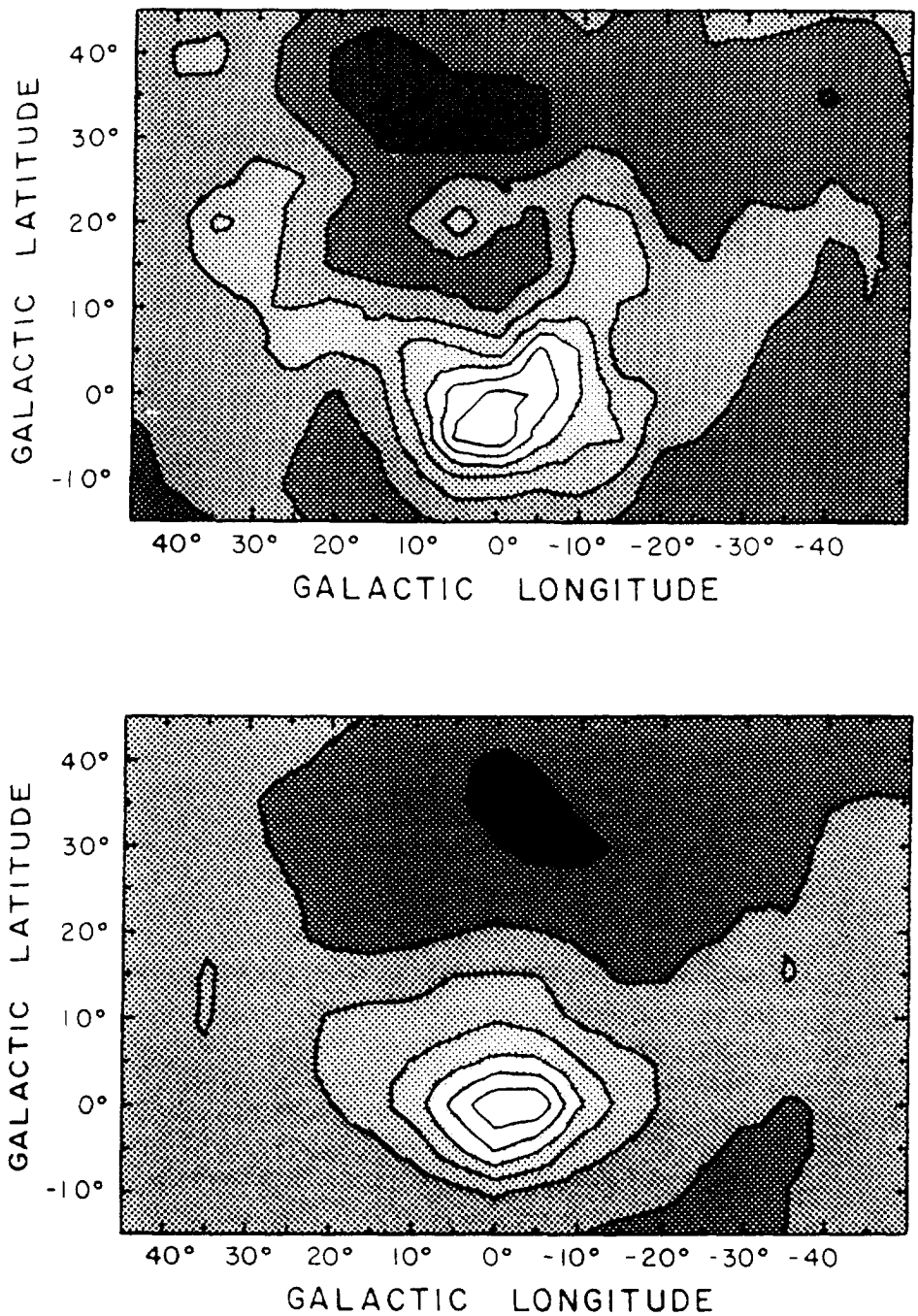

Fig. 2.6. Comparison of a map obtained by the MPE imaging Compton telescope from a short balloon flight to a map from simulated data for this flight, assuming a source at the Galactic centre only [165]. The map is constructed through projection of the measured events onto the sky by use of the imaging characteristics of the instrument [165]. The instrument angular resolution of $\simeq 10°$ suggests that the emission is fairly concentrated towards the Galactic centre direction, allowing source extents from point-like to $\leq 10°$. The poor energy resolution of the instrument scintillation detectors (12% FWHM) cannot constrain line energy and width, unlike Ge detector measurements.

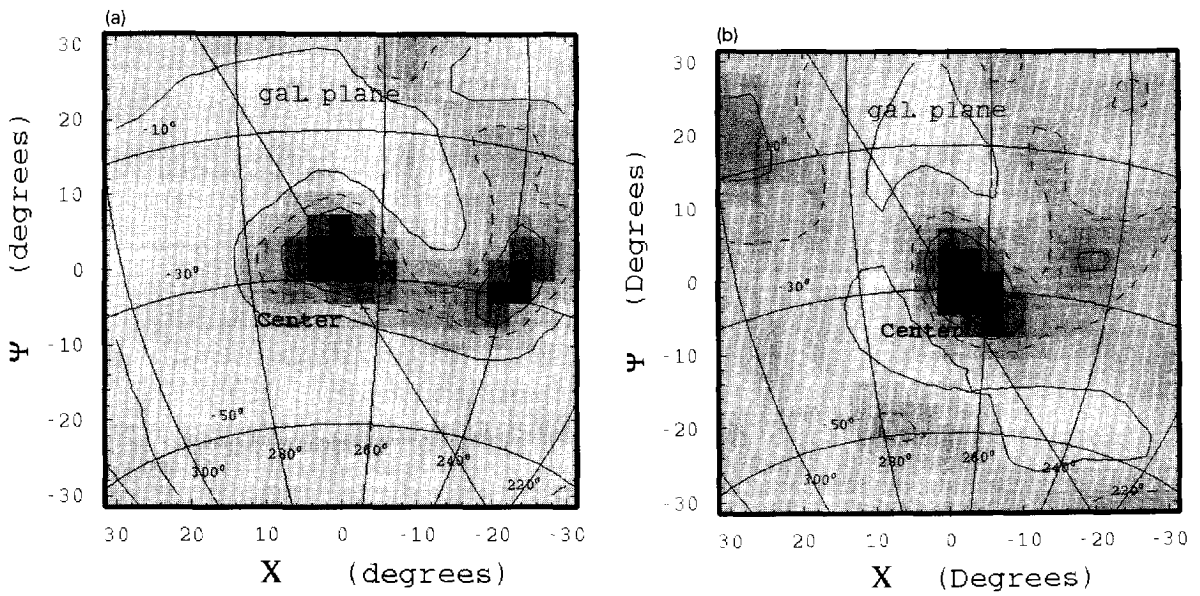

Fig. 2.7. Result from re-analysis of the MPE Compton telescope balloon flight data with the maximum-entropy technique [164]. Also in this analysis which makes full use of the instrumental imaging resolution through deconvolution with the instrument response the same result is obtained (compare Fig. 2.6). The deconvolved sky image of the actual measurement (a) is compared with an identical deconvolution of a Monte-Carlo simulation of the balloon flight data for a 'pointlike' source at the centre of the Galaxy (b). The exposure track of the balloon flight of a sky region towards the northern Galactic hemisphere, however, only puts weak constraints for emission further along the plane of the Galaxy. This result marks the first direct imaging attempt of the ^{26}Al emission.

direction with respect to the instrument axis. In spectral analysis and sky projection methods, the corresponding spectra and sky maps were subtracted after identical processing of the 'on' and 'off' datasets, to produce the final result. From straightforward event selections to constrain the photon arrival directions to the Galactic centre vicinity ($<15°$) the MPE team [165] was able to derive an energy spectrum for the Galactic centre region, which clearly showed a line at 1.8 MeV within the instrumental energy resolution of $\sim$12% (FWHM). The projected image from the data appeared very similar to a point source in the Galactic centre, folded through the instrumental response for this balloon flight [165] (Fig. 2.6). The low statistics of this short flight did not allow sensitive constraints on spatial source distribution, however. Only the broad supernova model of [86], derived from the radial CO distribution in the Galaxy, was claimed to contradict the MPE measurement at the 2σ level [165].

In a re-analysis of the same data a Maximum Entropy deconvolution method was applied [164] to determine an image of 1.8 MeV emission (see Fig. 2.7). This image confirmed that the emission is confined in the central part of the Galaxy; note however that the exposure of this balloon flight was mostly on the northern Galactic hemisphere and only weakly on the Galactic plane at distances $>20°$ from the centre. The derived flux of 4.9×10^{-4} ph cm^{-2} s^{-1} rad^{-1} was comparable to the other experiments (see Fig. 5.13 below).

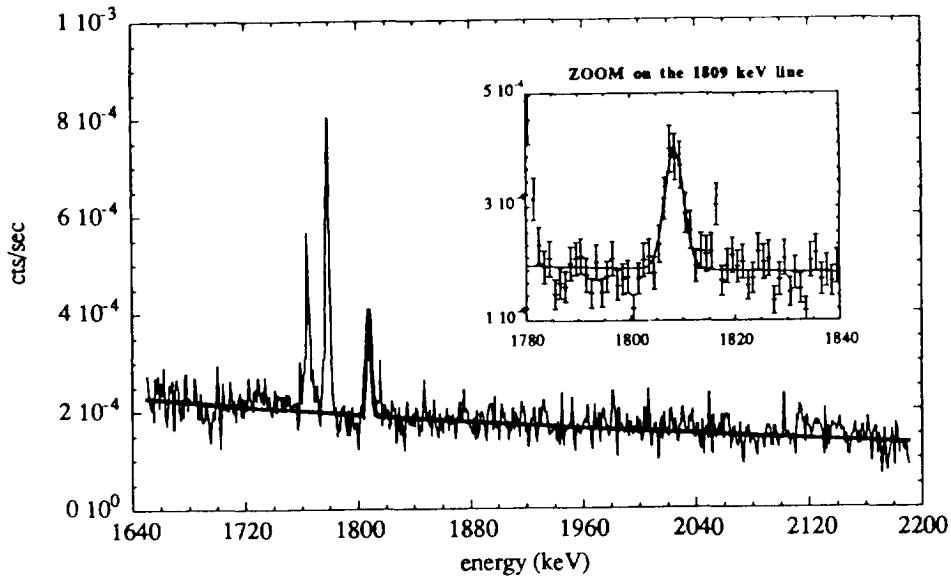

Fig. 2.8. Energy spectrum towards the direction of the Galactic centre measured with the HEXAGONE Ge detector from a balloon flight [53]. Several 'on/off' measurement pairs were analyzed independently to optimize background suppression. Several instrumental lines can be seen (including one at 1.8 MeV), which has been accounted for in the ^{26}Al result determination. Again the balloon flight data are inadequate to confirm the HEAO-C line identification.

2.6. HEXAGONE

This collaboration of French (Saclay and Toulouse) and US (San Diego and Berkeley) scientists developed another balloon instrument based on high purity n-type Ge detectors. The densely packed array of 12 Ge detectors with 5.5 cm diameter and 5.6 cm thickness was surrounded by a combination of BGO (a scintillation material that is more dense and hence more efficient than NaI, at the cost of reduced energy and timing resolution) scintillator bars of 5 cm thickness and a CsI(Na) scintillator active shield of 10 cm thickness, the respective masses being 240 kg and 60 kg. The CsI(Na) part provided the front shield, containing holes that defined a nominal 19° (FWHM) aperture. The effective field of view in this configuration was determined by simulations to be 22.5° (FWHM) wide, with a significant residual shield leakage.

The analysis of data from the May 1989 balloon flight from Alice Springs/Australia had 6.3 hours of Galactic centre exposure at its disposal [96,53]. The composite spectrum from this flight (Fig. 2.8) clearly shows the 1.809 MeV line at the expected energy, its width of 3.9 keV being compatible with the instrumental resolution of 3.1 keV. An instrumental line at the same energy results from the ^{27}Al(n,np)^{26}Mg* reaction of atmospheric neutrons with Ge detector instrument's material. The HEXAGONE flight data had sufficient accuracy to identify and correct for this instrumental line from the measurement itself (unlike the AT&T and GRIS data), yet this contamination is one of the major limitations of the sensitivity at 1.809 MeV. Nine sequences of 20 minute on / off pointing were individually translated into spectra and flux normalization factors for a set of Galactic distribution models. The total significance of celestial 1.809 MeV emission from the combined pointing sequences is $\sim 2\sigma$ only, with a point source flux value of $1.9 \pm 0.9 \times 10^{-4}$ ph cm^{-2} s^{-1} [53].

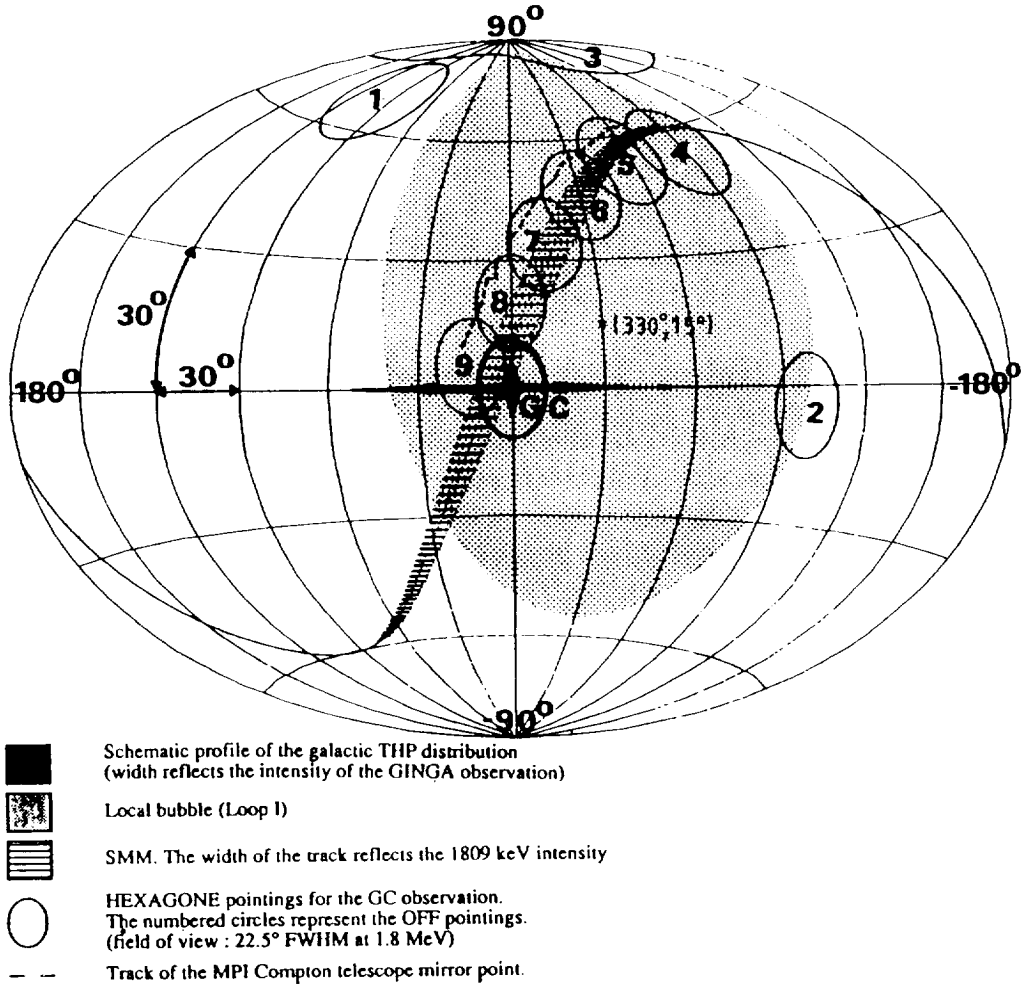

Fig. 2.9. Illustration of the problem of independent 'flat field' background measurements for ^{26}Al observations (from [97]). The celestial tracks for the instrument zenith axis generally move along the hatched area, such that 'off' pointings obtained through azimuthal changes of the instrument pointing end up in the sky regime of Loop I for all reasonably small Galactic centre source aspects. Therefore most measurements may be influenced by possible small and nearby low-level ^{26}Al emission from Loop I. The circles show the background fields for the HEXAGONE background measurements, the dashed line for the MPE Compton telescope. The hatched area represents the SMM 1.81 MeV intensity time profile measurement projected onto the sky, varying along a similar track due to the fixed instrument pointing towards the Sun. The shaded area corresponds roughly to the sky area subtended by Loop I.

The selection of background pointings for balloon observations and SMM may have an impact on their 1.809 MeV flux results. Malet et al. [97] discuss this issue and point out that the last 5 of the 9 HEXAGONE background measurements were taken from a region that includes the radio structure of Loop I, believed to be a remnant of supernova activity from the Sco-Cen stellar association, at a distance of ~170 pc (Fig. 2.9). The shell diameter of ~144 pc corresponds to an angular diameter of 116° in the sky, making difficult for balloon flights in the southern hemisphere to avoid background measurements including this structure. If a nearby ^{26}Al emissivity from Loop I is superimposed

onto Galaxy-wide emission models (as suggested in [12]), balloon instruments with ~20° apertures would measure preferentially the difference between local and Galactic ridge emissivity at 1.8 MeV. On the other hand, a large field-of-view instrument such as SMM (160° FWHM) would measure the sum of both components, with a correspondingly higher flux value. In [97] it is pointed out that the broad maximum of the SMM annual 1.809 MeV rate variation actually lies somewhat north of the Galactic plane, towards the centre of the North Polar Spur which is the radio bright part of the Loop I structure. We will return to this point below, in the discussion of the COMPTEL results.

2.7. *SMM imaging analysis*

The Gamma Ray Spectrometer on the SMM spacecraft has a large field of view of 160° (FWHM) at 1.8 MeV and no intrinsic imaging capability. However, Purcell et al. [124] applied a data selection method that sorts the primary spectra integrated onboard over 65 second intervals into 'source' and 'background', depending on whether the source region of interest is up to 13° outside or inside the region of the sky occulted by the Earth. This *Earth occultation* selection achieves an angular resolution of 22° (FWHM) for each scan position. It was applied in the inner 70° of the Galactic plane, at 5° steps (Fig. 2.10). The resulting structure of measured 1.809 MeV counts along the Galactic plane in longitude originates mainly from observational bias: exposure variations are incurred by the data selection criteria that filter out measurement times where the Earth limb is close to the interesting region of the sky. The lines in Fig. 2.10 represent convolutions of a set of assumed 1.809 MeV source distribution models with instrumental response and exposure and are drawn for comparison. Point-like emission from the Galactic centre only, as well as emission from only a ~10° wide region around the Galactic centre (as suggested by the MPE results of Section 2.5) are excluded by the analysis of [124]. All other diffuse models are compatible with this analysis of the SMM data. Purcell et al. [124] determine a flux value for the case of a Galactic centre point source (a conventionally used reference, although invalid in this case!) of 1.1×10^{-4} ph cm^{-2} s^{-1}. Moreover, they point out a particular excess at $l \sim 340°$ with a significance of 2.3σ and a count rate 4 times higher than at the Galactic centre itself. The Galactic centre "point source" flux determined from this analysis appears in agreement with the fluxes derived from the Ge detector balloon instruments, but inconsistent with the high MPE result at 1.9σ.

This imaging analysis from one instrument's data indicates the power of observations within large fields of view, whereby systematic biases for comparisons of different regions along the plane are minimized. In comparison, the different balloon campaigns all were plagued with instrumental and observational imperfections that raise concerns for direct result comparisons. Before discussing the findings from recent more sensitive measurements with the instruments aboard the Compton Gamma-Ray Observatory, we will review the astrophysical models for the nucleosynthesis of ^{26}Al and its distribution in the Galaxy. We shall see that several classes of astrophysical sources can explain an observationally suggested 2-3 $M_\odot$ Myr^{-1} of interstellar ^{26}Al. The results of CGRO suggest that massive stars are the most probable sources.

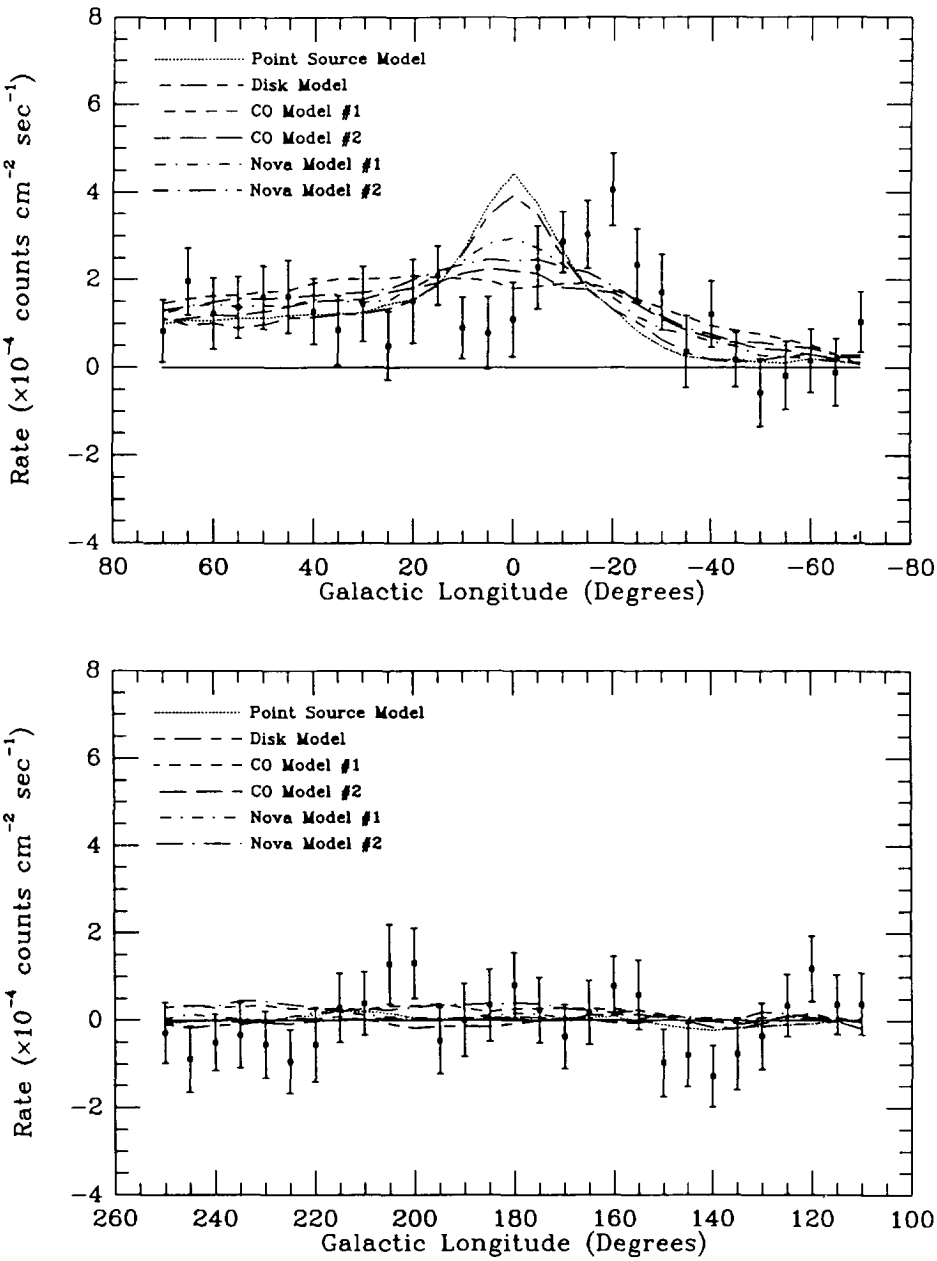

Fig. 2.10. Re-analysis of the SMM 1.81 MeV measurements using Earth occultations to select the data [124]. With this selection only an $\simeq 10°$ wide sky area is effectively exposed, allowing some imaging resolution along the plane of the Galaxy. The lines show convolutions of several source distribution models through the effective response of this analysis, for comparison. The lower panel shows the same analysis as applied to the direction towards the anticentre. Source models more concentrated towards the inner Galaxy are not favoured, as is a dominating Galactic centre source. There is remarkable excess 1.81 MeV emission from $l \simeq 340°$.

3. Nucleosynthesis of ^{26}Al

The main production mechanism of ^{26}Al in astrophysical environments is proton capture on ^{25}Mg, i.e. the ^{25}Mg(p,γ)^{26}Al reaction. Obviously, *proton rich or magnesium rich environments* (or both!) are needed for a substantial production of ^{26}Al.

Proton rich environments with sufficiently high temperatures for an efficient production of ^{26}Al are encountered in *hydrostatic H-burning* conditions, either in the convective *H cores of massive stars* ($T > 4 \times 10^7$ K) or in the *H shells and envelopes of low and intermediate mass stars* ($T \sim 5\text{-}9 \times 10^7$ K). They are also met in *explosive H- burning* conditions, at the surfaces of white dwarfs undergoing a *nova* explosion (peak temperature $T_P \sim 1.5\text{-}4 \times 10^8$ K); notice that in a particular class of novae, the *O-Ne-Mg rich*, large amounts of *both H and Mg* are available.

An environment rich in Mg can be found in the *carbon and neon shells of massive stars*, where ^{26}Al can be produced either *hydrostatically* ($T \sim 1 \times 10^9$ K) or *explosively* ($T_P \sim 2\text{-}2.5 \times 10^9$ K). The ^{25}Mg(p,γ)^{26}Al reaction proceeds rapidly at those high temperatures and, despite the low abundance of protons generated in those sites by reactions such as ^{12}C(^{12}C,p)^{23}Na, leads to large amounts of ^{26}Al.

After been produced, ^{26}Al has to be ejected in the ISM before destruction, for the gamma-ray photons of its decay to be observable. This can be easily achieved in the case of an *explosive* site, like e.g. a *nova* or a *supernova*, as well as in the case of an object suffering extensive *mass loss*, like a *Wolf-Rayet* star or a *red giant* in the Asymptotic Giant Branch phase (AGB). Obviously, the different regimes of temperature, density, timescale and initial composition in those astrophysical sites imply different modes for the production and destruction of this radioactive nucleus. We present the production and destruction mechanisms of ^{26}Al in Section 3.1, along with the uncertainties still affecting the most important nuclear reactions. Those uncertainties are due to the fact that reaction cross sections at astrophysical energies are too small to be measured with current techniques, making necessary extrapolations from higher energies; such extrapolations are often shaky, because resonances near the reaction threshold may completely dominate the cross section at low temperatures (e.g. [131]). In the subsequent sections we present, successively, the most important candidate sites that have been proposed up to now, i.e. Wolf-Rayet stars, massive stars exploding as SNII, AGB stars and novae. For each of those sources we discuss the uncertainties of the theoretical models, the yields of ^{26}Al, the ^{26}Al/^{27}Al ratio, and the associated radioactivities that may be of importance for gamma-ray line astronomy.

3.1. Nuclear physics

In proton rich environments the Mg-Al cycle (Fig. 3.1) was traditionally thought to operate at temperatures somewhat higher than those of the CNO cycle, i.e. at $T > 25 \times 10^6$ K. However, an investigation of the ^{27}Al(p,α) reaction showed that it is always slower than the ^{27}Al(p,γ) reaction [157]. This is somewhat surprising, in view of the experimentally deduced "rule" of (p,α) rates being always larger than (p,γ) rates, at least for nuclei with mass number $A < 20$. This experimental result indicates that *no Mg-Al cycle exists*, at any temperature.

In hydrostatic H-burning conditions ($T < 9 \times 10^7$ K) the ^{24}Mg(p,γ) reaction rate is not sufficiently rapid, and only ^{25}Mg may turn into ^{26}Al through the ^{25}Mg(p,γ)^{26}Al reaction. The destruction of ^{26}Al in those conditions is due to its β^+ decay for temperatures $T < 5 \times 10^7$ K and to ^{26}Al(p,γ)^{27}Si at

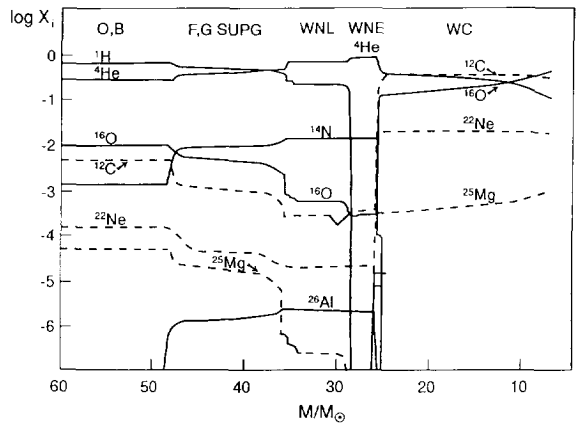

Fig. 3.5. Surface abundances (by mass fraction X) of a 60 $M_\odot$ star with mass loss as a function of remaining mass (i.e. of time). The different stages of the evolution are indicated in the upper part of the figure. The WR stage is divided in WNL (late), WNE (early) and WC, the first corresponding to reduced or no hydrogen at the surface (and to enhanced nitrogen abundance) and the last one to the absence of nitrogen and an overabundance of carbon. ^{26}Al is brought to the surface by the convective envelope of the yellow supergiant star, peaks during the WN phase and disappears in the WC phase. (Adapted from [102]).

3.2. *Astrophysical sites of ^{26}Al production*

3.2.1. *Wolf-Rayet stars*

Stars more massive initially than ~40 $M_\odot$, with metallicity $Z \sim Z_\odot$, suffer considerable mass losses already on the main sequence (e.g. [26]). The reason is the large radiation pressure exerced on their hot envelopes, which have effective temperatures $T_{\rm eff} \geq 30\ 000$ K. For the most massive of them ($M \geq 70\ M_\odot$), mass loss is so large that they remain always on the left side in the Hertzprung-Russel diagram, never moving to the red giant branch. The other massive stars ($40 \leq M/M_\odot \leq 70$) do move in the red giant region, where they suffer further mass loss and move again back to the blue. In both cases the initial hydrogen envelope of the star is stripped-off sooner or later, uncovering the former convective core. The products of the central H-burning through the CNO cycle (and, eventually, the Ne-Na cycle and the Mg-Al chain) appear then at the stellar surface. The star makes the first step in its life as a Wolf-Rayet (WR) star entering the WN phase, with a surface composition dominated by He and N. Some H exists in the WNL stars, but disappears later on, in the WNE stage (see Fig. 3.5). During the whole WR phase mass loss is maintained at very high levels ($M \sim 2\text{-}10 \times 10^{-5}\ M_\odot$/yr) and, in some cases, the former He core may be uncovered in its turn; the surface composition is then dominated by He and C (WC stars) and even C and O (WO stars) [see [92] for a recent review of the properties of those stars].

This senario accounts nicely for the main observational properties of single WR stars, like: the relationship between mass, luminosity and effective temperature; the surface chemical composition; the relative numbers of the various subtypes, as well as their distributions in galaxies with different metallicities. The initial metallicity of the stars plays, indeed, an important role in the overall picture, since the radiative force on the envelope depends on the amount of metallic ions it contains. A larger

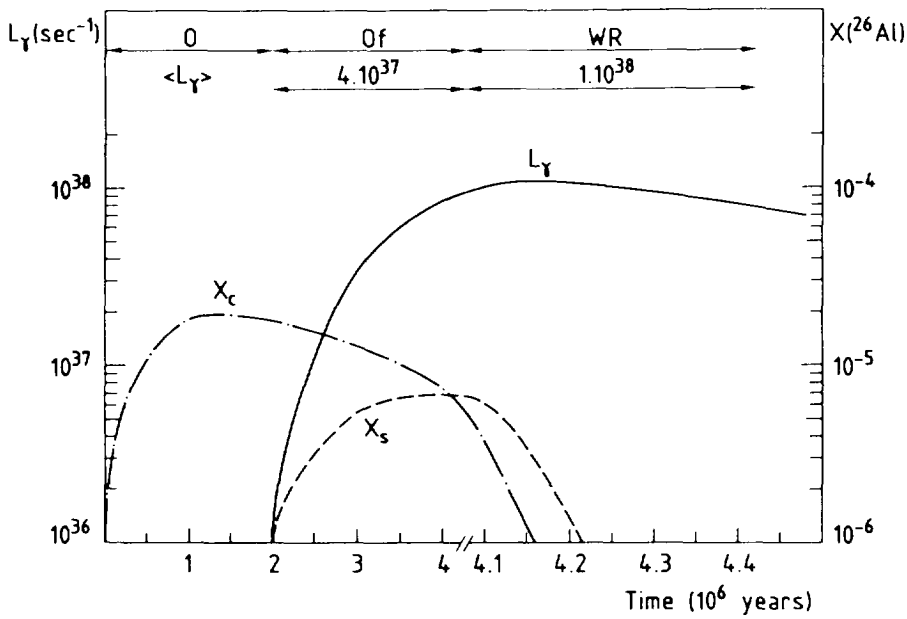

Fig. 3.6. Central (X_C) and surface (X_S) abundance of ^{26}Al and corresponding 1.8 MeV luminosity of a 100 $M_\odot$ star with mass loss as a function of time. The different stages in the evolution of the star appear in the upper part of the figure. Because of the time delay between its production in the stellar core and its appearance at the surface, the maximum atmospheric abundance of ^{26}Al is somewhat lower than its central one. (From [120]).

metallicity leads to higher mass losses on the main sequence and to an earlier stripping off of the core.

Hydrostatic core H burning in massive stars can lead to the production of significant amounts of ^{26}Al if the central temperature of the star is $T_c > 35\text{-}40 \times 10^6$ K, i.e. for stars more massive than $\sim$25 $M_\odot$ on the main sequence. As the convective stellar core gradually retreats, while the star still burns H on the main sequence, it leaves behind ^{26}Al that has been previously produced and mixed in the core. Thus, some ^{26}Al is found in the stellar envelope, where it β^+ decays to ^{26}Mg. Whether or not it will appear at the stellar surface depends on the mass loss. Stars with $M > 40\ M_\odot$ (for $Z \sim Z_\odot$) become Wolf-Rayet and regions processed by H burning finally emerge at the surface. Obviously, the higher the mass loss rate and/or the extent of the convective core, the more ^{26}Al will be ejected. Because of the time delay between its production in the stellar core and its appearence at the surface, the maximum atmospheric abundance of ^{26}Al is somewhat lower than the maximum central abundance (Fig. 3.6). During the subsequent phase of central He burning ^{26}Al is no more produced. Neutrons released through ^{13}C(α,n) in early He-burning efficiently destroy the remaining ^{26}Al in the stellar core, through ^{26}Al(n,α) and ^{26}Al(n,p) reactions. However, ^{26}Al continues to be ejected from the stellar envelope, and disappears only when the He burning products appear, in their turn, at the surface, at the WC phase [see [120] for details of ^{26}Al production in WR stars].

The injection rate of ^{26}Al in the interstellar medium by a star of mass M is:

$$\dot{m}_{26}(M,t) = \dot{M}(M,t)\, X_{26,S}(M,t)\,, \tag{2}$$

where $X_{26,S}(M,t)$ is the surface mass fraction of ^{26}Al and $\dot{M}(M,t)$ is the mass loss rate of the star.

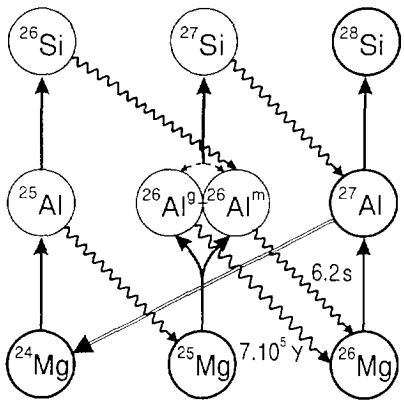

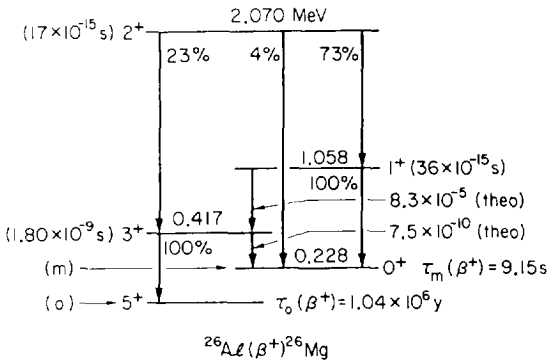

Fig. 3.1. Principal reactions involved in the synthesis of ^{26}Al in astrophysical sites. *Thick circles*: stable nuclei; *thin circles*: unstable nuclei; *Solid line arrows*: (p,γ) reactions; *wavy arrows*: β^+ decays; *double arrow*: (p,α) reactions. The ground and isomeric states of ^{26}Al (not thermalised below 4×10^8 K) are shown as separate nuclei, connected by electromagnetic transitions (*broken line*). Since the ^{27}Al(p,γ) reaction is more rapid than the ^{27}Al(p,α) reaction at all temperatures [157] there is no Mg-Al cycle.

Fig. 3.2. Decay scheme of ^{26}Al (from [168]).

higher temperatures (though the rate of the latter reaction in this temperature range is still rather uncertain; see below).

In the conditions of explosive H-burning in novae (timescales $\tau \sim 10^2$ s) the ^{24}Mg(p,γ) reaction is rapid enough to transfer substantial amounts of ^{24}Mg into ^{26}Al, through the ^{24}Mg(p,γ)^{25}Al(β^+)^{25}Mg(p,γ)^{26}Al chain. The interest of having an initial composition enriched in ^{24}Mg (usually, more abundant than ^{25}Mg) becomes then obvious. The destruction of ^{26}Al in those conditions is due to ^{26}Al(p,γ)^{27}Si. Notice that if ^{25}Al(p,γ)^{26}Si becomes more rapid than ^{25}Al(β^+)^{25}Mg, the efficiency of the process in producing ^{26}Al is reduced.

At the conditions of hydrostatic carbon burning ($T \sim 1 \times 10^9$ K, timescale $\tau \sim 10^3$ years) and explosive neon burning ($T_9 \sim 2$-3×10^9 K, $\tau \sim 1$ s) only the ^{25}Mg(p,γ)^{26}Al reaction is important for the production of ^{26}Al (i.e. no transfer from ^{24}Mg has time to occur). In such environments substantial amounts of neutrons may be produced through various secondary reactions, e.g. ^{13}C(α,n) or ^{22}Ne(α,n). ^{26}Al is then destroyed mainly by ^{26}Al(n,p) or ^{26}Al(n,α) reactions. If neutrons are not present in large quantities and if the timescale is sufficiently long ($>10^3$ s, i.e. in shell C-burning conditions), ^{26}Al is mainly destroyed by ^{26}Al(β^+). Indeed, at such high temperatures its β^+ decay rate is enhanced, due to the presence of an *isomeric state* ^{26}Al^m at 228 keV above the ground state ^{26}Al^g.

The consequences of the presence of the isomeric state on the production of ^{26}Al have been analysed in great detail in Ref. [168]. Contrary to ^{26}Al^g, the isomeric state (see Fig. 3.2) has a short lifetime $\tau_{26}^m \sim 9.2$ s, and *decays to the ground state of* ^{26}Mg, i.e. its decay is not accompanied by a photon emission. At temperatures $T < 4 \times 10^8$ K the two states are not equilibrated, the relevant thermalization time scale is longer than the time scales of nova explosions or of massive star evolution; consequently, ^{26}Al^g and ^{26}Al^m *have to be treated as separate species in nucleosynthesis calculations* for $T < 4 \times 10^8$ K. At higher temperatures equilibration between the two species is reached in timescales ≤ 9 s and the total positron emission rate for the entire ^{26}Al nucleus is [168]:

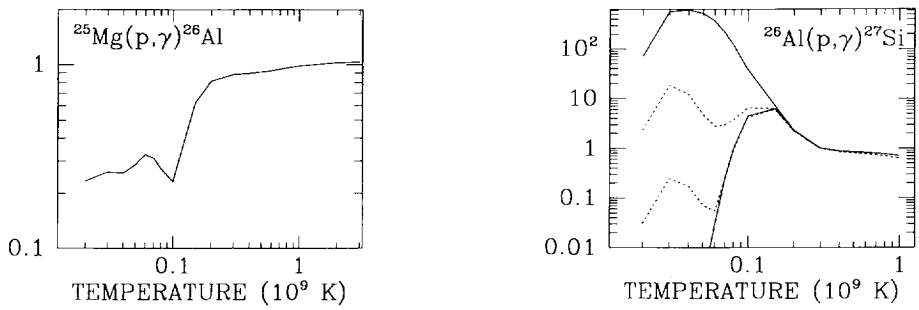

Fig. 3.3. The value of the ^{25}Mg(p,γ)^{26}Al rate according to a recent analysis [35] normalised to that of CF88 [23], plotted as a function of temperature. In the high temperature regime ($T > 2 \times 10^8$ K) the rate is equal to the CF88 value, but it is considerably smaller at lower temperatures.

Fig. 3.4. The value of the ^{26}Al(p,γ) rate according to two recent analyses [24,35] normalised to that of CF88 [23], plotted as a function of temperature. Upper and lower limits are given in both works. *Solid lines*: [35]; *dashed lines*: [24]. As in the previous case, there are no discrepancies with the CF88 value in the high temperature regime (except in the 1-2 $\times$ 10^8 K region) but the rate is quite uncertain at lower temperatures.

$$\lambda_{\beta^+}^{\mathrm{eff}}(^{26}\mathrm{Al}) \sim 10^{-2}\exp(-2.651/T_9) \quad \mathrm{s}^{-1}. \tag{1}$$

Having identified the main production and destruction paths of ^{26}Al in various environments, we give here a brief overview of the current status of the two most important reaction rates, namely ^{25}Mg(p,γ)^{26}Al and ^{26}Al(p,γ)^{27}Si. We include only information more recent than the latest compilation [23] (hereafter CF88) of astrophysical nuclear reaction rates. More details can be found in [35].

^{25}Mg(p,γ)^{26}Al: The key reaction in the production of ^{26}Al has been extensively investigated in recent years. The works of Ref. [130,71] provided the values of the strengths of the low energy resonances at E = 37 keV to 304 keV. A new reaction rate, based on all information available up to mid-94 has been derived [35]. It appears in Fig. 3.3, normalised to the CF88 value. In the high temperature range ($T_9 > 10^9$ K) the new rate is identical to the one in CF88. At $T_9 \sim 10^8$ K the new rate is lower by a factor of ~5 w.r.t the CF88 rate, due to a lower spectroscopic factor at the 136 keV resonance. At $T \sim$ 2-7 $\times$ 10^7 K the new rate is lower by a factor of ~3-4. In the case of novae the use of the new rate results in somewhat lower ^{26}Al yields, whereas in the case of WR stars a counterintuitive result is obtained, as discussed in Sect. 3.2.1. However, the uncertainties are still quite large in the low-temperature regime and work currently in progress may modify the situation considerably.

^{26}Al(p,γ)^{27}Si: Recent work on that reaction clarified the importance of several low-energy resonances [24], but considerable uncertainties remain still. The results of two recent evaluations are plotted in Fig. 3.4. At temperatures corresponding to nova explosions the new rate is ~5 times as large as the CF88 value. At temperatures corresponding to ^{26}Al production in AGB stars there is now an uncertainty by a factor of ~5-100 (up or down from the CF88 value). Finally, at even lower temperatures, appropriate to WR stars, the uncertainty of that rate is even larger (a factor of several hundred up and down the CF88 value). Notice, however, that ^{26}Al is mostly destroyed by β^+ decay in WR stars, so that this uncertainty does not affect by much its yield (except for the highest values of ^{26}Al(p,γ)^{27}Si).

The corresponding 1.8 MeV luminosity is given by

$$L_\gamma(M,t) = \frac{f\lambda_{26}N_A}{26}\int_{t_{WR}}^{t} \dot{m}_{26}(M,t)\exp[-\lambda_{26}(t-t')]\,dt', \tag{3}$$

where $f = 0.97$ is the branching ratio of the 1.8 MeV transition, N_A Avogadro's number, and t_{WR} marks the beginning of the WR phase. For illustrative purposes the 1.8 MeV line luminosity of a 100 $M_\odot$ star is displayed in Fig. 3.6 as a function of time. It has a maximum value of $\sim 10^{38}$ s^{-1} and an average one of $\sim 6 \times 10^{37}$ s^{-1}. Such a star would be visible by a detector with sensitivity $F \sim 3 \times 10^{-6}$ cm^{-2} s^{-1} like *INTEGRAL*, at a distance $D = (L_\gamma/4\pi F)^{1/2} \sim 300$ pc. The closest WR star, γ^2 Vel, is at a distance of ~300 pc, but the 1.8 MeV emission detected by *COMPTEL* in its direction should probably be attributed to another source (see Section 5).

The total mass of ^{26}Al ejected by a WR star of mass M and still surviving at time t is:

$$m_{26}(M,t) = \int_{t_{WR}}^{t} \dot{m}_{26}(M,t)\exp[-\lambda_{26}(t-t')]\,dt'. \tag{4}$$

Actually, the time between the onset of the WR phase and the death of the star is lower than $\tau_{26} \sim 1 \times 10^6$ years, at least for WR stars with $Z \sim Z_\odot$, who have an average lifetime of $\sim 5 \times 10^5$ years. The exponential decay factor in (4) is then ~0.7-1 and can be omitted in a first approximation.

Several calculations of ^{26}Al production in WR stars have been performed in the past ten years [38,39,120,21,167,115,101,99,15,78]. A meaningful comparison between them is rather difficult, because of the different stellar models and different physical ingredients (mass loss, treatment of convection, reaction rates) that were used. However, it is rather encouraging that, despite those differences, results similar to within a factor of ~3 are found for stars of a given mass. Those calculations show that stars in the mass range $40 < M/M_\odot < 120$ and solar metallicity eject in the ISM a few 10^{-5} - 10^{-4} $M_\odot$ of ^{26}Al (depending on stellar mass), during the $\sim 5 \times 10^5$ yr of their WR stage. In Fig. 3.9 appear the results of some recent works, performed with different stellar models, but with basically the same nuclear physics, i.e. the rate of ^{25}Mg(p,γ)^{26}Al reaction from [71]. Notice that, despite the smaller value of the [71] rate w.r.t. the CF88 one, a larger yield of ^{26}Al is obtained with the new rate than with the old one! As explained in [101], where calculations with both rates are reported, this is due to the fact that ^{26}Al is produced later in the lifetime of the star with the new rate and has less time to decay before being ejected.

Notice that calculations with the Schwarzschild criterion for convection result in larger amounts of ^{26}Al than calculations with *overshooting* [15]. The extent of an overshooted convective core is larger than what is obtained with the Schwarzschild criterion, since it is determined by the annihilation of the velocity of the ascending fluid elements and not merely of their acceleration; having more fuel available, stars calculated with overshooting last longer than their Schwarzschid counterparts. The effect on the production of ^{26}Al in WR cores can better be understood with the help of Fig. 3.6, obtained with the old rate and a large amount of overshooting: the central ^{26}Al abundance peaks early on (at $\sim 10^6$ yr) and subsequently decreases by β^+ decay by a factor of ~2 before ^{26}Al is brought to the surface. With the new lower rate and/or with no overshooting the peak appears just before core H-exaustion, being almost contamporaneous with the ejection, i.e. ^{26}Al has no time to decay in the stellar core.

An important feature of the production of ^{26}Al by WR stars is the *dependence of the ^{26}Al yield on metallicity*. The production of ^{26}Al is proportional to the available ^{25}Mg which depends on the initial stellar metallicity (notice that this is true for H-burning in massive stars, but not necessarily in other sites; see below). On the other hand the destruction of ^{26}Al by β^+ decay or ^{26}Al(p,γ) does not depend on metallicity. Thus, the net yield of ^{26}Al should be proportional to Z, if all other things were the same. However, the initial metallicity has another effect, since it determines the mass loss rate on the main sequence, as mentioned above: the larger the metallicity, the larger is the mass loss and the corresponding ^{26}Al yield. Recent calculations show that for a 60 $M_\odot$ WR star: $m_{26} \propto (Z/Z_\odot)^{2.2}$ [101]. Finally, metallicity has one more effect, since it determines (again via mass loss) the minimum mass of a star that may become WR. According to [92] stars with initial mass as low as 25 $M_\odot$ may become WR stars, if their metallicity is $\sim 2Z_\odot$. This should increase the relative number of WR stars in the inner Galaxy, where the average metallicity is larger than in the solar neighborhood. This metallicity dependence should be taken into acount in evaluating the galactic ^{26}Al production and the collective 1.8 MeV emissivity of WR stars (see Sections 4.4 and 4.5).

Results of the first calculations of ^{26}Al yields in WR stars in *binary systems* have been recently reported [15]. In close binaries the mass loss of the the primary star may considerably increase by interaction with the secondary (somehow imitating the effect of an enhanced metallicity). The main uncertainty here comes from the unknown fraction f of the ejected material that leaves the system, escaping accretion onto the secondary. It is found that this mechanism is not significant in the case of massive WR stars ($M > 50 M_\odot$, that loose much mass anyway), but may help less massive stars to eject some ^{26}Al. *Rotation* may also play a similar role [78], but the associated uncertainties are too large for any meaningful conclusion.

The central and surface abundances of ^{27}Al in WR stars are somewhat reduced by processing through the Mg-Al chains. The resulting X_{26}/X_{27} ratio in the WR wind is found to be $(X_{26}/X_{27})_{WR} \sim 2\text{-}5 \times 10^{-2}$, depending somewhat on stellar mass and metallicity.

The most massive WR stars go through the WC phase and may eject in their winds some ^{60}Fe, produced by neutron capture nucleosynthesis in their He burning cores. This radioactive nucleus has a lifetime of $\sim$2.2 Myr, i.e. comparable to the one of ^{26}Al, and decays by emitting gamma-ray photons of 1.173 and 1.332 MeV. Calculations [122,113] show that the amount of ^{60}Fe ejected by WC stars is $\sim 10^4$ times lower than the one of ^{26}Al, far too low to be important even for gamma-ray astronomy with INTEGRAL. However, ^{60}Fe may also be produced by SNII, in interesting amounts for INTEGRAL (see Sections 3.2.2 and 6).

3.2.2. Advanced evolution and explosion of massive stars

The advanced evolution of Wolf-Rayet stars is rather uncertain today, because of the important, and difficult to quantify, role of their mass loss. In extreme cases those stars may be "evaporated", leaving a presupernova star of only a few $M_\odot$, which explodes probably as SNIb supernova [176]. Because of the high mass loss rates during their whole life such stars never develop important *shell H-burning*. The evolution of less massive stars ($10 < M/M_\odot < 25$) is not much affected by mass loss, at least for initial metallicities $Z \leq Z_\odot$. Such stars do develop shell H-burning at temperatures $\sim 7\text{-}9 \times 10^8$ K. Some ^{26}Al may be produced there and be ejected in the ISM through the final supernova explosion. The calculations made so far show that the amounts of ^{26}Al produced in the H-shell are relatively

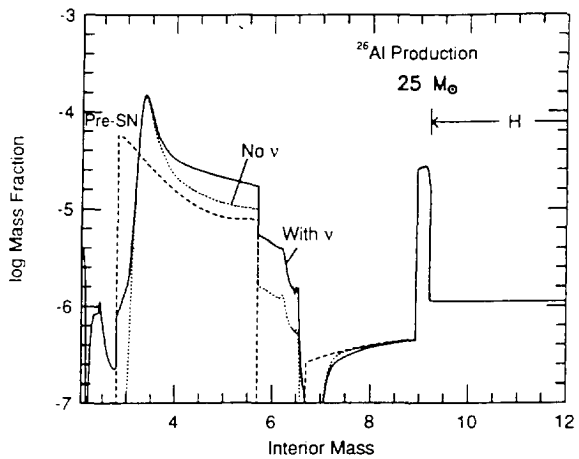

Fig. 3.7. ^{26}Al abundance profile (by mass fraction) inside a 25 $M_\odot$ star. ^{26}Al is produced in two regions: in the H shell ($\sim$ 8-12 $M_\odot$) and in the O-Ne shell (2-6 $M_\odot$). Dashed lines: production in the pre-supernova star (hydrostatic); dotted lines: explosive nucleosynthesis; solid line: total, including neutrino-induced nucleosynthesis (From [70]).

small and do not make an important contribution in the overall ^{26}Al yield of those stars (less than $\sim$15%, see Fig. 3.7).

Much more important seems to be the production of ^{26}Al in the carbon and neon shells of massive stars, just prior to the supernova explosion. The importance of this site for the production of ^{26}Al was first pointed out by [5], using previously developed models for the evolution of massive stars, of initial mass 30-40 $M_\odot$. They found that, following hydrostatic core carbon burning, a convective carbon shell is formed, its innermost zones undergoing shell C-burning at temperatures $T \sim 1 \times 10^9$ K. While the core experiences neon, oxygen and silicon burning, approximately half of the carbon is hydrostatically consumed in the shell. When the stellar core collapses, the outgoing shock wave heats the inner zones of the carbon shell at peak temperatures $T_P \sim 1.8\text{-}2.5 \times 10^9$ K, sufficient to ignite explosive nucleosynthesis. However, only a small part of the shell meets explosive burning conditions, because of the steep density gradient in that region, so that most of the shell is ejected unprocessed by the explosion. Thus, the nucleosynthesis products of the carbon shell come mainly from its hydrostatic, not explosive, burning.

Those results were confirmed by subsequent studies [175,106], with models of $15M_\odot$ and $25M_\odot$ stars. These works emphasised an important point, already identified by [5]: the sensitivity of the hydrostatically produced ^{26}Al to the treatment of time dependent convection in the carbon and neon shells. Indeed, ^{26}Al is produced only in the inner and hotter layers of those shells, while convection subsequently dilutes it in the upper an cooler regions, where ^{26}Al is mainly destroyed by β^+ decay. In the temperatures prevailing in those regions its lifetime against β^+ decay is only $\sim 10^3$ s, due to the contribution of the isomeric state. This is comparable to the convection timescale ($\sim$500-10^4 s) and, consequently, ^{26}Al is in local equilibrium in those layers. The treatment of time-dependent convection is then quite important in determining the steady state abundance of this nucleus in hydrostatic carbon shell burning. The current lack of a satisfactory theory of convection makes quite uncertain the predicted yields of ^{26}Al in that site (see [4] for a hydrodynamic treatment of oxygen shell burning, nicely illustrating the difficulties of the treatment of nucleosynthesis in such sites).

The above works, as well as a previous one [161] studied also the *explosive nucleosynthesis* of ^{26}Al in the carbon and neon shells of the same stars, heated by the passage of the shock wave. They found that in layers with $T_P > 2.0 \times 10^9$ K the small amount of remaining carbon and increasing amounts of neon are burned during the explosion, while for temperatures $T_P > 2.7 \times 10^9$ K all carbon and neon is destroyed. Considerable amounts of ^{26}Al were found to be produced in those layers of *explosive neon burning*, and smaller ones in the layers of explosive carbon burning. The reason seems to be partly the larger proton concentration (leading to a greater production of ^{26}Al) and partly the smaller neutron irradiation (leading to a smaller destruction of ^{26}Al) in the neon layers.

Finally, the study of [175] pointed out the dependence of ^{26}Al on the initial stellar metallicity. Indeed, the abundance of ^{22}Ne, the main neutron producer, is directly proportional to that metallicity, since ^{22}Ne is the main product of the He-burning chain $^{14}N(\alpha,\gamma)^{18}F(\beta^+)^{18}O(\alpha,\gamma)^{22}Ne$ and ^{14}N is the main outcome of the previous CNO cycle. Obviously, a larger ^{22}Ne concentration in the layers of ^{26}Al synthesis means a larger destruction for this nucleus. On the other hand, the abundance of ^{25}Mg comes mainly from the carbon and neon burning reactions, i.e. the production of ^{26}Al is insensitive to the initial metallicity. For $Z = 2.5Z_\odot$ [175] find that the *net* production of ^{26}Al is ~ 2 times lower than in the case with solar metallicity. Notice that this trend is opposite in the case of WR stars. In both cases it should be taken into account in the calculation of the galactic emissivity of those objects.

The works of the late 70ies clarified most of the important points in the supernova nucleosynthesis of ^{26}Al, but suffered from large uncertainties in the stellar models and in nuclear physics, since the rates of many important reactions were poorly known. The situation improved considerably in the late 80ies in both fronts. The rates of $^{25}Mg(p,\gamma)^{26}Al$ and $^{26}Al(n,p)$ and $^{26}Al(n,\alpha)$ reactions were experimentally determined. A major advancement came from the explosion of SN1987A, a $\sim$20 $M_\odot$ star in the Large Magellanic Cloud, which gave to theoreticians the opportunity to refine considerably their models, comparing them to observations of unprecedented accuracy. Two groups calculated the amount of ^{26}Al from such a star [155,178], finding results similar to within a factor of three, a rather satisfactory situation, taking into account the differences in the stellar codes. On the other hand, it was found that the uncertainty in the $^{12}C(\alpha,\gamma)$ rate affects considerably the results, since this reaction determines largely the position and the extent of the various pre-supernova layers. A "nucleosynthetically optimum" value for that rate, equal to 1.7 times its CF88 value, has been recently proposed [169].

Still, the problem of convection remains as the major one. Besides the poorly known extent of overshooting (see previous section) calculations suffer from other uncertainties such as, for instance, *semi-convection*. This situation arises in stellar zones where the molecular weight decreases sufficiently rapidly outwardly as to reduce the buoyancy of a (convectively) rising fluid element; in these conditions, some compositional mixing may still take place, but on relatively long timescales, less than a tenth of the thermal diffusion timescale. The sensitivity of the ^{26}Al yield to this effect is nicely illustrated in a recent detailed study [169] of nucleosynthesis in presupernova stars of various masses. Two recipes for semi-convection are employed in this work, that "approximately bound the possibilities", according to the authors: "nominal" semiconvection, proceeding at a rate 0.1 times the thermal diffusion rate; and "restricted" semi-convection, proceeding at a rate a thousand times smaller. The effect on the pre-supernova yields of ^{26}Al is shown in Fig. 3.8 as a function of stellar mass. It is clearly seen that: (i) the yield of ^{26}Al is not a monotonic function of the stellar mass, depending in a complicated way of the stellar physics; and (ii) the ^{26}Al yield depends crucially on the treatment

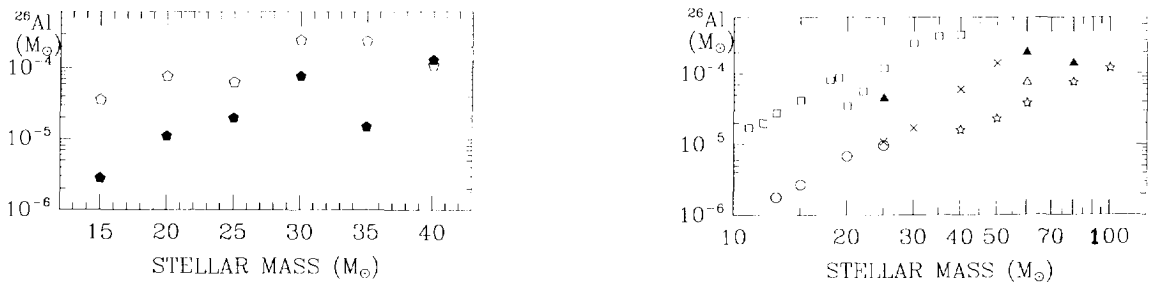

Fig. 3.8. ^{26}Al amounts in pre-supernova stars of various masses; They are produced by hydrostatic nucleosynthesis only, prior to the explosion. Two different prescriptions for semiconvection are used in the calculations of [169]: *Black symbols*: restricted semi-convection; *open symbols*: nominal semi-convection (see Section 3.2.2).

Fig. 3.9. ^{26}Al yields of massive stars as a function of stellar mass from several recent calculations. *Squares*: SNII total (pre-explosive + explosive) from [70]; *circles*: SNII explosive only from [156]; *asterisks*: WR stars from [115]; *filled triangles*: WR stars from [100]; *open triangles*: WR stars from [101]; X: WR stars from [78]. All WR stars are calculated with metallicity $Z = Z_\odot$, except those of [100] (filled triangles), calculated with $Z = 2Z_\odot$.

of semi-convection and may vary by factors of 3-12. In that study [169] it is found that restricted semi-convection leads to large overproduction of ^{18}O (produced in the He layers) and they favour nominal semiconvection, leading to large amounts of ^{26}Al. Notice that those are *pre-supernova* yields and they are expected to be modified by the subsequent explosive nucleosynthesis, although probably not by much for stars with $M \geq 35\ M_\odot$ [169].

A rather "exotic" mechanism for producing ^{26}Al (and other fragile nuclei) in SNII has also been proposed [178]: *neutrino induced nucleosynthesis*. The flux of neutrinos from the collapsed stellar core is so high ($\sim 10^{58}$ are emitted), that some of them, especially the higher energy τ and μ neutrinos, may interact with nuclei in the overlying Si, O, Ne, C, He and H layers. Single neutrons and protons are ejected from the de-excitation of those nuclei and subsequently interact with other nuclei present, modifying somehow the classical scheme of explosive nucleosynthesis. A ~50% enhancement to the explosive production of ^{26}Al in a 20 $M_\odot$ star is found in detailed calculations of that effect. The major uncertainty in that study is the number of neutrinos energetic enough (i.e. with energies $E >$ 6-8 MeV) to induce that kind of nucleosynthesis, since the neutrino spectrum emitted from the SNII core collapse is largely unknown. Indeed, detailed calculations suggest that the neutrino spectrum is truncated in its high and low energy tails [107] and that the corresponding effect on the explosive nucleosynthesis (and the production of ^{26}Al in SNII) may have been overestimated; see, however, alternative discussions in [180].

The current status of ^{26}Al production in SNII and WR stars is summarised in Fig. 3.9. The results of the Santa-Cruz group [169,70] include pre-supernova nucleosynthesis with "nominal" semi-convection and neutrino-induced nucleosynthesis (i.e. they represent maximum ^{26}Al production in SNII, under optimal conditions). It turns out that, in their case, the larger the stellar mass, the larger is the contribution of presupernova stage to the production of ^{26}Al: in the 35 $M_\odot$ star the explosion actually destroys (by photodisintegration) the hydrostatically synthesized ^{26}Al in the inner neon layers, but produces some more in the outer neon layers, so that the overall explosive production is negligible [179]. It appears then that the amount of explosively produced ^{26}Al decreases with stellar mass in [169] (and presumably in [70]). This is in disagreement with the results of

[156] which also appear in Fig. 3.9 and concern only explosive nucleosynthesis: the ^{26}Al yields clearly increase with stellar mass in that case. Moreover, the yields of [156] are considerably smaller than the corresponding ones (i.e. explosive nucleosynthesis only) of [169,70] . Those differences should be obviously attributed to the different presupernova structure of the stellar models used in those calculations, and illustrates clearly (along with Fig. 3.8 for the pre-supernova case) the current uncertainty in the ^{26}Al yields from the C and Ne layers of SNII.

The results presented in this section concern the advanced nucleosynthesis and evolution of stars with $12 \leq M/M_{\odot} \leq 35$, i.e. stars that are not heavily affected by mass loss (at least with $Z \leq Z_{\odot}$). The advanced evolution of more massive stars ($M \sim 40$-$85\ M_{\odot}$) with mass loss was recently studied [176]. It was found that in the pre-supenova stage such stars develop a structure corresponding to much lighter ones, i.e. C-O cores of $\sim 5\ M_{\odot}$ only, that characterize also $25\ M_{\odot}$ stars. Although ^{26}Al production in those WR descendents is not calculated in [176], it is estimated that such stars may also give a few $10^{-5}\ M_{\odot}$ of ^{26}Al. That estimate is, however, even more uncertain than those of Fig. 3.9.

The theoretical X_{26}/X_{27} ratio of SNII is currently somewhat larger (by a factor of ~ 5) than the one obtained in nucleosynthesis calculations in the late 70ies. The most recent calculations of SNII nucleosynthesis [169,70] give: $X_{26}/X_{27} \sim 5\text{-}7 \times 10^{-3}$ for stars with mass $M = 15$ to $35\ M_{\odot}$. This ratio is the lowest among all sources of ^{26}Al and does not favour SNII at the origin of the pre-solar ^{26}Al.

SNII are also interesting sources of ^{60}Fe, which may be produced either by neutron captures in the He-burning shell prior to the explosion, or by explosive nucleosynthesis in the inner layers. The calculations of [169,70] show that the produced amount of ^{60}Fe may be as large as $\sim 10^{-4}\ M_{\odot}$ in some cases (the negligible ^{60}Fe yields in [156] are probably due to an insufficiently extended network). The resulting diffuse γ-ray flux in the ^{60}Fe lines is lower than one tenth of the corresponding ^{26}Al γ-ray emission, i.e. of the order of $\sim$a few 10^{-6} ph cm^{-2} s^{-1}, making its detection marginally possible for future instruments, like INTEGRAL (see Section 6). Notice that the ^{60}Fe yields of [169,70] suffer from the same uncertainties resulting from the treatment of semi-convection as the corresponding yields of ^{26}Al.

3.2.3. AGB stars

Stars of intermediate or low mass ($\leq 9 M_{\odot}$) spend the last part of their active life on the Asymptotic Giant Branch of the Hertzprung-Russel diagram. At that phase of its evolution a star has terminated He burning in its core and consists of: a degenerate and inert carbon-oxygen core, surrounded by a He-shell, a H-shell and (part of) the original H-envelope, which has been reduced by mass loss during the first ascent of the red giant branch. The envelope is completely convective, but the depth of its penetration inside the star is poorly known, since it depends (once more) on the treatment of convection.

H and He burn intermittently at the bases of the corresponding shells, in the following way (Fig. 3.10). After core He exaustion, while H still burns in a "remote" shell, He ignites in the shell immediately surrounding the inert C-O core. Its ignition pushes the material of the H-shell outward, to such low temperatures and densities that the H-shell is effectively extinguished. As its fuel is progressively exausted, the He-burning shell slowly migrates outwards, until it almost reaches the He-H interface. Then the H-shell ignites again and He-burning dies down temporarily. In its turn,

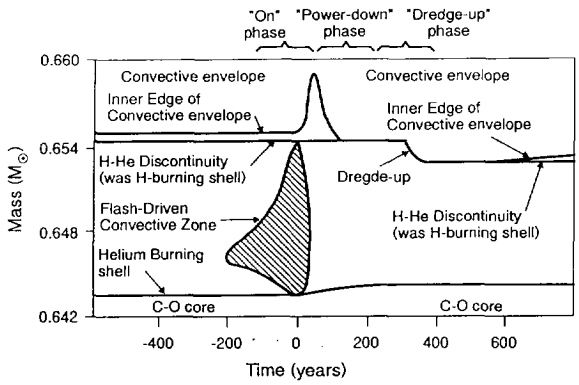

Fig. 3.10. Physical processes affecting the nucleosynthesis inside an AGB star before, during and after a thermal pulse (Adapted from [79]).

the H-burning shell migrates outwards, laying down its He-ashes. When the layer of those He-ashes becomes thick enough, its temperature and density are appropriate to ignite He again, in an almost explosive way. The H-shell is pushed outwards by this *He-shell flash* and the cycle of the *thermal pulses* starts again. The duration of the flash is very brief (a few years to decades) and relaxes to a quiescent He-burning phase $\sim$ hundred times longer, while the duration of the H-burning episodes is ten times longer yet. Those numbers depend heavily on the mass of the C-O core (i.e. the initial stellar mass), the longer durations corresponding to the smaller masses.

^{26}Al may be produced in the H-burning shell of AGB stars, where temperatures $\sim 7 \times 10^7$ K are easily encountered. It may also be produced at the base of the convective H envelope by *hot bottom burning* (e.g. [72]), provided that the temperature of that region is sufficiently high ($T > 5 \times 10^7$ K). In that case, the transport of the nucleosynthesis products to the stellar surface is immediate. Hot-bottom burning probably occurs in the more massive AGB stars ($M > 5\ M_\odot$), as observations seem to suggest. Indeed, bright AGB stars in the Large Magellanic Cloud are found to be enriched in s-elements (a signature of He-burning) and to have C/O<1, while He-burning in that site should give C/O>1. This has been interpreted as due to CN cycling in the bottom of the H-envelope, burning C to N and keeping the atmospheric C/O<1. Independently of the occurence of the hot-bottom burning, the convective envelope periodically descends down to the H-shell (when H-burning is, temporarily, off) and brings to the surface the H-burning products of that shell and ^{26}Al.

Products of the He-burning shell may also be mixed in the upper layers after a thermal pulse and finally to the surface, after the next dredge-up episode. This may be of interest for the production of ^{26}Al in the more massive AGB stars ($M > 5M_\odot$): according to theory, those stars develop high enough temperatures in the base of their He-shell ($> 2.5 \times 10^8$ K) to activate the ^{22}Ne(α,n)^{25}Mg reaction; some ^{25}Mg may be mixed in the regions of ^{26}Al production, enhancing considerably the ^{26}Al yield. Observations do not seem to support this idea, since some of the produced ^{25}Mg should also be dredged-up to the surface, together with carbon, oxygen and other He-burning products, like s-isotopes (produced by neutron captures on heavy nuclei); however, no observational evidence exists up to now for strange Mg isotopic ratios at the surfaces of AGB stars enriched in s-elements [77]. This suggests that the neutron source is not ^{22}Ne(α,n)^{25}Mg (but probably ^{13}C(α,n)^{16}O) and that ^{26}Al is produced in those stars solely from the initial ^{25}Mg (notice that hot bottom burning could

blur the effects of He-burning on the Mg isotopic pattern).

The first study of the synthesis of ^{26}Al in that complex environment was made fifteen years ago [108]. It was based on previous estimates concerning the thermodynamic conditions, the dredging-up and the mass loss of stars with $M \sim 5\text{-}7M_\odot$ during this evolutionary phase. It was found that nucleosynthesis at the bottom of the convective H envelope may produce abundance ratios $X_{26}/X_{27} \sim 0.5\text{-}1$. On the basis of those computations it has been argued in a very qualitative way, that red giants could significantly contribute to the production of ^{26}Al at the Galactic level. Due to a lack of accurate stellar evolution models, most of those calculations assume that all the initial ^{25}Mg in the H envelope is transformed in ^{26}Al [18,56]. This is clearly an unrealistic assumption, leading to an upper limit of $m_{26} \sim 10^{-4}\ M_\odot$ of ^{26}Al per AGB star. Such a conclusion is also reached in a recent study [10] where only the evolution of the stellar envelope is properly followed, while the evolution of the core is treated schematically. Despite this simplification and the rather optimistic conclusion, that work illustrates clearly the impact of the unknown depth of the convective envelope on the production of ^{26}Al: for a $6M_\odot$ star, a value of $\alpha = 1.5$ (the ratio of the mixing length to the pressure scale-height in the envelope) leads to $m_{26} \sim 10^{-4}\ M_\odot$, while a value of $\alpha = 1$ leads to $m_{26} \sim 10^{-7}\ M_\odot$.

The only detailed and completely self-consistent calculation of ^{26}Al production in AGB stars, up to now, concerns stars of 1-3 $M_\odot$, and is performed with up-to date opacities and reaction rates [112,54]. Neither ^{25}Mg enrichment from the He-shell, nor hot-bottom burning is found in that study. ^{26}Al is found to be produced in the H-shell by the complete burning of the pre-existing ^{25}Mg, at temperatures $T \sim 5 \times 10^7$ K. The total amount of ^{26}Al ejected by the 3 $M_\odot$ star is $\sim 3 \times 10^{-8}\ M_\odot$ in $\sim 7 \times 10^6$ y. Notice, however, that the results of that calculation cannot be generalised to all AGB stars, since hot-bottom burning is expected to occur only in more massive stars ($> 4\text{-}5\ M_\odot$).

Finally, notice that, contrary to the cases of WR and SNII, no study of the dependence of AGB ^{26}Al yields on metallicity exists today. In principle, if ^{26}Al is produced in the H-burning shell or by hot-bottom burning, its yield should be proportional to the initial ^{25}Mg content, i.e. to metallicity. However, the physical conditions of the envelope depend also on metallicity and it is difficult to say how they will affect the ^{26}Al yield.

The X_{26}/X_{27} ratio of AGB stars has received considerable attention over the years. If ^{26}Al is produced only in the H-burning shell, then the resulting X_{26}/X_{27} ratio in the ejecta is ~a few 10^{-3} [54] (and a slowly varying function of time and stellar mass). If it is produced by hot-bottom burning, that ratio is much more uncertain and can be larger than unity, especially if most of the ^{25}Mg is turned into ^{26}Al. The same is true if ^{25}Mg from the ^{22}Ne(α,n)^{25}Mg is mixed in the H-shell; however, this case is rather improbable, as discussed above. Because of their large X_{26}/X_{27} ratio AGB stars are prominent candidate sources for the ^{26}Al found in the early solar system.

The s-process taking place in the He-burning shells of AGB stars could also produce radioactive nuclei of interest for γ-ray line astronomy, like ^{60}Fe. However, the uncertainties in the stellar models, concerning the activation of the ^{22}Ne(α,n) and ^{13}C(α,n) reactions, the dredging-up mechanism etc., make very difficult the evaluation of the corresponding yields.

3.2.4. Novae

Theoretical models of nova explosions suggest that accretion of a critical mass of H-rich material on the surface of a white dwarf (WD) leads to a thermonuclear runaway. Matter is accreted from a companion star filling its Roche lobe. The material at the base of the accreted envelope is degenerate,

so that matter accumulates with no pressure increase while it is heated by the luminosity of the white dwarf and quiescent H-burning at a low rate at these low temperatures. The temperature rises rapidly, as well as the rate of the nuclear burning, and when the Fermi temperature ($\sim 10^8$ K) is exceeded, the increased thermal pressure causes the envelope to begin expanding. The accreted mass necessary to trigger the runaway varies widely with the mass of the white dwarf, from $\sim 10^{-3}$ $M_\odot$ for a M_{WD}=0.2 $M_\odot$, to $\sim 10^{-7}$ $M_\odot$ only for M_{WD} = 1.4 $M_\odot$. This is due to the fact that the ignition temperature is more easily attained in the case of the massive white dwarfs, with their higher surface gravities creating larger pressures. The peak temperature ($T_P \sim$ 150-400 $\times 10^6$ K) and the corresponding timescale ($\tau \sim$ a few 10^2 s) depend essentially on the mass of the white dwarf and its envelope, as well as on the available energy ([84,59] and references therein).

The nucleosynthesis of the hot-CNO cycle constrain the energetics of the nova explosion. The rate of nuclear energy generation at high temperatures ($T > 10^8$ K) is limited by the timescale of the slower (and time-independent) positron decays, particularly of ^{14}O ($\tau \sim$ 102 s) and ^{15}O ($\tau \sim$ 176 s); it is also determined by the total number of initial CNO nuclei. On that basis, a distinction is made between *slow* novae, with ~solar composition and *fast* novae, with composition enriched in CNO.

This scenario of nova explosions has been studied in detail with hydrodynamic models by a few groups [147,80,148,109], which reproduce in a rather satisfactory way most of the observational data, like the light curves in various wavelengths, the masses and velocities of the ejecta ($M_{ej} \sim 10^{-7}$-10^{-3} $M_\odot$, i.e. roughly the accreted mass, and $u_{ej} \sim 5 \times 10^2$-$10^4$ km s^{-1}) and the abundances in the ejecta. The analysis of the abundance observations shows that (see [59] for a review):

(i) H is depleted w.r.t. He in the ejecta;

(ii) the CNO nuclei are considerably enriched, with N being typically the most abundant (a signature of CNO cycle operation); and

(iii) about 1/3 of all novae show a strong enrichment of neon, usually accompanied by enhancements of the $Z > 10$ elements (Mg to Si); the implications of that class of *O-Ne-Mg rich novae* for the production of ^{26}Al will be discussed below.

The first detailed studies of the synthesis of ^{26}Al in explosive H-burning conditions were made in the early 80ies [6]. As in most subsequent works, they concerned "post-processing" calculations, i.e. with no coupling between the nuclear network and the hydrodynamics, by simply adopting thermodynamic conditions of realistic nova models. They showed that on long timescales (>10 s) ^{24}Mg may also be transformed in ^{26}Al through the ^{24}Mg(p,γ)^{25}Al(β^+)^{25}Mg(p,γ)^{26}Al chain, since there is enough time for the beta decay of ^{25}Al to occur. In that case the theoretical upper limit to the resulting ^{26}Al yield is given by the initial amount of (^{24}Mg+^{25}Mg). Those results were confirmed by subsequent calculations [68,44,173,178], leading to production ratios $X_{26}/X_{27} \sim$ 0.1-1 and to corresponding mass fractions $X_{26} \sim 10^{-4}$, for material with solar initial composition.

A major revision in the rates of many relevant reactions [172], concerning essentially unstable nuclei (in some cases by many orders of magnitude), showed that an important leakage may occur out of the Mg-Al cycle, through ^{27}Si(p,γ) (Notice that this was prior to the discovery that no Mg-Al cycle exists). Consequently, the production of ^{26}Al was found to be considerably reduced with respect to previous estimates: only a few times 10^{-7} (by mass fraction) for *hot* novae ($T_P > 200 \times 10^6$ K) and a few 10^{-5} for *cold* ones ($T_P < 200 \times 10^6$ K). Subsequent calculations with the [71] rate for ^{25}Mg(p,γ) reaction, found even lower results: $X_{26} \sim 10^{-5}$ only, for a cold nova with solar composition [112]. Taking into account that a nova ejects on the average $M_{nova} \sim 10^{-4}$ $M_\odot$, the average ^{26}Al yield

of a C-O nova turns out to be $\sim 10^{-11}$-10^{-9} $M_\odot$, depending on its peak temperature and composition (CNO enriched or not).

It should be stressed that uncertain reaction rates and thermodynamic conditions are not the only factors affecting the production of ^{26}Al in novae, which is particularly sensitive to the modelling of the site. A major difficulty comes from the treatment of *convection*, the time-scale of which is comparable to the nuclear one, i.e. a few 10^2 s. In such conditions time-dependent convection should be used, which has indeed been done in one case (see below); but the associated uncertainties are quite large, since no satisfactory treatment of convection exists yet. The impact of the treatment of convection on the ^{26}Al yield has been studied in a schematic way up to now, in parametrized, two-zone, calculations [174,112]. ^{26}Al is produced in the lower and hotter zone. Convection brings fresh fuel from the upper zone and removes the fragile nuclei (among them ^{26}Al) from the burning region up to the colder zone, where they can be preserved before being ejected in the ISM. In some cases spectacular production enhancements are found for ^{26}Al, by factors ~10-30, depending on the adopted physical conditions. This illustrates clearly the uncertainties affecting all current nucleosynthesis computations in novae.

The results presented so far concern novae from C-O white dwarfs with $M_{WD} < 1.25\ M_\odot$, resulting from stars with M <6-7 $M_\odot$. In the past years, interest has focused on more massive white dwarfs with O-Ne-Mg composition, resulting from stars with $M \sim$8-11 $M_\odot$. Indeed, a distinct subclass of novae, associated with an underlying O-Ne-Mg rich white dwarf, seems to be a promising candidate for the production of ^{26}Al. The existence of those objects, first discussed by [81] is based on spectroscopic observations of Nova V693 CrA 1981 and Nova V1370 Aql 1982. The observed overabundances of intermediate mass elements Ne-Na-Mg-Al-Si cannot be explained by the explosive nucleosynthesis itself and should be attributed to material dredged-up from the underlying white dwarf. In that case the initial abundance of Mg may be of the order of 10% or more, i.e. a thousand times its solar value, and the corresponding ^{26}Al production may be greatly enhanced.

Several groups have performed one-zone parametrised calculations of nucleosynthesis in novae on O-Ne-Mg white dwarfs, making plausible assumptions about the initial composition (generally amounting to 25-75 % of O-Ne-Mg by mass fraction) [44,174,171,112,109]. It was shown that high peak temperatures ($T_P > 2.5 \times 10^8$ K) and/or long timescales ($\tau >$ a few 10^2 s) do not favour the production of ^{26}Al. On the contrary, at low peak temperatures (around $\sim 1.5 \times 10^8$ K) the final ^{26}Al mass fraction may be as high as $X_{26} \sim 2 \times 10^{-2}$. Those results are confirmed in a recent work, which is the first study coupling hydrodynamics (with time-dependent convection) to nucleosynthesis of ^{26}Al [149] (remember, however, that the uncertainty from the treatment of convection affects hydrodynamic calculations as well). It is found that, starting with an initial composition of ~50% O-Ne-Mg, novae of M_{WD} = 1., 1.25 and 1.35 $M_\odot$ may produce $X_{26} \sim 2 \times 10^{-2}$, 10^{-2} and 7×10^{-3}, respectively. This trend of decreasing X_{26} with M_{WD} is interesting, since the less massive the white dwarf is, the greater is the amount of accreted and ejected matter; the range is probably from $M_{nova} \sim 10^{-4}\ M_\odot$ for $M_{WD} \sim 1.\ M_\odot$, down to $M_{nova} \sim 10^{-7}$-$10^{-8}\ M_\odot$ for $M_{WD} \sim 1.4\ M_\odot$. This calculation suggests that $\sim 1\ M_\odot$ novae eject up to $\sim 10^{-6}\ M_\odot$ of ^{26}Al and, therefore, are excellent candidates for ^{26}Al production. Notice, however, that the masses of O-Ne-Mg rich white dwarfs are expected (from stellar evolution calculations) to be larger than 1.2 $M_\odot$, so that the above result for the 1 $M_\odot$ O-Ne-Mg nova should be considered as of rather academic interest.

Finally, a recent calculation investigates the impact of the remaining uncertainties in key nuclear reaction rates on the ^{26}Al yield of O-Ne-Mg novae [35]. The adopted model is neither a parametrised,

one-zone, nor a hydrodynamic one, but follows the analytic prescriptions of [91]. The resulting temperature profiles compare favourably with detailed hydrodynamic calculations, at least near the peak, where most of the nucleosynthetic action takes place. The authors find that the nuclear uncertainty that may considerably affect X_{26} (by a factor of $\sim$3 from its "canonical" value of $\sim 10^{-2}$) is the unkown strength of the resonance at 188 keV in the ^{25}Al(p,γ)^{26}Si reaction.

Notice that the interpretation of O-Ne-Mg rich novae as originating from massive white dwarfs ($>1.2\ M_\odot$) has been recently questioned. Indeed, massive novae are expected to eject only $<10^{-5}$ $M_\odot$ of material, while the mass ejected by the neon nova QU Vul 1984 was determined to be 10^{-4}-$4 \times 10^{-3}\ M_\odot$ and the one of nova Her 1991 $\sim$ 7-9 $\times 10^{-5}\ M_\odot$ [89]. It has been suggested then [137,138] that O-Ne-Mg rich novae may originate from C-O white dwarfs ($M \sim 1\ M_\odot$), accreting matter at very high rates ($\sim 10^{-6}\ M_\odot$/yr, instead of the $10^{-9}\ M_\odot$/yr assumed in the classical senario). The accreted material is slowly burned into He and then (via mild flashes with little mass ejection) into C,O, Ne and Mg; thus, the C-O white dwarf is covered by a thin layer of O-Ne-Mg. When the accretion rate slows down to $\sim 10^{-9}\ M_\odot$/yr, the conventional senario occurs with H burning in a thermal runaway and the O-Ne-Mg rich material being (partially) ejected. This alternative scenario has the advantage of explaining how a low mass O-Ne-Mg white dwarf may be formed. Although its authors are optimistic as to the resulting yield of ^{26}Al, no self-consistent nucleosynthesis calculation in that site exists up to now.

As in the case of AGB stars, the X_{26}/X_{27} ratio in novae depends very much on the existence of progenitor nuclei with enhanced abundances. In the case of O-Ne-Mg rich novae it may attain quite large values, of the order of 1-10, as recent calculations show [149,35]. This is the largest X_{26}/X_{27} ratio that may be obtained in any site of ^{26}Al production; it constitutes an important argument for a nova origin of Galactic ^{26}Al, based on the X_{26}/X_{27} ratio [27].

Nova explosions produce also several other radioactive nuclei [84]. The most interesting for gamma-ray line astronomy is ^{22}Na ($\tau_{22} \sim 3.75$ yr), produced by the hot Ne-Na cycle. The nuclear uncertainties affecting the abundance of that isotope in novae are analysed in detail in the recent work of [35], where an average mass fraction of $X_{22} \sim 3 \times 10^{-4}$ in the ejecta of O-Ne-Mg rich novae is obtained. The substantial difference in the yield of ^{22}Na between that work and the one of [149] (a factor of ten) is obviously due to the different modelling of the nova nucleosynthesis (i.e. parameterised in the former case vs. hydrodynamic in the latter).

3.3. A non-thermonuclear origin for the galactic ^{26}Al?

A possibility of non thermonuclear origin for the interstellar and meteoritic ^{26}Al has been recently suggested [29], prompted by the discovery of gamma-ray line emission from the de-excitation of ^{12}C and ^{16}O nuclei in the Orion complex. The gamma-ray lines at 4.4 and 6.1 MeV have been detected by COMPTEL at flux level of $\sim 1 \times 10^{-4}$ cm^{-2} s^{-1} [13]. At the Orion distance of $\sim$500 pc, this flux corresponds to an emissivity of $\sim 2 \times 10^{39}$ s^{-1}. This emission is attributed to the interaction of rapid C and O nuclei with the hydrogen nuclei of the Orion complex. Notice that the inverse process, i.e. rapid protons on the Orion C and O nuclei, could also be invoked but it produces a much larger ionisation rate for the same emissivity. The widths of the lines, much larger in the former than in the latter case could, in principle, be used to distinguish between the two possibilities, but the energy resolution and sensitivity of COMPTEL are not sufficient for that.

The heavy nuclei could be the ejecta of massive stars that exploded in Orion and may have been accelerated to relatively low energies (~10-30 MeV/nucleon) by the shock waves of the explosions. In that case, the spallation of the heavy nuclei in the Mg-Si region could produce ^{26}Al nuclei through e.g. ^{26}Mg(p,n)^{26}Al, or ^{28}Si(p,ppn)^{26}Al. Taking into account the corresponding cross sections and allowing for the (completely unknown) energy spectrum of those heavy nuclei, it is found that the production rate of ^{26}Al in Orion should be $\sim 2 \times 10^{38}$ s^{-1}, i.e. about one tenth of the excitation rate of ^{12}C nuclei [29]. Supposing that this production rate has remained ~constant in the past $\tau_{26} \sim 10^6$ yr, a duration smaller than the estimated age of the Orion complex, one obtains $\sim 5.4 \times 10^{51}$ ^{26}Al nuclei Myr^{-1} or $\langle \dot{m}_{26} \rangle_{\text{Orion}} \sim 10^{-4}\ M_\odot$ Myr^{-1}.

If the same process takes place in the $N_{\text{GMC}} \sim 500$ or so giant molecular clouds (GMC) that are currently thought to existe inside the solar circle (i.e. inside a radius $R_\odot \sim 8.5$ kpc around the galactic centre), the galactic rate of ^{26}Al production is:

$$\dot{M}_{\text{GMC}} = \langle \dot{m}_{26} \rangle_{\text{Orion}} N_{\text{GMC}} \sim 0.05\ M_\odot \text{Myr}^{-1}\,.$$

Needless to say that this number should be considered only as indicative, the uncertainties of this scenario being much larger than in all the previously considered cases. Indeed, neither the duration nor the magnitude or the spectrum of the energetic particle irradiation is known. But there is an observational argument against Orion-type clouds producing most of the galactic ^{26}Al: indeed, in that case there should be an even more intense diffuse galactic emission at 4.4 MeV from the de-excitation of ^{12}C, which is not observed [128].

3.4. Comments

A few general remarks should be made on the nucleosynthesis of ^{26}Al in various astrophysical sites:

- The time-scale for the ejection of ^{26}Al from the above astrophysical sites is $\tau \ll \tau_{26}$ for all the explosive sites (novae and supernovae), $\tau \sim \tau_{26}$ for WR stars and $\tau > \tau_{26}$ for AGB stars (for the most massive of them, $\tau \sim \tau_{26}$). In the latter case it is not the total quantity of ^{26}Al ejected by the AGB winds that has to be taken into account, but only an average production over $\sim 10^6$ y.
- In all the models of the nucleosynthetic sites of ^{26}Al the treatment of convection constitutes one of the major difficulties. But it affects the ^{26}Al yield much more in the case of SNII (by factors 3-12 in the presupernova stage) and nova (factors of > 10), than in the case of WR stars (factor ~2-3). The situation is even more difficult in the case of AGB stars, because of the complex interference of convection, dredge-up and mass-loss.
- Uncertainties in nuclear reaction rates have been considerably reduced in the past years. They affect now the yield of ^{26}Al less than astrophysical factors (like e.g. convection in general, or initial composition in the case of O-Ne-Mg rich novae). Only in WR stars one may expect a 'surprise' from the badly known behaviour of the ^{26}Al(p,γ) reaction rate at temperatures $\sim$ 2-6 $\times 10^6$ K (see Section 3.1).

4. Production and distribution of ^{26}Al in the galaxy

In order to evaluate the total amount of ^{26}Al ejected in the ISM by the previously discussed astrophysical sites in the last $\tau_{26} \sim 10^6$ yr, one needs to know their galactic frequency. For a more accurate evaluation, their galactic distribution is also needed, since the ^{26}Al yield depends in some cases on metallicity, which is a function of position in the Galaxy. The corresponding ejection rate of ^{26}Al can be estimated by the expression:

$$\dot{M}_{26}^{G} = \langle m_{26} \rangle_S \, f_S, \tag{5}$$

where: $\langle m_{26} \rangle_S$ ($M_\odot$) is the average amount of ^{26}Al ejected by each source, and f_S (Myr^{-1}) the source frequency of occurence in the Galaxy (at least during the last millions of years). As discussed in Sections 2 and 5.6, observations indicate that $\dot{M}_{26}^{G} \sim$ 2-3 $M_\odot$ Myr^{-1}.

In some cases the source frequency can be determined by observations. In other cases (like AGB stars) it has to be derived by combining observations and theoretical arguments, involving the stellar *Initial Mass Function* (IMF) and the galactic *Star Formation Rate* (SFR). Notice that in all cases except novae, the average yield $\langle m_{26} \rangle_S$ is also defined with the use of an IMF. Finally, in the case of low mass AGB stars, ejecting their ^{26}Al over periods longer than τ_{26}, $\langle m_{26} \rangle_S$ above should be replaced by $\langle \dot{m}_{26} \rangle_S \tau_{26}$, where $\langle \dot{m}_{26} \rangle_S$ is the average ejection rate of ^{26}Al by the star.

The frequency of occurence of stars with mass between M_1 and M_2 in the Galaxy can be estimated by:

$$f_S = \mathrm{SFR} \int_{M_1}^{M_2} \Phi(M) \, \mathrm{d}M, \tag{6}$$

where the IMF $\Phi(M)$ is normalised, as usual, to:

$$\int_{M_{LOW}}^{M_{UP}} \Phi(M) \, M \, \mathrm{d}M = 1, \tag{7}$$

with $M_{LOW} \sim 0.1 \, M_\odot$ and $M_{UP} \sim 100 \, M_\odot$, respectively.

Observations suggest that the galactic SFR today is $\sim$3 $M_\odot$ yr^{-1} (e.g. [125]). For any reasonable IMF this corresponds to $\sim$5 stars yr^{-1} and we adopt $f_G \sim 5 \times 10^6$ stars Myr^{-1} for the birthrate of stars of all masses in the Galaxy. In principle, the SFR should be included in the integral (6), since it is a function of the time $t - \tau(M)$ at which the star of mass M and lifetime $\tau(M)$ is born. However, for stars with mass $M \geq 1.5 \, M_\odot$(and corresponding lifetimes $\tau(M) \leq 2 \times 10^9$ yr), which are the most interesting for the production of ^{26}Al, we may reasonably assume that the galactic SFR has remained approximately constant at its current value and adopt Eq. (5). [Notice, however, that one cannot exclude *fluctuations around an average value*, by factors $\sim$3 as derived in models of chemodynamical galactic evolution [17]. With this hypothesis the *death rate* of stars (needed for the calculation of ^{26}Al ejection) is the same as their *birth rate* (given by SFR and f_S). Moreover, we shall see in Sec. 4.3 that this $f_G \sim 5 \times 10^6$ stars Myr^{-1} is compatible with the independently derived supernova rate in the Galaxy.

The value of the integral in (6) depends on M_1 and on the form of the IMF. In the following we adopt the recently derived IMF [76] for the solar neighborhood: it is a multiple slope power-law

IMF $\Phi(M) \propto M^{-(1+X)}$, with $X = 1.7$ above 1 $M_\odot$. We make the assumption that it has been the same all over the Galaxy for the past few billions of years.

4.1. AGB stars

Low mass AGB stars originate from stars with masses $M_1 \sim 1.0\ M_\odot$ and $M_2 \sim$3-4 $M_\odot$. With the previously described IMF, the fraction of stars with mass between $M_1 = 1\ M_\odot$ and $M_2 = 4\ M_\odot$ is $w \sim 9 \times 10^{-2}$ and their galactic frequency (deathrate): $f_{\rm LAGB} \sim w f_{\rm G} \sim 5 \times 10^5$ stars Myr^{-1}. According to the calculations of [54] reported in Sec. 3.4, an average low-mass AGB star of $\sim 3\ M_\odot$ may eject up to $\langle m_{26}\rangle_{\rm AGB} \sim 10^{-8}\ M_\odot$ of ^{26}Al. The ejection rate of ^{26}Al from the galactic population of those low mass AGB stars is:

$$\dot{M}_{\rm LAGB} \sim 5 \times 10^{-3}\ \frac{\langle m_{26}\rangle_{\rm LAGB}}{10^{-8}}\ \frac{f_{\rm LAGB}}{5\ 10^5}\ M_\odot\,{\rm Myr}^{-1}\,, \tag{8}$$

i.e. a factor of $\sim 6 \times 10^2$ lower than the observationally derived rate. Thus, it seems that low mass AGB stars have a negligible contribution to the interstellar ^{26}Al, a conclusion also supported by the COMPTEL results as will be discussed in Section 5.

In the case of massive AGB stars ($M_1 \sim$ 4-5 $M_\odot$ and $M_2 \sim 9\ M_\odot$) the corresponding number fraction is $w \sim 5 \times 10^{-3}$ and their galactic frequency $f_{\rm MAGB} \sim 3 \times 10^4$ stars Myr^{-1}. If each one of them produces on average $\langle m_{26}\rangle_{\rm MAGB} \sim 3 \times 10^{-5}\ M_\odot$ of ^{26}Al by hot-bottom burning, as suggested by [10], their collective production in the Galaxy could be as large as:

$$\dot{M}_{\rm MAGB} \sim 1\ \frac{\langle m_{26}\rangle_{\rm MAGB}}{3\ 10^{-5}}\ \frac{f_{\rm AGB}}{3 \times 10^4}\ M_\odot\,{\rm Myr}^{-1}, \tag{9}$$

i.e. they could almost account for the total galactic ^{26}Al. As we shall see below, such a possibility cannot be excluded by the COMPTEL data. Notice, however, that the extreme sensitivity of their ^{26}Al yield to the mixing length prescription (see Sec. 3.4), could make their contribution as small as the one of their low mass cousins.

4.2. Novae

In the case of *novae*, the most prolific producers of ^{26}Al are the O-Ne-Mg rich ones: according to recent calculations, each one of them may eject up to $\sim 10^{-6}\ M_\odot$ of ^{26}Al[35,149]; an average of $\langle m_{26}\rangle_{\rm ONeMg} \sim 3 \times 10^{-7}\ M_\odot$ is adopted in view of those results. The frequency of novae in the Galaxy has been a subject of active research for many years, the original estimates of more than $\sim$100 novae/yr being considered now as excessive. Recent work has shown that the nova rate in external galaxies (per unit luminosity) varies with Hubble type [41]. On the basis of the current values of the nova rates in LMC, M33, M31, NGC25128 and three ellipticals in the Virgo cluster as callibrators, a nova rate of 24 novae/yr has been recently proposed [40]. In any case, the current uncertainty in the nova rate is much smaller than the uncertainty in the ^{26}Al yield of novae, so we shall adopt a "generous" estimate of 30 novae yr^{-1}, as in most older studies. According to several estimates, the ONeMg novae constitute $\sim$1/3 of the nova population, although that fraction may be as low as $\sim$10%, as recently argued [89]. Again, this uncertainty is smaller than the one of the nova

yield of ^{26}Al, so we adopt a galactic rate of $f_{\mathrm{ONeMg}} \sim 10\ \mathrm{yr}^{-1}$. Their galactic production rate of ^{26}Al could then be as high as:

$$\dot{M}_{\mathrm{nova}} \sim 3\,\frac{\langle m_{26}\rangle_{\mathrm{ONeMg}}}{3\times 10^{-7}}\,\frac{f_{\mathrm{ONeMg}}}{10^{7}}\,M_{\odot}\,\mathrm{Myr}^{-1}, \tag{10}$$

i.e. O-Ne-Mg novae seem to be serious candidates, at least in view of the recent nucleosynthesis calculations at that site. We shall see below that the COMPTEL observations seem to exclude the possibility that novae dominate the Galactic ^{26}Al emission.

4.3. Massive stars (core collapse supernovae)

Massive stars exploding as SNII (or as SNIb, if they have lost a large part of their hydrogen envelope) are among the most promising sources of ^{26}Al. The frequency of supernovae in the Galaxy has been recently evaluated [151] on the basis of (i) historical evidence and (ii) observations of supernovae in galaxies of different types and luminosities. For the Milky Way, a Sb or Sc type galaxy of luminosity $\sim 2.3\times 10^{10}\ L_{\odot}$, a rate of 2.5 supernovae of all types per century has been derived. About 80% of them belong to the class of SNII+SNIb, which leads to an average death rate of massive stars of ~ 2 per century in our Galaxy. Notice that this number is in agreement (within a factor of two) with the frequency derived from the procedure decribed in Sec. 4.1: indeed, with $M_{\mathrm{l}} \sim 10\ M_{\odot}$ as lower mass limit for stars exploding as SNII+SNIb one obtains $w \sim 2\times 10^{-3}$ and $f_{\mathrm{SN}} \sim 10^{4}\ \mathrm{Myr}^{-1}$. According to Fig. 3.9 each one of them ejects on average $\langle m_{26}\rangle_{\mathrm{SN}} \sim 8\times 10^{-5}\ M_{\odot}$ of ^{26}Al. Their collective production rate of ^{26}Al in the Galaxy is then:

$$\dot{M}_{\mathrm{SN}} \sim 1.6\,\frac{\langle m_{26}\rangle_{\mathrm{SN}}}{8\times 10^{-5}}\,\frac{f_{\mathrm{SN}}}{2\times 10^{4}}\,M_{\odot}\,\mathrm{Myr}^{-1}. \tag{11}$$

Taking into account the current uncertainty in supernova yields (more than a factor of 3) it seems that exploding massive stars may be the dominant sources of galactic ^{26}Al (but they could, as well, produce less than 0.5 $M_{\odot}$).

In fact, the contribution of SNII to the galactic amount of ^{26}Al has a long story. SNII are thought to be the major galactic producers of the stable isotope ^{27}Al and it was suggested that the galactic ^{26}Al production of SNII should be correlated to that of ^{27}Al [27]; another motivation for such a correlation was the fact that in the late 70ies the isotopic production ratio $(X_{26}/X_{27})_{\mathrm{SN}}$ ~a few 10^{-3} suffered from less uncertainties than the absolute ^{26}Al yield of SNII (due to a lack of detailed models of SNII explosions). Supposing that supernovae produced all the ^{27}Al($X_{27} \sim 2X_{27}^{\odot} \sim 6\times 10^{-5}$) in the galactic ISM (that is, in a mass $M_{\mathrm{ISM}} \sim 5\times 10^{9}\ M_{\odot}$) during the past $T_{\mathrm{G}} \sim 10^{10}$ years (the age of the Galaxy), the quantity of ^{26}Al produced by supernovae with $(X_{26}/X_{27})_{\mathrm{SN}} \sim 5\times 10^{-3}$ during the last $\tau_{26} \sim 10^{6}$ years should be:

$$M_{26}^{\mathrm{G}} \sim (X_{26}/X_{27})_{\mathrm{SN}}\,(\tau_{26}/T_{\mathrm{G}})\,X_{27}\,M_{\mathrm{ISM}} \sim 0.30\,M_{\odot} \tag{12}$$

if *nucleosynthesis at constant rate* is assumed all over the galactic history [notice that this method allows to circumvent the uncertainties on the galactic rate of SNII, which was poorly known in the late 70ies]. Thus, it seemed that supernovae fall short of producing a Galactic quantity of a few $M_{\odot}$ of ^{26}Al by a factor of ~10; stated in a different way, if supernovae were at the origin of ~3 $M_{\odot}$ of ^{26}Al in the ISM, they should have overproduced ^{27}Al by a factor of ~10 [27]. This argument

was used for some time as conclusive evidence against the SNII origin of galactic ^{26}Al. However, if the assumption of constant rate nucleosynthesis is dropped, and *galactic chemical evolution* effects are taken into account (as they should), the supernovae contribution may be considerably modified, as was subsequently shown with the use of simple, analytical models of galactic chemical evolution including *infall* [31]. Such models are quite successful in reproducing several observational features of the solar neighborhood in the framework of a simple parametrisation of the infall rate $f(t)$ as a function of time:

$$f(t) = \frac{k}{t + \Delta} M_g(t) , \tag{13}$$

where $M_g(t)$ is the mass of the galactic gas and Δ a time constant. In a recent work [34] it is shown that in such models the relationship (12) becomes:

$$M_{26}^G \sim (k + 1) (X_{26}/X_{27})_{SN} (\tau_{26}/T_G) X_{27} M_{ISM} , \tag{14}$$

i.e. the mass of galactic ^{26}Al is increased with respect to the one in the closed box model by a factor $k + 1$. Physically, this is explained by the diluting effect that infall has on the concentration of the stable isotope ^{27}Al (by a factor $\sim k + 1$), effect which does not operate on ^{26}Al, because of its short lifetime. It is easily seen that models with $k = 4$, which seem plausible from galactic evolution arguments, lead to $M_{26}^G \sim 1.5\ M_\odot$. Such a conclusion is also reached in a recent numerical calculation of evolution of the galactic disk with infall, leading to a total quantity of $\sim 2\ M_\odot$ of ^{26}Al in the Galaxy [158], not very different from the estimate in the beginning of this section. It seems then that there is no incompatibility between the two roles of SNII as producers of both ^{26}Al and ^{27}Al in the Galaxy.

We feel, however, that the above "chemical evolution" arguments on the interstellar ^{26}Al may not be very constraining, since they correlate a stable isotope (^{27}Al), produced by 10^{10} years of galactic evolution, to a very short-lived one (^{26}Al), produced only during the last 10^6 years. This large discrepancy in the relevant timescales makes such a correlation somewhat speculative, despite the (probably) common origin of the two isotopes. Indeed, it is not known when the bulk production of ^{27}Al in the Galaxy took place and even the most succesful models of galactic chemical evolution reproduce data only up to solar system formation, i.e. 4.5 Gyr ago. Such models cannot be claimed to reproduce the last $\sim 10^9$ years and, in particular, the current interstellar medium, characterised by important composition inhomogeneities. For instance, the nearby ($\sim$500 pc) Orion nebula seems to be metal deficient by a factor of ~ 2 w.r.t. the Sun, contrary to what is expected from galactic chemical evolution models. Besides, such models give an *average* nucleosynthesis rate over some large interval of time; it may well be that the actual galactic nucleosynthesis rate in the last few 10^6 or 10^7 years is considerably above or below this average value.

It is certainly interesting to find that chemical evolution models show compatibility between the SN production of both ^{27}Al and ^{26}Al. However, they can hardly be used to *predict* the current ^{26}Al content of the Galaxy, at least not to better than a factor of ~ 10 [indeed, the stellar yields of [170] fit the solar values to a factor of ~ 3; a larger uncertainty factor is introduced from uncertainties in star formation rate across the Galaxy, the current mass profile of the Galactic disk, etc.].

4.4. WR stars

Early estimates of the contribution of WR stars to the galactic ^{26}Al content were based on an uncertain evaluation of their total number and distribution in the Galaxy [120,20,114,123]. This was done by extrapolating data concerning the WR density in the solar neighbourhood and low metallicity regions like the Large and Small Magellanic Clouds. The reason was that WR catalogues are complete only within $R \sim 2.5$ kpc from the Sun, where $N_R \sim 100$ WR stars have been observed up to now [163], while the inner galactic regions are obscured by dust. Their galactic number may be roughly estimated as: $N_{WR} \sim N_R (R_\odot/R)^2$, where $R_\odot = 8.5$ kpc is the distance of the Sun to the Galactic centre (since no WR stars have been observed outside the solar circle). One obtains then: $N_{WR} \sim 1100$, or a galactic frequency $f_{WR} \sim 2200$ Myr^{-1}, since their average lifetime is ~ 0.5 Myr.

Their galactic frequency may also be estimated as in Section 4.1, i.e. using an IMF and the current SFR. The lowest mass of a single star that may become WR is the important factor for the evaluation of that number. Calculations show that for stars with solar metallicity $M_l \sim 40\ M_\odot$. For larger metallicities this limit gets lower, since the radiation pressure on the stellar envelope becomes more important. Taking into account the observed galactic metallicity gradient of $d(\log Z)/dr \sim -0.07$ dex/kpc [142] an average galactic metallicity of $Z_G \sim 2Z_\odot$ can be defined. Stars with such a metallicity may become WR if their mass is as low as $M_l \sim 25\ M_\odot$ [92]. The procedure of Section 4.1 gives then a number fraction $w \sim 4 \times 10^{-4}$ and a corresponding galactic frequency $f_{WR} \sim 2 \times 10^3$ Myr^{-1}, i.e. consistent with the independent estimate above.

From the yields of Fig. 3.9, valid for solar metallicity WR stars, an average ^{26}Al yield of $\sim 6 \times 10^{-5}\ M_\odot$ can be derived. As stressed in Sec. 3.2, the ^{26}Al yield of a WR star varies with metallicity as $m_{26} \propto (Z/Z_\odot)^2$. The ^{26}Al yield of a WR star with an average metallicity of $Z_G \sim 2Z_\odot$ becomes then $\langle m_{26} \rangle_{WR} \sim 2 \times 10^{-4}\ M_\odot$. Their collective production of ^{26}Al in the Galaxy is:

$$\dot{M}_{WR} \sim 0.4 \frac{\langle m_{26} \rangle_{WR}}{2 \times 10^{-4}} \frac{f_{WR}}{2 \times 10^3} M_\odot \,\mathrm{Myr}^{-1} \tag{15}$$

(see also [115–118,143,144,99]. Taking into account that the overall uncertainties (from the stellar models and the galactic frequency) are not larger than a factor of ~ 3 it seems that WR stars cannot produce more than $\sim 20\%$ of the galactic ^{26}Al. Only a major change in the low temperature behaviour of the ^{25}Mg(p,γ)^{26}Al and ^{26}Al(p,γ) rates could modify this conclusion.

4.5. A consistent calculation of galactic ^{26}Al production

In principle, the galactic yield of a stellar population depends not only on the IMF, the SFR and the galactic metallicity gradient, but also on the galactic distribution of that population. For instance, if all WR stars were concentrated in the galactic centre region, where the metallicity may be as large as $Z_{GC} \sim 3Z_\odot$, their yields of Fig. 3.9 ($Z = Z_\odot$) should be multiplied by $(Z_{GC}/Z_\odot)^2 \sim 9$. This extreme example shows that the galactic distribution of the sources may affect, via the galactic metallicity gradient, the amount of galactic ^{26}Al, at least in the case of sources with metallicity dependent yields. In practice, it turns out that the effect is much smaller than the other uncertainties of the problem and can be ignored in a first approximation. One further reason to neglect it comes from the fact that none of the candidate sources has a well known galactic distribution, as will be discussed in the next section. However, as theoretical models improve and uncertainties are reduced, one may expect

that this effect will eventually have to be taken into account. This will be the case, in particular, if a detailed galactic map of the 1.8 MeV emission exists and one wants to check its compatibility with the theoretical picture. Formally, the rate of ^{26}Al ejection in the Galaxy is:

$$\dot{M}_{26} = \mathrm{SFR} \int_0^{R_G} 2\pi R \, \mathrm{d}R \, \sigma(R) \int_{M_1}^{M_2} \Phi(M) \, Y[M, Z(R)] \, \mathrm{d}M, \tag{16}$$

where R is the galactocentric radius, R_G = 15 kpc the radius of the Galaxy, $\sigma(R)$ the adopted source surface density, M_1 and M_2 the corresponding mass limits of the stellar sources (as defined in the previous sections) and $Y[M, Z(R)]$ the ^{26}Al yields as a function of stellar mass and metallicity (itself a function of position). Such a formalism was introduced in [143], with the product SFR $\int_{M_1}^{M_2} \Phi(M) \, \mathrm{d}M$ for massive stars normalised to the observed frequency of SNII+SNIb. As we shall see below, the adopted $\sigma(R)$ has a large impact on the resulting spatial distribution of the 1.8 MeV emission.

4.6. Galactic distribution of the sources of ^{26}Al

From the discussion of the previous paragraphs, it appears difficult to eliminate any one of the candidate sources of ^{26}Al on the basis of their nuclosynthetic yields alone. Indeed, each one of them may have a galaxywise production of up to $\sim$1 $M_\odot$ Myr^{-1}, i.e. close to the observational requirements (except, perhaps, low-mass AGB stars). In view of that difficulty encountered by theory, it has been suggested that the spatial distribution of the 1.8 MeV emission could help to discriminate between the candidate sources, since each one of them is expected to have a distinct spatial "signature" in the Galaxy. This suggestion is based, implicitly, on the assumption that ^{26}Al does not move far away from its sources during its $\sim 10^6$ year lifetime. This is obviously a quite reasonable assumption in the case of novae and AGB stars, each one of them ejecting at relatively low velocities very small amounts of matter, that are rapidly decelerated in the interstellar medium. On the other hand, SNII and WR stars eject several $M_\odot$ of matter at average velocities of $\sim 10^3$ km s^{-1}, that may travel during $\sim 10^5$ years and go through a few hundred pc (depending on the ambient density) before stopping. This is a small distance compared to the scalelength of the galactic disk ($\sim$3 kpc), so that, even in this case, the diffusion of ^{26}Al should not "blurr" the gross features of the source profile as a function of galactic longitude; however, it could certainly alter the source profile at smaller scales and, in particular, the latitude distribution (the scale-height of a young population being $<$100 pc, see below).

Most of the effort in the late 80ies consisted in finding plausible galactocentric distributions $\sigma(R)$ for the various candidate sources and then calculating the corresponding longitude flux profile [86,120,31,114,66,67,166]. Unfortunately, none of the candidate sources has a directly observable distribution, because of obscuration by gas and dust in the inner Galaxy and/or poor statistics. WR stars are observed mostly in the solar neighborhood, their catalogue being complete only up to $\sim$2.5 kpc from the Sun [163]. Supernova explosions have not been observed for the last $\sim$400 years in the Galaxy, and the $\sim$150 observed SN remnants do not reveal the nature of the explosion i.e. ^{26}Al producing SNII vs. ^{26}Al "sterile" SNIa (see [88] for an analysis of the distribution of galactic SN remnants). Similar uncertainties affect also the distributions of novae (e.g. [85]) and AGB stars.

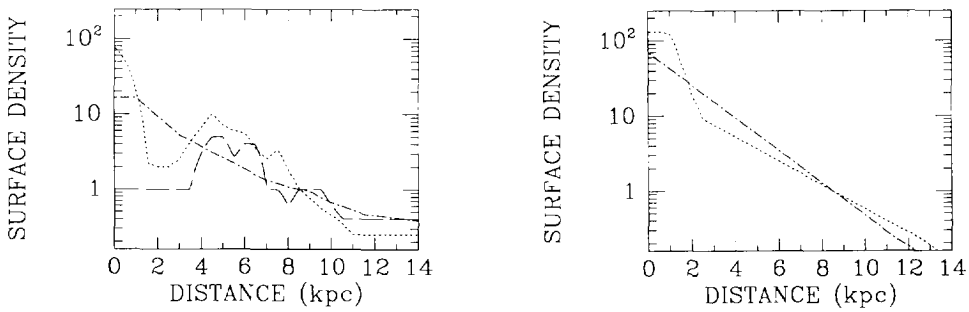

Fig. 4.1. Plausible radial distributions of young stars (age $<10^8$ years) in the Galaxy. *Dotted line*: H_2 clouds (from [136]); *Dashed line*: giant HII regions (from [136]); *Dashed-dotted line*: SNII in external spiral galaxies (from [9]). All distributions (surface densities) are normalised to 1 at the solar position (radius $R = 8.5$ kpc).

Fig. 4.2. Plausible radial distributions of old stars (age >a few 10^9 years) in the Galaxy. *Dashed-dotted line*: exponential disk profile with scale radius $r = 3$ kpc, corresponding to the IRT observations [73] (often referred to as "flat nova" distribution). *Dotted line*: Radial distribution of novae in M31 according to [141] and [31] (often referred to as "sharp nova").

In view of the uncertainties in the galactic distribution of the candidate ^{26}Al sources, one has to rely on "tracers" observed either in our Galaxy or in external spiral galaxies. Many such tracers have been proposed up to now, and we discuss below a few that seem the most appropriate. For that purpose we distinguish two classes of sources:

(1) Those belonging to a *young population* (age $< 10^8$ years), including the most massive AGB stars ($M > 5\ M_\odot$), SNII ($M > 10\ M_\odot$) and WR stars ($M >$ 25-40 $M_\odot$ for single WR stars, depending on metallicity). Those extreme Pop. I objects have a small scaleheight ($h_Z < 100$ pc, at least inside the solar circle) and their galactic distribution can be traced either by giant HII regions or giant molecular clouds (GMC). Indeed, there is an excellent spatial correlation between massive star forming dense cores, as detected by IRAS in the CS line (normally excited at H_2 densities $>10^4$ cm^{-3}) and velocity integrated CO contour maps, tracing GMC [14]. Also, giant HII regions are ionised by the UV flux of embedded or nearby massive stars, and observations in spiral galaxies show that supernovae occur preferentially in their vicinity. Thus, the galactocentric distributions of giant HII regions or GMC (both presenting a maximum in the "molecular ring", at $R \sim 4$ kpc, Fig. 4.1) can be reasonably used as tracers of this young population. Notice, however, that the surface density of H_2 in the innermost galactic regions ($R < 2$ kpc) is difficult to evaluate; this is also true for the star formation rate there, since there are observational indications for turbulence and/or large scale magnetic fields that could prevent star formation even in the presence of large amounts of H_2 [61]. This point is important for the determination of the emissivity of that region, compared e.g. to the one expected from the molecular ring (see below). Finally, independently of their actual radial distribution, young objects are expected to be found inside *spiral arms*. Indeed, it is currently thought that star formation in the Galaxy takes place predominantly inside spiral arms, especially in the case of massive stars, and observations of SNII in spiral galaxies strongly support this argument. Objects with lifetimes shorter than the $\sim 10^8$ year revolution period of the Milky Way (which sets the survival timescale for the spiral pattern), are expected to be found in such a configuration.

(2) Those belonging to a *relatively old population* (age >a few 10^9 years), like the small AGB stars ($M < 2\ M_\odot$) and novae. For those objects the galactic survey of the InfraRed Telescope offers a

reliable tracer, since the observed emission is thought to reflect the distribution of G and K giant stars; it corresponds to an exponential distribution with scalelength ~3 kpc and scaleheight ~170 pc [73]. Superimposed to it is a bulge population of radial extent ~1 kpc with an exponentially decreasing density profile. The disk IRT distribution is similar to the luminosity profile of our Galaxy, used in several studies as "flat nova" distribution. The disk+bulge configuration presents a particularly enhanced density profile in the central kpc of the Galaxy; this is the reason of the pronounced central peak in the nova distribution of M31, presented sometimes as "sharp nova" distribution [67,135,164]. Notice that the introduction of a bulge is equivalent to the introduction of a point source in the Galactic Center as far as the resulting longitude profile is concerned, but flattens considerably the latitude profile in that region. However, it is not clear whether the galactic bulge should be taken into account in the discussion of ^{26}Al sources: it has been claimed [83] that it is even older than the galactic halo, its population being formed more than 10^{10} years ago. AGB stars with $M > 1.5\ M_{\odot}$ or O-Ne-Mg novae are much younger objects and should not be associated to a bulge distribution in that case. Notice also that it is not certain that the O-Ne-Mg novae, the most important ^{26}Al producers among novae, belong to an old population. Although the O-Ne-Mg white dwarfs probably come from stars with $M > 7\ M_{\odot}$, it is the interaction with the companion that determines the nova phenomenon. The corresponding timescale depends both on the mass of the companion and the distance of the two components, and neither of those two quantities is known in the case of O-Ne-Mg novae. Companion masses, kinematics and scale-height of novae in the solar vicinity suggest an age $\sim 5 \times 10^9$ years, but observations are dominated by the more frequent CO novae and may not be quite relevant (except if the recently proposed scenario of [138] for O-Ne-Mg novae is correct). In any case, O-Ne-Mg novae cannot belong to the young population (as defined above), since it is difficult to imagine all of them having both their components more massive than $\sim 5\ M_{\odot}$ (i.e. with lifetimes $<10^8$ years). Finally, notice that the "old" population of ^{26}Al sources has two marked differences w.r.t the "young" one: a larger scaleheight (150-400 pc in the former case vs. <100 pc in the latter) and no correlation with the spiral pattern (because of its age>10^8 years). The latter point probably offers the only reliable method to discriminate between the two populations, through the corresponding longitude profile. The latitude profile is a less good tracer, since diffusion of ^{26}Al away from its sources may alter the scaleheight of a young population (see the discussion in the beginning of this section).

4.7. Theoretical emissivity profiles of the galaxy at 1.8 MeV

An axisymmetric distribution of sources in the Galaxy, with a surface density $\sigma(R)$ and a scale-height h (which may also be a function of galactocentric radius R) has a volume density:

$$\rho(R, Z) = \frac{1}{2h}\,\sigma(R)\exp\left(-\frac{Z}{h}\right), \tag{17}$$

where Z is the distance from the galactic plane. By definition $\rho(R, Z)$ is normalised to:

$$\sigma(R) = \int_{-\infty}^{\infty} \rho(R, Z)\,\mathrm{d}Z\,. \tag{18}$$

If each of the sources has an emissivity $Q(R)$ (in photons s^{-1}), the differential flux received on Earth (in photons $cm^{-2}\ s^{-1}\ sr^{-1}$) from a direction with galactic longitude l and latitude b is given

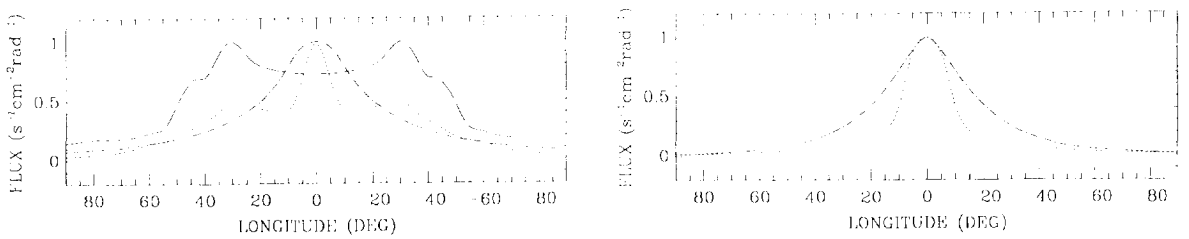

Fig. 4.3. Flux profiles as a function of galactic longitude, corresponding to the radially summetric distributions of young stars of Fig. 4.1. *Dotted line*: H_2 clouds; *Dashed line*: giant HII regions; *Dashed-dotted line*: SNII. All flux profiles are normalised to maximum value=1. The peaks at longitude $l \sim \pm 30°$ correspond to the molecular ring of the H_2 and HII distributions. The intensity of the central peak in the case of H_2 is quite uncertain, depending on the unknown star formation rate in the inner Galaxy.

Fig. 4.4. Flux profiles as a function of galactic longitude, corresponding to the radially summetric distributions of old stars of Fig. 4.2. *Dashed-dotted line*: exponential disk profile with scale radius r = 3 kpc. *Dotted line*: Radial distribution of novae in M31. Those two longitude profiles are often encountered in the literature of γ-ray line astronomy as "flat" and "sharp" nova distributions, respectively. In the case of our Galaxy the contribution of the bulge is quite uncertain (see text).

by:

$$\mathrm{d}F(l,b) = \frac{1}{4\pi}\int_0^\infty \rho(l,b,S)\,Q(l,b,S)\,\mathrm{d}S\mathrm{d}\sin b\,\mathrm{d}l\,, \tag{19}$$

where S is the distance along the line of sight. The heliocentric coordinates (l,b,S) are related to (R,Z) by: $Z/S = \sin b$ and $R^2 = R_\odot^2 + r^2 - 2rR_\odot\cos l$, $R_\odot$ = 8.5 kpc being the distance of the Sun from the Galactic centre and r the distance from the Sun of the projection of the source on the Galactic plane.

Defining $\Sigma(R) = \sigma(R)\,Q(R)$ one obtains for the expected longitude profile of a population of sources with radial surface density $\sigma(R)$ and scale-height h the following expression:

$$\frac{\mathrm{d}F}{\mathrm{d}l} = \frac{1}{4\pi}\int_0^\infty\int_{-b_{\max}}^{b_{\max}} \frac{\Sigma(r,l)}{2h}\exp\left(-\frac{r\tan b}{h}\right)\mathrm{d}b\,\mathrm{d}r\,. \tag{20}$$

Assuming mirror symmetry between the northern and southern galactic hemispheres and for small detector apertures ($b_{\max} < 10°$), or for distributions with small scale-heights, the integral in latitude may be performed analytically, leading to:

$$\frac{\mathrm{d}F}{\mathrm{d}l} = \frac{1}{4\pi}\int_0^\infty \frac{\Sigma(r,l)}{r}\left[1-\exp\left(\frac{-r\tan b_{\max}}{h}\right)\right]\mathrm{d}r\,. \tag{21}$$

This derivation of the longitude profile follows the one given in [62], as used in [120,114–119,121]; a somewhat different derivation of the longitude flux profile is given in [86,31].

Application of Eq. (21) in the radial distributions of young populations (Fig. 4.1) leads to the longitude profiles presented in Fig. 4.3. Depending on the assumed SFR in the inner Galaxy one obtains either a peaked flux profile or a hollow one in the direction of the galactic centre. The molecular ring at $l = \pm 30°$ is more or less prominent, its importance being inversely proportional to

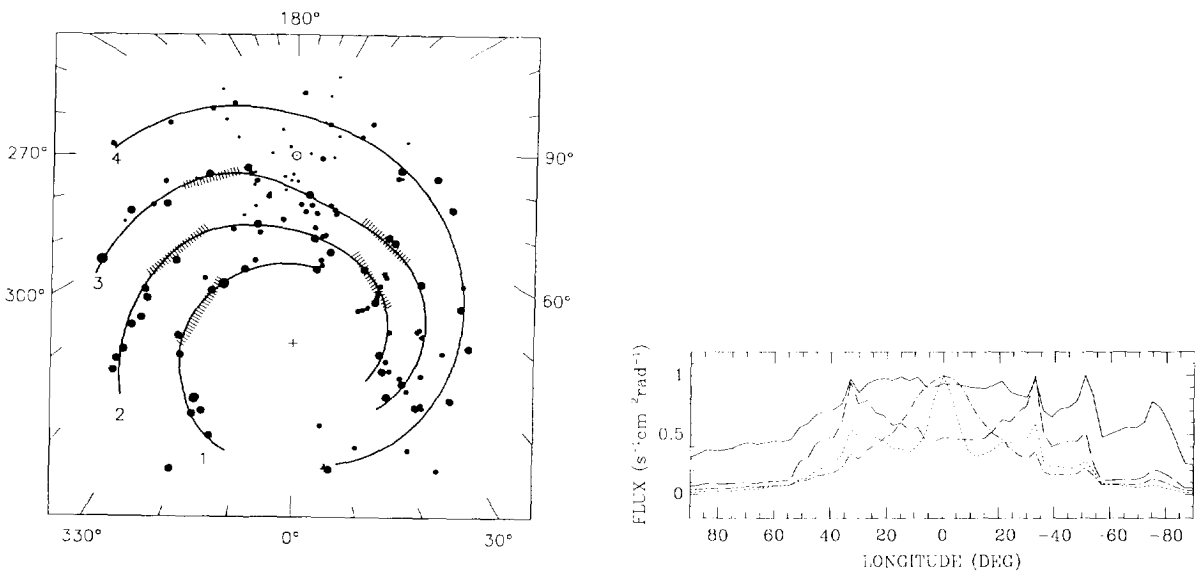

Fig. 4.5. Spiral structure of our Galaxy from observations of HII regions (from [60,152]). Enhanced flux is expected on Earth when the line of site is tangent to the spiral arms. Notice, however, that the spiral structure of the inner Galaxy is poorly known.

Fig. 4.6. Flux profiles as a function of galactic longitude, corresponding to the radially summetric distributions of young stars of Fig. 4.1, superimposed on the spiral pattern of Fig. 4.5. The arm/interarm density contrast is taken to be 5 and the ^{26}Al yields are assumed to be independent of metallicity. *Dotted line*: H_2 clouds; *Dashed line*: giant HII regions; *Dashed-dotted line*: SNII. *Solid line*: a uniform density distribution is also displayed for illustrational purposes. Spiral arms are clearly distinguished at longitudes $l \sim +32°$, $-32°$, $-52°$ and $-75°$ (the last one only in the uniform density case).

that of the central peak. Results for the old population distributions of Fig. 4.2 appear in Fig. 4.4. No features at $l = \pm 30°$ are obtained in this case, but there is a similarity with the young population: in both cases the importance of the central peak is quite uncertain, depending on the bulge contibution (for "old" objects) or on the SFR in the inner Galaxy (for "young" objects). In view of such results, obtained by several authors in the 80ies [86,120,31,114,66,67] it was argued [115] that, contrary to initial expectations, longitude profiles with axisymmetric distributions cannot help to discriminate between an old and a young population; and latitude profiles are not of much help either, in view of the previous discussion. The situation becomes even more confused if the possibility of metallicity dependent yields is considered [115].

In fact, it seems that the only possibility to discriminate between the two populations is through the detection (or the absence) of asymmetric features in the longitude profile, as suggested a few years ago [115,127]. Such features are expected in the case of the young population, in the direction of the tangents to the spiral arms of the Galaxy. Unfortunately, our knowledge of the spiral structure of the Milky Way is still very poor and even the number of the spiral arms is under debate. Preliminary works adopted, for illustration purposes, a two-arm logarithmic spiral pattern and showed clearly that the *generic feature* of such distributions is an asymmetric longitude profile with several superimposed "spikes" on it [115,116]. In a subsequent work [117,118] a more "realistic" four-arm spiral pattern was adopted, based on observations of HII regions and pulsar dispersion measurements [60,152] (Fig. 4.5). The results, corresponding to the three distributions of Fig. 4.1 appear in Fig. 4.6. The

spiral arms appear clearly at $l \sim 30°$, $-30°$, $-50°$ and $-75°$; notice that the $l = \pm 30°$ directions correspond to the molecular ring. The arm/interarm density contrast is one more free parameter in such calculations.

5. The 1.8 MeV sky after CGRO

The launch of the NASA Compton Gamma-Ray Observatory (CGRO) in April 1991 for a mission of 5-10 years [57] is a major step in astronomical measurements of the MeV sky. The OSSE scintillation-detector and the COMPTEL imaging telescope aboard CGRO have the sensitivity to probe the distribution of ^{26}Al with unprecedented accuracy. For the first time, in particular, the COMPTEL all-sky survey, completed in November 1992, provides a complete coverage of the Galaxy.

5.1. COMPTEL instrument characteristics and data analysis

The COMPTEL imaging telescope aboard the CGRO implements the same detection principle as the MPE Compton telescope described in Section 2.4 (for details on the instrument see [134]). An incident photon first Compton scatters in an upper layer of detectors, and is absorbed in a lower layer of detectors with high-Z material. The detector planes are composed of 7 (in the upper layer) and 14 (in the lower layer) cylindrical detector modules of ~28 cm diameter each. The upper detector consists of liquid scintillator tanks filled with NE213A, a scintillation material that allows pulse shape discrimination between events originating from neutron interactions vs. photon and/or electron Compton scatterings; this provides a means to suppress background from atmospheric neutrons at the low-altitude orbit of the CGRO (400 km). The detector thickness of 8.5 cm was chosen to optimize the probability of a single Compton scatter interaction for MeV photons traversing the scintillator. The lower detector plane consists of NaI(Tl) scintillator crystals, chosen to maximize the total absorption probability with a thickness of 7.5 cm. Each detector module is viewed by a set of 8 (upper) and 7 (lower) photomultipliers and achieves a positional resolution of the interaction within the scintillator of better than 2 cm, through the Anger camera principle (whereby the relative amplitudes of the signal in a set of photomultipliers viewing a single scintillation detector are evaluated to yield an estimate for the interaction location within the detector). The total width of the telescope's angular response is ~3.8° (FWHM) at 1.8 MeV, with a telescope energy resolution of 8% (FWHM) at this energy.

Within the ~1 steradian field of view the imaging information recorded per detected photon can be used to reconstruct sky intensity distributions that are compatible with the measured data. This is done by projection of the measurement onto a three-dimensional data space that retains the full imaging parameters of each event: the Compton scatter angle, as calculated from the measured energy deposits in the upper and lower detectors, and two angles describing the direction of the scattered photon from the upper towards the lower detector. In this imaging data space, an idealized instrument response (i.e. a distribution for a large number of measured events [45]) to a point source in the sky would be a cone centered on the direction of the source, with an opening angle of 90°: for a photon scattered at a given angle in the upper detector, the difference between the source direction and the direction of the scattered photon should be this same angle. Blurring of such an idealized response originates from the limitations in detector energy resolution and incomplete absorption of

the measured MeV gamma-rays in the lower detector plane. These effects result in a broadening of the Compton scatter angle measurement.

Those imperfections in the reconstruction of the interaction locations in both detectors lead to an uncertainty in the scattered photon's direction angles, two of the three imaging parameters of the primary measurement. Typically, at 1.8 MeV the COMPTEL angular response width of 1.6° (1 σ) is composed of a contribution from the detector energy response of 1° and a location uncertainty of 1.3°; at lower energies the contribution from the energy measurement dominates, while at higher energies the location uncertainty limits the angular resolution. Reconstruction of images from the event distributions in the COMPTEL data space is indirect. A convolution of assumed sky intensity distributions with the (multi-dimensional) instrumental response function and exposure yields hypothetical distributions of data in this same data space, which are then compared to the actual measurement. An image result is obtained by iteration of the sky intensity model until satisfactory agreement of these hypothetical data and the actual measurement is achieved. Typical source statistics for ^{26}Al emission is $\sim 10^4$ recorded events for a 10^6 sec exposure – populating a data space with typically 10^5 pixels at one degree binning. Naturally, if each pixel in the sky is considered as a free and independent parameter, large families of sky images can be found to be consistent with the measured data. Therefore the image determination uses prior knowledge or additional constraints to select meaningful images.

The *Maximum Entropy* method iterates sky images with slowly increasing level of detail, to constrain over-interpretation of the data in general [146]. In this method, an initial image (in general chosen to be a flat map) is used as a reference in the determination of the image entropy in iterations of the deconvolution process. Successive iterations are obtained by adjustment of the tested sky intensity distribution, where the amount of adjustment in each pixel is determined both from its impact on improving the fit in data space, and its contribution to the image entropy. In early iterations, the weight factors of fit improvement and entropy favour the entropy criterion and thus reveal only image features that are strongly enforced by the data; in late iterations, the entropy constraint is reduced and the fit quality criterion aims at an overall maximum likelihood image. Simulations of typical fluctuations for COMPTEL measurements of the 1.809 MeV line from diffuse emission have been performed to determine the effects of overfitting, and the impact of the choice of the initial map on the sequence of reconstructed images. For the data of the combined Galactic plane observations five such iterations are considered by the COMPTEL team to produce an image that best represents the measurements [74].

For determination of specific parameter values of the 1.809 MeV sky, a *Maximum Likelihood* method is used to test sky model distributions with a small number of free parameters, such as location and intensity of a single point source [42], or the normalization for a 2-dimensional model such as the measured CO distribution [146]. The significance of detection of 1.809 MeV emission is determined through a maximum likelihood fit of a 1.8 MeV point source above the instrumental background. Scanning the point source position over the sky results in a map of likelihood values over the sky. These likelihood values comprise conservative significance estimates for the case of extended diffuse emission as seen from the ^{26}Al sources, due to the assumption of one single point source only. More realistic and astrophysically modelled source distributions are tested on the COMPTEL data also with the Maximum Likelihood fit method, comparing the convolved data from such a source distribution plus an instrumental background model to the actually measured data in the imaging data space. This yields relative ratings for candidate source distributions, only adjusting intensity

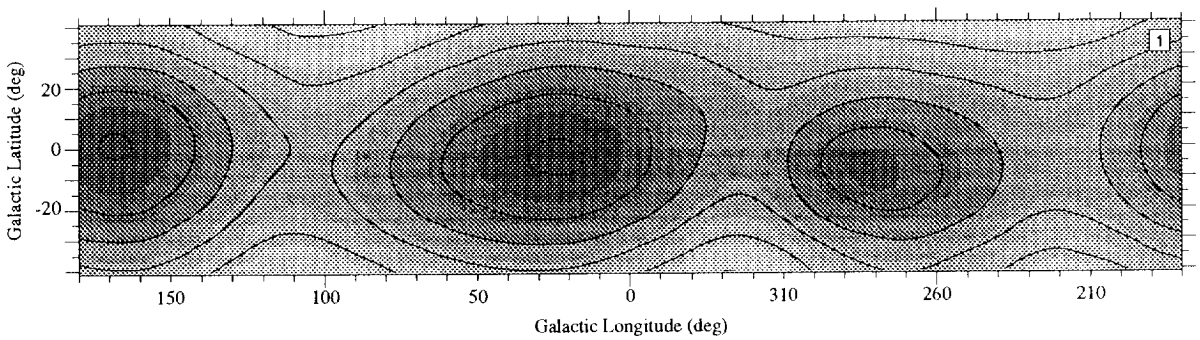

Fig. 5.1. Exposure of the Galaxy in the COMPTEL sky survey measurements [50]. The number of events recorded from a standard point source (10^{-5} ph cm^{-2} s^{-1}) at each position is represented in a linear greyscale.

normalization parameters in the fitting process. Another, more simplified, analysis is performed for plausibility and consistency checks [46], selecting the primary events on their imaging parameters with the effect of a narrower acceptance field on the sky of about 10-12° FWHM specified by selection parameters, where the raw data can be inspected directly for an 1.8 MeV excess. It avoids the above multi-dimensional convolutions and allows scanning the distribution of 1.8 MeV signal excess within the instrument field of view (however at the cost of reduced spatial resolution).

5.2. *COMPTEL galactic plane results*

The COMPTEL team combined all data from more than 25 observation periods that exposed parts of the Galactic plane during the CGRO all-sky survey for 1.8 MeV analysis [50]. The exposure along the plane (Fig. 5.1) is deepest in the first Galactic quadrant and in the anticentre region, and weakest (about three times lower) in the second quadrant (around $l = 120°$). In spite of dominant background signal with instrumental line features at 1.46 MeV and 2.23 MeV a spectrum for the Galactic centre region clearly shows the 1.8 MeV line (Fig. 5.2), after subtraction of a background spectrum as derived from several observations at high galactic latitudes. The 1.8 MeV line feature fits a Gaussian with instrumental width and nominal line position.

For imaging analysis 200 keV wide energy bands are binned into the three-dimensional data space. Maps of likelihoods for scanning an assumed point source through the sky (Fig. 5.3 middle) clearly show that the energy band of the ^{26}Al line (centered at 1.8 MeV) reveals emission from the plane of the Galaxy. The same analysis in adjacent energy bands (centered at 1.6 and 2.0 MeV, respectively) produces irregular structures mainly (see Fig. 5.3 top and bottom) with a low level of significance. The sky image that results from deconvolution of 1.8 MeV band data with the maximum entropy method and a background method that accounts for continuum emission [74] (Fig. 5.4) confirms the pronounced emission at 1.8 MeV along the plane of the Galaxy. The inner Galaxy stands out as dominant feature, but the real novelty of the map is the irregular structure along the plane and the pronounced emission regions far away from the inner Galaxy e.g. in the Carina, Vela, and Cygnus regions. Apparently, the 1.809 MeV emission is not smoothly varying along the plane of the Galaxy, and the source regions are clustered and possibly not confined to a narrow (stellar) disk.

Fig. 5.5 shows the longitudinal emission profile obtained from the maximum entropy image, together with an uncertainty estimate from the bootstrapping method [74]. Bootstrap analysis samples

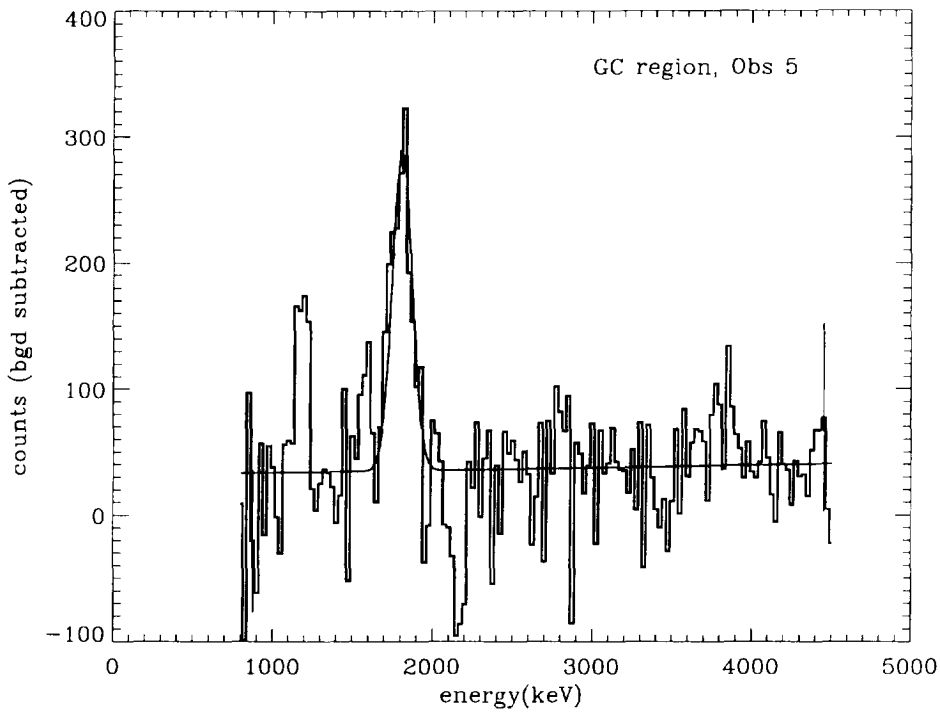

Fig. 5.2. Energy spectrum measured by COMPTEL from the inner Galaxy [50]. The region $\simeq \pm 30°$ around the Galactic centre direction is included, background as estimated from observations at high Galactic latitudes has been subtracted.

the measured data again many times, with subsequently identical imaging analysis on each sample to produce 'bootstrap sample skymaps'; the intensities obtained from these maps scatter around the actual measurement and measure the overall statistical uncertainty in the imaging procedure. It is clear that several structures in the image are of marginal significance by themselves. However the overall irregularity and pronounced emission regions in the inner Galaxy, at longitudes 35°, 2°, 285°, 310° and 345°, and in Vela and Cygnus appear well established.

Sky-images from the models presented in Section 4 and corresponding to the axisymmetric case of Figs. 4.3 and 4.4 are shown in Fig. 5.6 [119,121] for direct comparison with the observations. The small extent in latitude of the flux from young objects is due to the neglect of any diffusion of ^{26}Al away from its sources. In principle, such a diffusion should be taken into account, reducing the usefulness of the latitude extension as a discriminator between old and young sources. More realistic sky images for young objects, taking into account the spiral pattern of the Galaxy are presented in Fig. 5.7. The "patchy" and asymmetric structure of the images is in marked contrast with the smooth and symmetric behaviour of Fig. 5.6. Apparently this young object model corresponds better (albeit not perfectly) to the sky images obtained by the Compton Observatory.

Several of the observed features can be readily identified with known structures: this is the case for features at longitudes 35°, 285° (Carina arm) and 310°, which correspond to directions tangent to the spiral arms. Other features of the 1.8 MeV map, however, have no counterpart in the theoretical maps.

Some model comparisons to the data have already being performed by the COMPTEL team [50].

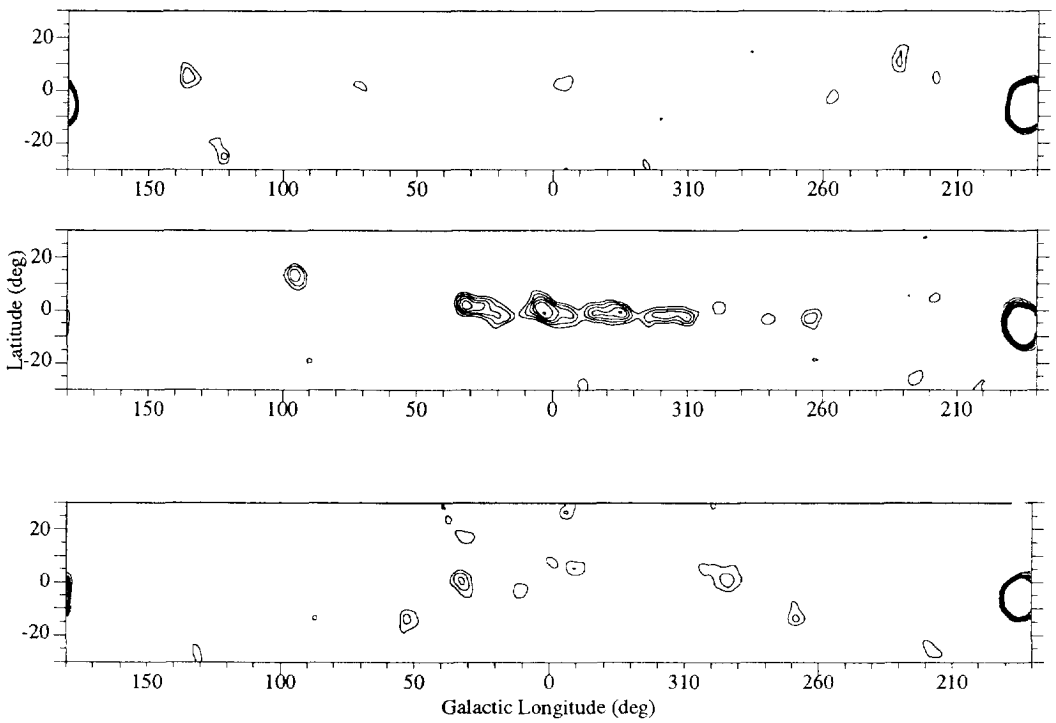

Fig. 5.3. Maps of source likelihoods in COMPTEL data for three energy bands: one band centered on the ^{26}Al gamma-ray line (centre), and two adjacent energy bands above (bottom) and below (top) the ^{26}Al band [50]. Here background was estimated from the measurements themselves using a special filtering technique. Continuum emission is still included in this analysis, as can be seen from the strong Crab feature in the anticentre in all energy bands. The 1.8 MeV energy band clearly shows emission along the plane of the Galaxy, not observed in the adjacent energy bands. The emission is found to be surprisingly irregular along the plane.

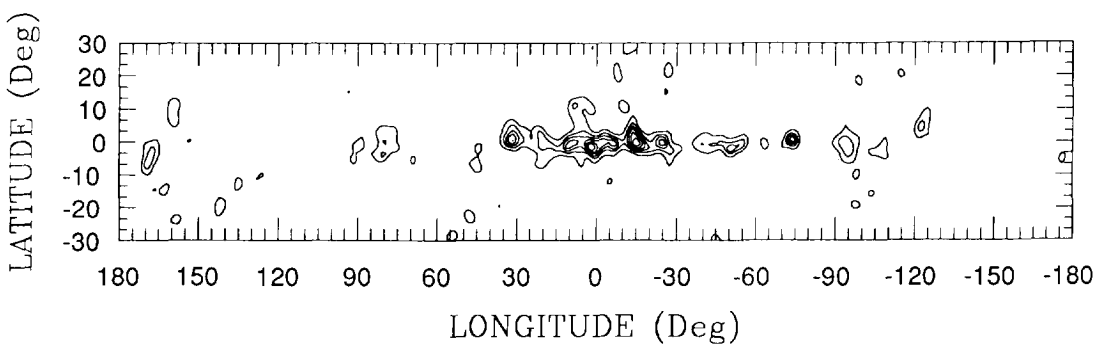

Fig. 5.4. Intensity skymap from the COMPTEL 1.8 MeV data of the sky survey [50]. Here the maximum-entropy technique (see text) has been employed to determine a plausible deconvolved image from the data. The detailed instrumental imaging response has been applied, background was estimated from adjacent energy bands of the same observations, hence include observation-specific background fluctuations as well as effectively a subtraction of continuum emission. The irregular structure (Fig. 5.3) is confirmed, a global preference of emission from the fourth Galactic quadrant is observed.

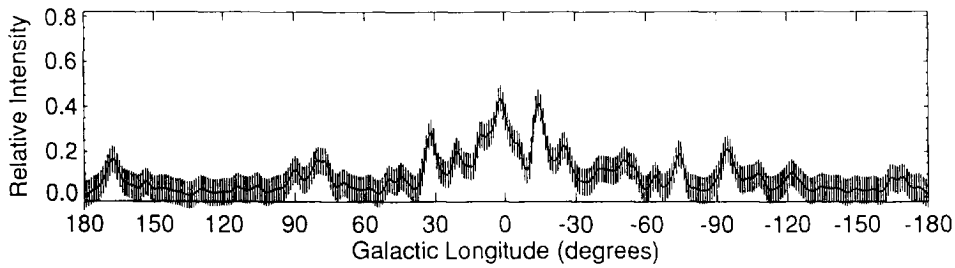

Fig. 5.5. Projection of the COMPTEL image (Fig. 5.4) along the Galactic plane, obtained from integration in a latitude range of $\pm 5^{\circ}$. The remarkable emission from outer regions towards the directions of Carina, Vela, Cygnus, and the anticentre is clearly visible.

First, symmetric distributions corresponding to the galactic nova population (i.e an exponential disk with or without a bulge contribution) were compared to the data. It was found that the introduction of the bulge did not improve the fit, thus ruling out an important contribution from that component of the Galaxy (characterising, as discussed in Section 4, low mass AGB stars and C-O novae). The flux from the inner Galaxy (i.e from $l < 30^{\circ}$) and the ^{26}Al mass coresponding to the exponential ^{26}Al distribution are $F \sim 3 \times 10^{-4}$ cm^{-2} s^{-1} and $M_{26} \sim 3\ M_{\odot}$, respectively, i.e. similar to the original HEAO-3 values. Secondly, COMPTEL data were directly compared to the CO emission profile as a function of the galactic longitude (Fig. 5.8 from [37]), which is a tracer of molecular gas and, presumably, massive star forming regions. [It is on the basis of that longitudinal profile, azimuthally averaged, that the galactocentric H_2 distribution of Fig. 4.1 is derived]. Notice, however, that not all features of the CO profile correspond to the two-dimensional representation of the spiral structure features in the Taylor and Cordes [152] map (Fig. 4.5). It is found that the CO profile gives no better fit to the COMPTEL data than the simple exponential disk, even if an appropriate metallicity dependence for the ^{26}Al yields of SNII and WR stars is taken into account [50] (see Sections 3.3 and 3.4). This, somewhat surprising, result is probably due to the fact that the improvements to the fit (w.r.t. the exponential disk case) brought by features common in the two maps, are cancelled by features that are not common. The derived flux from the inner Galaxy and the corresponding ^{26}Al mass are not very different from the case of the exponential disk – in all cases the COMPTEL team derives $\simeq 3 \times 10^{-4}$ ph cm^{-2} s^{-1} rad^{-1} and $\simeq 3\ M_{\odot}$ of ^{26}Al.

5.3. *Inferences from the COMPTEL results*

The first conclusion that can be drawn from the results of COMPTEL is that the irregular appearance of the 1.8 MeV emission most probably excludes novae and low mass AGB stars as major sources of galactic ^{26}Al. The low individual yield of each of these sources (Sections 4.1 and 4.2) requires a very large number of them to explain the observed flux and, consequently, a smooth flux distribution is expected; there is no way to justify the clustering of such sources to the degree reflected in the COMPTEL image. (Notice also that the central bulge of the Galaxy is not seen as a particularly outstanding 1.8 MeV source.) This leaves SNII, WR and massive AGB stars as possible major contributors, with possible low level contribution from other source types.

The second point is that at least three out of the eight "hotspots" in the COMPTEL data can be readily identified with directions tangent to the spiral arms. This can be hardly considered as

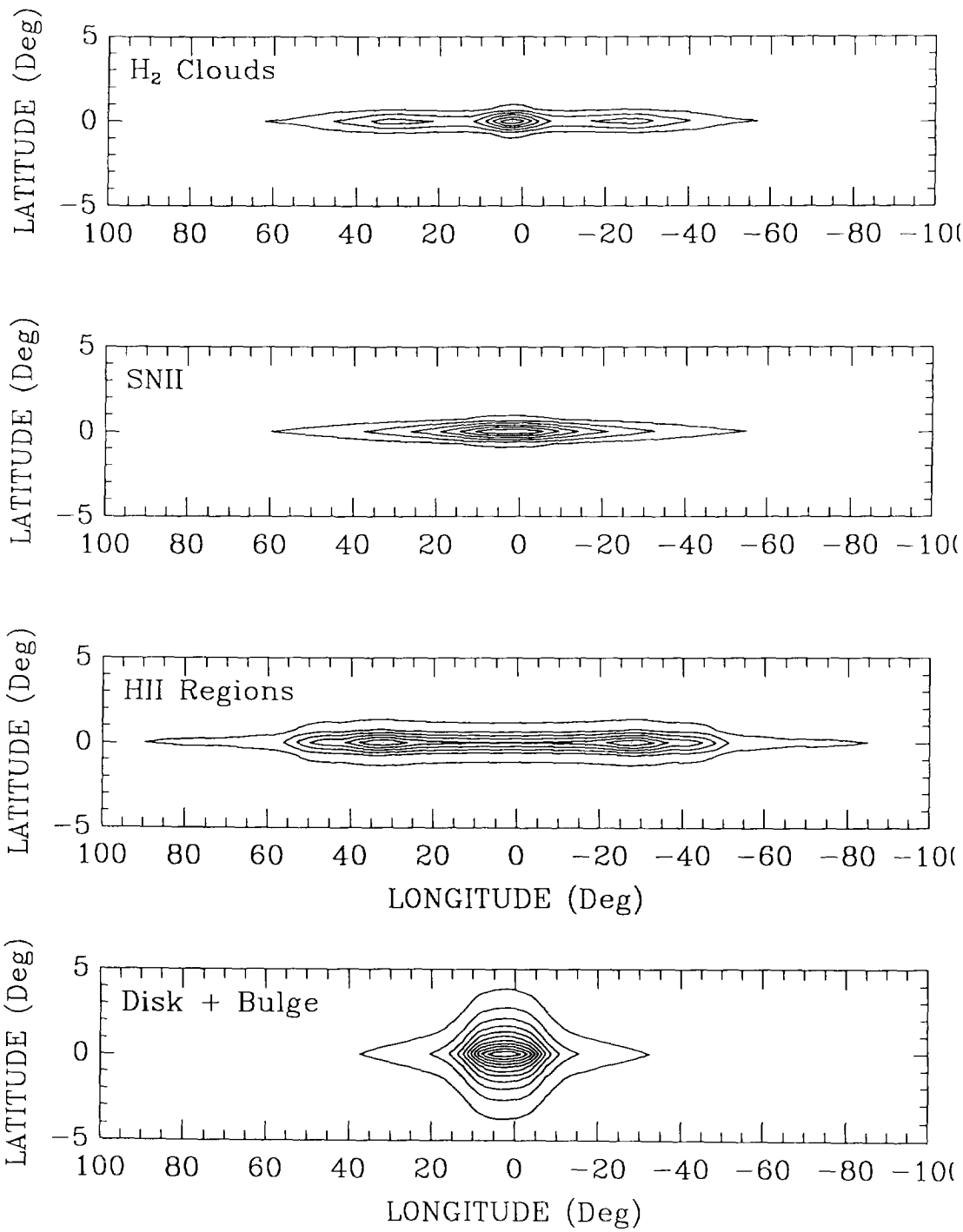

Fig. 5.6. Sky images corresponding to the symetric flux profiles of the source tracers discussed in Section 4, Figs. 4.3 and 4.4. The distributions of young objects (H_2 clouds, SNII and HII regions) have a scale height $h = 80$ pc. The distribution of old objects (disk+bulge) has a scale height $h = 300$ pc and is more extended in latitude; the contribution of the bulge is quite prominent. Notice, however, that ^{26}Al from young objects could diffuse away from its sources, extending the coresponding emissivity in latitude (see text). Iso-contours are at 15% levels from the maximum in the first three cases and at 10% levels in the last one.

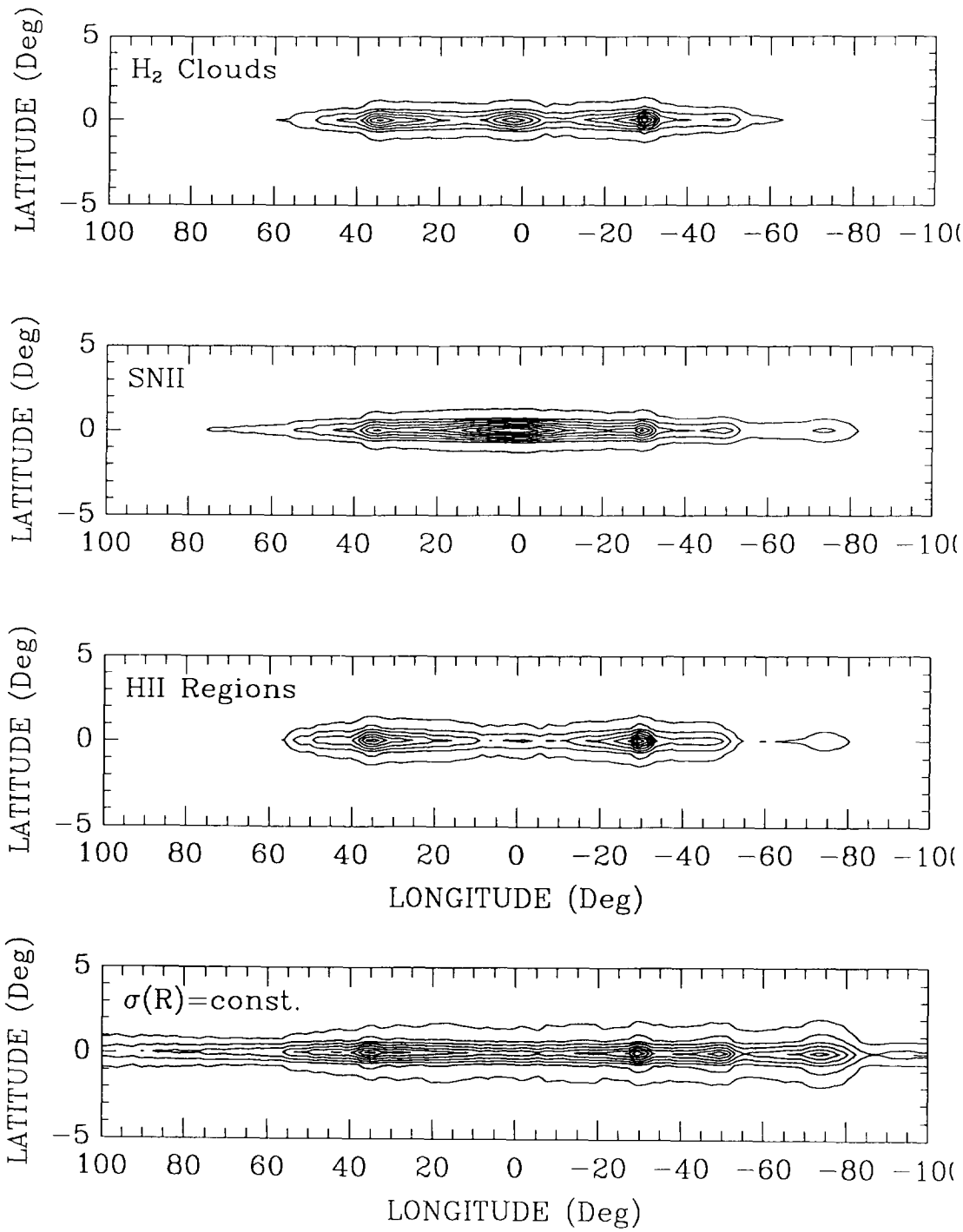

Fig. 5.7. Sky images corresponding to the asymmetric flux profiles of Fig. 4.6, taking into account spiral structure. All distributions have a scale height $h = 80$ pc. Iso-contours are at 10% levels.

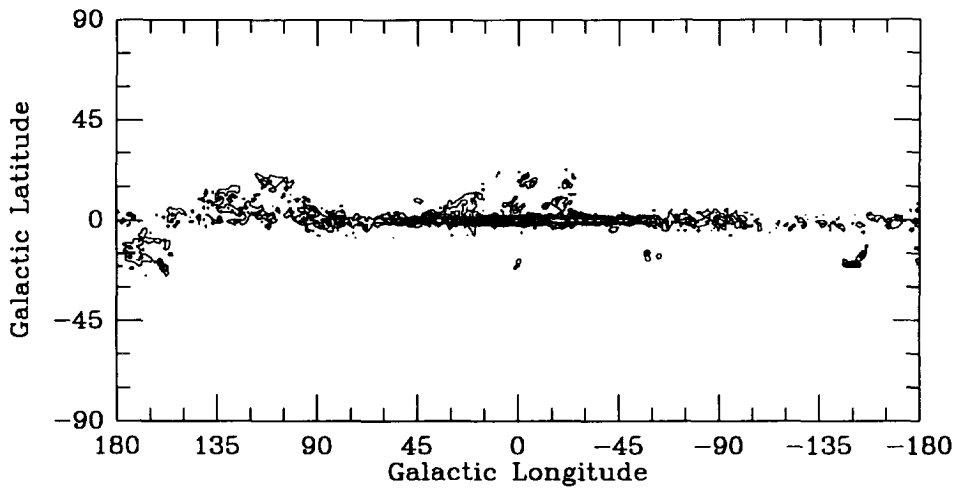

Fig. 5.8. Model for the Galactic distribution of molecular gas, as based on CO measurements [37]. Molecular gas can be assumed to trace formation of massive stars (see text). This distribution has been used a.o. in the COMPTEL analysis.

a coincidence, since it has been anticipated by theory [115]. It is one of the major COMPTEL results, since for the first time 1.8 MeV sources can be identified with (most probable) sites of star formation; it will obviously contribute to a better understanding of their nucleosynthetic activity in the past million of years.

The other four hotspots, however, do not fit in the spiral image of Fig. 4.8 and this is, perhaps, the most interesting of the new COMPTEL results concerning the 1.8 MeV emission. Indeed, it can be reasonably argued [49] that the observed image suggests a two-component origin for the 1.8 MeV emission, i.e. a "global" component following the spiral pattern of the Galaxy, on which are superimposed several localised regions of intense activity. Those localised regions could be nearby individual sources, like the Vela supernova remnant (see next Section), but also regions of enhanced massive star formation somewhat outside the spiral pattern. Such "deviations" from the global nucleosynthetic activity of the Galaxy are conceivable, and in fact there are examples suggested by observations in other spectral regimes: for instance, the Galactic centre vicinity clearly presents a dynamical configuration which is unstable and is most likely determined by unusual recent activity; the Sgr A East supernova remnant can be understood as the result of ~40 supernovae in the GC vicinity within the last few 10^5 years [103]. In any case, the detection (and eventual identification) of those hotspots offers a most valuable tool, allowing to probe the recent nucleosynthetic activity of the Galaxy in the past 10^6 years.

The central hot spot of 1.8 MeV emission derived by the COMPTEL analysis appears located slightly off the Galactic centre ($l = 2.0°$, $b = -1.5°$) at the 2σ confidence level. If confirmed, this may be an important discovery. First, this again argues against classical novae ot low mass AGB stars dominating the ^{26}Al production, since it requires a degree of clustering that is quite improbable for such sources; moreover, the bulge component of a nova distribution would be symmetric, most likely. Therefore an origin from massive stars is more plausible for this Galactic centre feature. Notice that the CO measurements from the inner Galaxy peak actually towards the same direction away from the Galactic centre at $l = 1.2°$ [37], indicating that the molecular mass density is highest in this

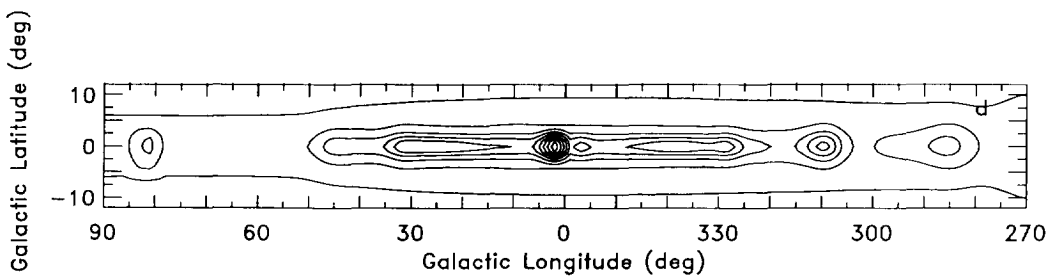

Fig. 5.9. Empirical model of Galactic distribution of ^{26}Al sources, based on H_{II} region measurements, free electron distribution as deduced from pulsar dispersion measurements, with tentative addition of an asymmetric Galactic centre region bar component [25]. This presents an example of a multi-component ^{26}Al source model, mostly based on plausible tracer data, yet adding new components as suggested by the ^{26}Al measurement. Possibly, ^{26}Al observations are better tracers of the massive stars in the Galaxy, due to the 10^6 yr sampling time, larger than the characteristic times for massive star signatures in radio and X-ray data.

direction. On the other hand, recent COBE near-infrared maps suggest that the spiral structure of the Galaxy only extends inward up to a radius of about 2.5 kpc; further inward the Lindblad resonances are not visible in warm dust emission. A bar structure extending up to 5 kpc is suggested by the data, with the near end of the bar pointing towards the Sun into the first quadrant. Such a structure could result in higher measured flux from the near side of the bar, resulting in an asymmetric central feature, provided that the ^{26}Al production is distributed homogeneously along this structure (e.g. [63]). However the increased path length in the far side of the bar may counterbalance for such a homogeneously active bar region, as pointed out by [25]. In that Reference it is argued that the observed asymmetry of the molecular gas distribution within the inner few degrees of the Galaxy (see review by [58]) suggests some asymmetric star formation activity within the bar (at least during its last rotation period of $\sim 10^8$ years) as a more plausible explanation for the asymmetry in the COMPTEL 1.809 MeV image (see Fig. 5.9).

It is plausible also that the large loop structures that are apparent in radio and X-ray maps of the Galaxy are residuals of past and preferentially nearby supernova activity, hence related to ^{26}Al production at some (low) level. Del Rio et al. [43] discuss possible contributions from these loops (Fig. 5.10). Loop I, the closest feature, brings to mind the proposal [12] of local and hence almost omnidirectional origin of the 1.809 MeV emission. In fact some of the apparent global asymmetry observed on the Galactic scale in the COMPTEL map could possibly originate from an underlying Loop I contribution.

Looking at the 1.809 MeV emission regions that COMPTEL discovered far from the inner Galaxy, the direction of Cygnus presents a view to the local spiral arm out to 4 kpc distance, with a variety of candidate ^{26}Al sources along the line-of-sight. In particular, the Cygnus Superbubble, a ring of soft X-ray emission with 13° diameter centered at the Cyg OB2 stellar association (at $l = 80°$) is a remarkable object aligned with the observed COMPTEL 1.8 MeV feature. The Cygnus Superbubble is speculated to originate from steady energy input from 30-100 supernovae over the last few million years [19], making it a promising candidate for ^{26}Al production. Its contribution to apparent 1.809 MeV emission was estimated [129] as 1×10^{-6} ph cm^{-2} s^{-1}. Also, about 20 identified Wolf-Rayet stars are located in this direction, significantly contributing to the observed emission at a flux level of approximately 1-4 $\times$ 10^{-5} ph cm^{-2} s^{-1} [129]. It is intriguing, however, that the observed emission

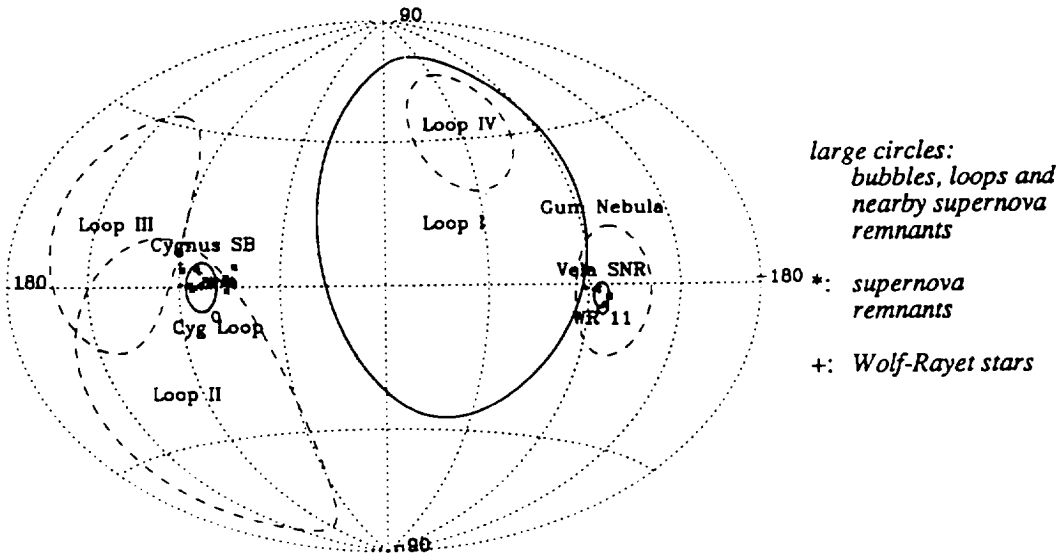

Fig. 5.10. Structures in the sky from loops that may be attributed to recent supernova activity [43]. These loop structures are clearly identified in radio and X-ray measurements, from their synchrotron and thermal emission, respectively. If supernovae and massive star winds created these loops, and these objects are among the dominating ^{26}Al sources, extended 1.809 MeV emission is expected from these regions, although at levels below current instruments' sensitivity.

does not obviously correlate with the positions of these Wolf Rayet stars. The Cygnus Loop itself, the brightest radio and X-ray source and a known supernova remnant at 700 pc distance, is not an apparent source in the COMPTEL image, as expected from the theoretical ^{26}Al yields of Section 3.2.2.

5.4. The Vela region

The COMPTEL discovery of a 1.809 MeV signal from the Vela region [52,47,49] highlights an extraordinary opportunity for the study of ^{26}Al sources: the study of individual source objects. The direction of Vela at Galactic longitude ~260°-265° is found between spiral arm features of the Galaxy (the Carina arm at $l \sim 275°$ and the possible outer part of the Perseus arm around $l = 240°$), towards a sparsely populated region with a few prominent nearby objects. The Vela pulsar at $l = 263.9°$ and $b = -3.3°$ is the X- and gamma-ray-bright compact remnant of the Vela supernova, with a spindown age estimated to 11500 years. The supernova shell is one of the most prominent features in the X-ray sky, with its extent of about 3.5° radius and its fine structures that have recently been analysed as proof of association of the Vela pulsar and remnant with the supernova event [8].

The feature observed by COMPTEL at 1.8 MeV (Fig. 5.11) is encompassed by the X-ray observed Vela supernova remnant [7,8]. The total 1.809 MeV flux from this feature of 3.6 10^{-5} ph cm^{-2} s^{-1} is comparable to the flux from the Galactic centre hot spot [52]. In a recent work [110] the candidate ^{26}Al sources within the Vela region are studied in detail. It is found that extended contributions from novae or from the Gum nebula are possible with integrated fluxes of ~10^{-5} ph cm^{-2} s^{-1} within the total COMPTEL field of view of 1 sr. Localized candidate sources that can be associated with the

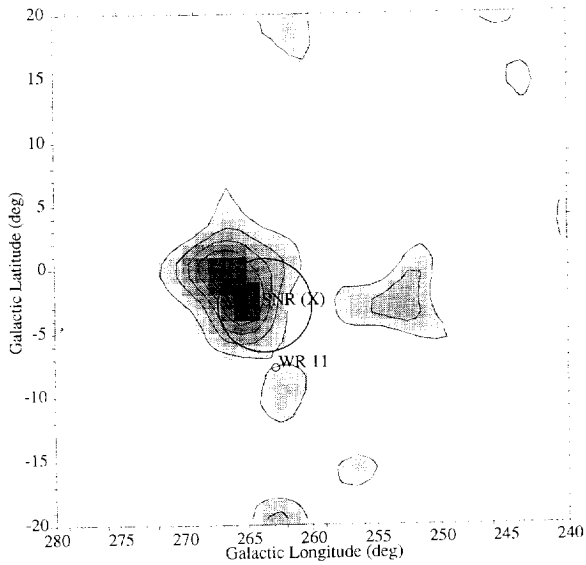

Fig. 5.11. Zoom of the COMPTEL skymap result (Fig. 5.4) in the Vela region [49]. The observed emission feature appears consistent with the Vela supernova remnant shell as observed in X-rays (large circle). The small circle marks the position of the Wolf Rayet star closest to the Sun, probably not significantly contributing to the observed emission. Other candidate source objects are probably negligible [110]. Therefore this region may prove to calibrate ^{26}Al yields from individual source objects.

observed emission feature are the Vela supernova remnant and the Wolf-Rayet / O star binary system γ^2 Velorum.

Fig. 5.12 displays the uncertainty in the ^{26}Al yield of current core collapse supernovae [169,70] as applied to Vela in the context of the COMPTEL measurements [52]. The hatched area indicates how different assumptions about convection and nuclear reaction rates affect the ^{26}Al yield for a 25 $M_\odot$ supernova progenitor, while the solid, dashed, and dotted lines show model calculations for different progenitor masses of 25, 35, and 15 $M_\odot$.

The distance to the Vela pulsar is a subject currently under discussion and refined study. Classical estimates were based on the similarity of supernova shells in the Galaxy, in particular the Cygnus Loop and IC433; their apparent diameters and distance estimates were used [104] to derive a Vela distance of 500 pc. Based on the same grounds but using more recent data on these objects Oberlack et al. [110] evaluate it to 210-230 pc (doted vertical line in Fig. 5.12); they caution, however, that dissimilarities of these remnants may result in substantial systematic errors. Other distance estimates can be derived from the Vela pulsar interstellar scintillation, which yields a very uncertain distance estimate of 120 pc only. Other recent distance estimates are shown in Fig. 5.12 for comparison (hatched bars in the bottom part): Analysis of ROSAT X-ray emission from the Vela pulsar also results in a distance estimate as close as 125-160 pc [11]. On the other hand the supernova shell measurement by ROSAT with its projectile-type structures on the periphery is more consistent with a distance of 400±200 pc [8]. In this estimate, the remnant has been interpreted as spherically inhomogeneously expanding debris, providing the opportunity for purely geometrical determination of the pulsar position at the time of the supernova. Therefore Vela pulsar proper motion measurements, currently underway with adequate precision with VLBI radio telescopes, can be expected to reduce

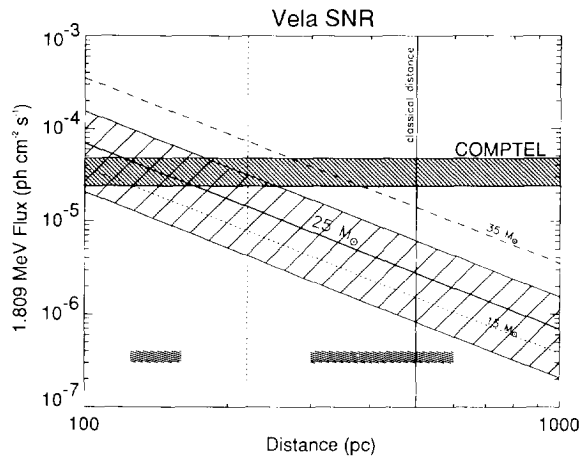

Fig. 5.12. Supernova model ^{26}Al yields for the Vela supernova, for a variety of model parameters. The yields are translated into measured flux at 1.809 MeV, as a function of distance to the Vela supernova. The lines indicate the yield variations obtained from variation of the progenitor mass (15, 25, and 35 $M_\odot$, respectively, from the bottom). The yield varies roughly one order of magnitude for a given progenitor mass, as indicated by the hatched area for the 25 $M_\odot$ case. This uncertainty originates from different assumptions about convective mixing in the burning zone, and from different nuclear reaction rate assumptions. The COMPTEL measured flux range (horizontal hatched area) is compatible with the more optimistic yields, provided that the distance to the Vela supernova is closer than about 300 pc. Current Vela distance estimates (hatched bars in the bottom regime of figure) range from 125 pc (from X-ray measurement interpretation as Vela pulsar polar cap emission [11]) to 600 pc (from various sources, including the most pessimistic supernova remnant age determination from geometrical considerations based on Mach-cone like projectile structures at the outer X-ray circumference of the supernova remnant [8]).

the distance uncertainty; comparison of the 1.809 MeV measurement to the model predictions will provide then new information. Apparently the assignment of the measured excess in the Vela region to the Vela SNR only is plausible only if either distance or nucleosynthesis models (or both) are favourably modified, within their current uncertainties, nevertheless.

The other prominent object within this region is the Wolf-Rayet / O star binary system γ^2 Velorum at $l = 262.8°$ and $b = -7.7°$. It houses the nearest Wolf-Rayet star, called WR11 in van der Hucht's catalogue [163], at an estimated distance of 300-450 pc [162,36]. The Wolf Rayet star's initial mass has been estimated from the mass function of the binary system, both for a Roche-lobe overflow model and for a "luminous blue variable" model for the binary system evolution. Initial masses of 50 and 60 $M_\odot$, respectively, where obtained, placing WR11 into the regime of massive Wolf Rayet stars with a correspondingly promising high yield in ^{26}Al. The effect of the binary companion on the evolution of the Wolf Rayet star and its yield of ^{26}Al is uncertain. Recent nucleosynthesis models for WR11 [15] produced substantially higher ^{26}Al yields than earlier estimates [115,101] used in the analysis of [110]. This is however most likely due to the different stellar models of these calculations, while the presence of the binary companion probably implies reduced rather than enhanced ^{26}Al yields [15]. Still, the predicted yield is probably below the sensitivity of COMPTEL, even for several months of exposure.

In conclusion, it appears that the COMPTEL flux measurement from Vela is difficult to explain if the Vela supernova remnant and/or the WR star γ^2 Vel are assumed at their "canonical" distances of 500 pc and 450 pc, respectively. Favourable assumptions about the distance to Vela and the ^{26}Al

yield of supernovae can bring the predicted flux to the level of COMPTEL sensitivity and explain this intriguing observation (see Fig. 5.12). A minor contribution from WR11 is possible, although the extent of the observed feature in the COMPTEL map towards γ^2 Vel is insignificant and within the noise regime of the measurement. Additional COMPTEL and INTEGRAL observations are needed to clarify the situation. In summary, it appears that the Vela region offers the unique opportunity to study individual ^{26}Al sources and derive constraints on nucleosynthetic yields, free from uncertainties on the spatial distribution of the sources.

5.5. *OSSE results*

The Oriented Scintillation Spectrometer instrument (OSSE) aboard the CGRO consists of four identical large-area NaI(Tl) scintillation detectors (33 cm diameter, 10 cm thickness), with an optically coupled 7.6 cm thick CsI(Na) scintillation crystal at the backside in "phoswich"" configuration. The complete detector system is actively shielded by an annulus of NaI(Tl) scintillation detectors. A tungsten slit collimator defines a nominal field of view of $3.8° \times 11.4°$ (FWHM). Each detector unit has its own single-axis positioning system with 192° rotation range. The typical data recording mode employed for 1.809 MeV studies operates two pairs of detectors in parallel, toggling between "source" and "background" pointings in two-minute intervals. The background pointings typically are located 12° off the source direction towards the long side of the instrument field of view. For Galactic plane observations, the "position angle" (defined as the angle between the long axis of the aperture and the Galactic pole) was chosen in the vicinity of 90°, such as to have background pointings out of the plane. Owing to the 511 keV study from the Galaxy as primary science objective, the offset for the background pointings in most observations is somewhat small for 1.809 MeV background definition. The effective field of view at 1.809 MeV is somewhat larger than the purely geometrically defined $3.8 \times 11.4°$ wide collmator opening, with a slower falloff towards large incidence angles and a remaining plateau from residual shield leakage, such that the background pointings still expose the source field partly, reducing the net celestial signal.

Data analysis first subtracts the average of the adjacent background spectra for each 2-minute source spectrum and for each of the four detector units. The resulting source spectra are accumulated per detector for each observation period. Folding an assumed celestial source distribution model through the instrumental response and exposure for each detector yields a comparison of predicted flux versus measured flux per observation. The analysis of the OSSE data shows the 1.809 MeV line standing out at the 6σ significance level [87]. As in the case of the COMPTEL data, the OSSE team does not find a preference for any of the 'classical' candidate source distributions. However, neither the COMPTEL emission map (Fig. 5.5) seems to fit the OSSE observations, at least in a preliminary analysis [87]. Yet, for all source models a positive correlation of predicted and observed fluxes is found, for a set of 205 observations. The OSSE flux value determined for the Galactic centre observation (assumed to be a point source) is considerably lower than the measurements prior to CGRO but in agreement with the COMPTEL image results.

5.6. *Observational summary*

Gamma-ray emission from radioactive ^{26}Al is definitively detected in our Galaxy, at a level which is clearly above the nominal sensitivity of several γ-ray experiments in the last 15 years. The launch

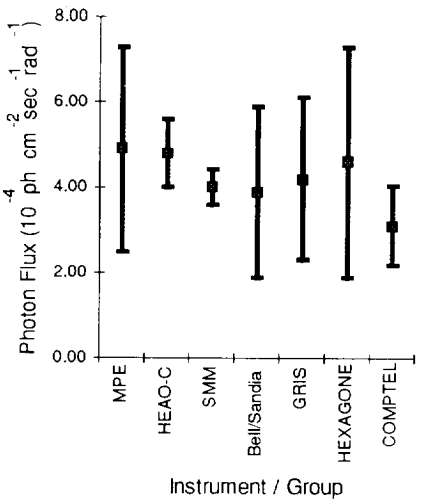

Fig. 5.13. Comparisons of flux values for all instruments (with their uncertainties) for the inner Galaxy [50]. The values are not strictly comparable, as their determination method varies between instruments; mostly (for the non-imaging instruments), assumed source distribution models have been normalized towards the Galactic centre direction, and then integrated within the central radian to derive a flux value. Although no highly significant discrepancies are observed, the variations may indicate trends: large field-of-view instruments without imaging capability may include more 1.809 MeV emission in their data from regions far outside the inner Galaxy due to residual shield leakage, or else their assumed distribution model differences to the COMPTEL 1.8 MeV image may cause their normalization to include several bright regions in the inner Galaxy, rather than just the immediate centre vicinity. In both cases the measured fluxes as converted to these units (i.e. per rad) would be systematically high. Future imaging / small field-of-view observations are needed to clarify this issue.

of CGRO considerably improved our understanding of this cosmic radioactivity. Still, after several years of observations many issues remain yet unsettled.

The ^{26}Al radioactivity is clearly a Galactic phenomenon, since the COMPTEL images show that the 1.809 MeV emission extends along the Galactic plane. Neither a point source at the Galactic centre (often used for the interpretation of measurements in the 80ies with large field-of-view detectors) nor a nearby local bubble of ^{26}Al (as suggested by [12]), are favoured by the COMPTEL results. The COMPTEL data are relatively well fit with a model of an exponential disk galaxy. However, the irregularity of the derived 1.809 MeV image raises doubts as to the adequacy of this fit: even if the uncertainties due to the nonlinear imaging method and the proximity of the instrument's sensitivity threshold are considered, it is clearly established that the 1.8 MeV sky is asymmetric with respect to the Galactic centre direction. This asymmetry raises doubts on analysis methods whereby measured flux is converted into a Galactic amount of ^{26}Al through radially symmetric Galactic distribution models.

The irregularity of the observed images and the lack of information on the distances of the emitting regions do not allow to draw better estimates as to the Galactic amount of ^{26}Al. The total measured flux from the inner Galaxy has been used over the years as a reference to compare results from different instruments. [We note once more that referring to an equivalent point source flux from the Galactic centre is misleading]. Fig. 5.13 compares the measured 1.809 MeV fluxes for the central radian of the Galaxy. Although all data are compatible within their quoted uncertainties, it is seen that the CGRO results fall on the low end of the range of values. This may be attributed to instrumental

reasons, i.e. some 1.809 MeV emission from the outer Galaxy leaking through the shield detectors that define the aperture of the instruments.

The irregularity seen in the COMPTEL intensity map along the galactic plane suggests that at least some of the 1.8 MeV emission is due to sources lying outside the main star locations in the Galaxy [47] (i.e. the exponential disk for low mass stars and the spiral pattern for more massive ones). The distances to these "peculiar" sources is unknown. It is possible that only the closest of them appear above the COMPTEL sensitivity limit, while more distant and fainter ones dissappear in the instrument's noise. Therefore it is is misleading to assign to such peculiar sources an average distance of 8-10 kpc in model fits evaluating the mass of galactic ^{26}Al. Among the five prominent 1.8 MeV sources found in the central radian of the COMPTEL map, three may be associated with tangents to spiral arms and one with the galactic centre region. The flux in the remaining two hotspots amounts to ~10-30% of the total 1.8 MeV flux from the inner Galaxy (depending on the assumed level of large scale flux under those hotspots, which is probably below the COMPTEL sensitivity limit). Assuming that those two peculiar sources are nearby (i.e. that their flux is due to a negligible amount of ^{26}Al) one finds the mass of galactic ^{26}Al reduced by as much as ~30%; in other terms, the amount of ^{26}Al in the Galaxy is closer to 1.5-2 $M_\odot$ in that case. On the contrary, in the opposite (and more improbable) case of remote "peculiar" hotspots, the mass of galactic ^{26}Al is correspondingly increased.

6. Summary and outlook

The epochal detection of a galactic γ-ray line at 1.8 MeV, due to the decay of ^{26}Al, boosted theoretical as well as experimental and observational work on the origin of the ~1.5-3 $M_\odot$ of ^{26}Al currently present in the interstellar medium. Now, after more than ten years of intense theoretical and experimental investigation, some light is shed on the origin of this radioactive nucleus. It is true that from the theoretical point of view the situation has not changed by much since the previous major review on the subject: indeed, "... deciding among the sources of ^{26}Al is more difficult than ever ..." [31]. Theoretical models of all the candidate sites (novae, AGB stars, WR stars and SNII) suffer from considerable uncertainties, that allow no preference for one of them. But the results of the COMPTEL telescope aboard CGRO gave a new impetus to the field since they allowed to eliminate: (i) a unique point source in the Galactic centre and/or a nearby local bubble in that direction, the detected flux being diffuse in the galactic plane; (ii) an important contribution from the galactic bulge, signature of a very old population, and (iii) any class of sources involving a large number of sites with low individual yields (like novae or low mass AGB stars), since a smooth flux distribution is expected in that case.

Still, several ^{26}Al sources maintain their candidacy after the COMPTEL results: massive AGB stars (with mass 5-9 $M_\odot$), type II supernovae and Wolf-Rayet stars. At present there is no observational test to discriminate between those sources, since their spatial signatures are expected to be rather similar to each other. In fact, all of them may contribute significantly to the ^{26}Al emission, depending on their galactic location. Indeed, WR stars are expected to be more numerous and to have enhanced ^{26}Al yields in the inner Galaxy, because of the larger metallicity in that region. Thus, the 1.8 MeV emission of the inner Galaxy (a few 10^{-5} cm^{-2} s^{-1} at $l < 2°$) may be dominated by the ^{26}Al production of ~1000 WR stars. Because of this metallicity dependence, the WR emissivity of the

outer Galaxy is expected to be quite weak, unable to account for the detected flux. On the other hand, the dependence of the ^{26}Al yield of SNII on metallicity is expected to be opposite to that of WR (see Sec. 3.2). Thus SNII may dominate the 1.8 MeV emission outside 20° of longitude (see [115] for a discussion of the 1.8 MeV distribution with metallicity dependent yields). Finally, nothing can be said at present for the role of massive AGB stars, in view of their very uncertain yields.

The irregular 1.8 MeV emission detected by COMPTEL along the galactic plane reveals, better than any other tracer, the sites of current nucleosynthetic activity in the Galaxy. A complete identification with other known distributions does not seem plausible, at present. However, a very tempting identification can already be made of several 1.8 MeV "hotspots" with tangents to the spiral arms. Indeed, three out of the eight COMPTEL hotspots correspond to the spiral arm tangents at galactic longitude $l \sim 32°$, $-50°$ and $-74°$, respectively. Similar features appear not only on HII maps (used to derive the galactic spiral pattern), but also on longitude profiles of CO distribution, high energy γ-ray emission (>100 MeV) detected by SAS-2 and COS-B, as well as Far InfraRed (FIR) emission, detected by IRAS (see [150] for a recent review). All those distributions are thought to be tracers of massive star formation sites in the Galaxy. Their similarity to the COMPTEL map suggests again a massive star origin of the interstellar ^{26}Al. Notice that the central peak in all those distributions appears to be off the galactic centre direction, by ~2° to the left. The interpretation of this feature in terms of asymetric activity in a central galactic bar needs further investigation; in any case, it holds important clues as to the stellar activity in the innermost regions of the Galaxy.

Two of the remaining COMPTEL hot spots, at $l \sim 80°$ and $-90°$ are certainly not related to spiral features. The former can be identified with the Cygnus region, presumably created by WR stars and the activity of several tens of supernovae in the past million of years, which may well account for the detected 1.8 MeV flux of $\sim 2 \times 10^{-5}$ cm^{-2} s^{-1} from that region. The feature at $l \sim -90°$, which still waits confirmation by an independent measurement, coincides with the Vela region where only two sources have been identified: the Vela supernova and γ^2 Vel, the closest WR star. Assuming that one of them is indeed at the origin of the detected flux, the COMPTEL measurement allows to have the first direct estimate of its individual ^{26}Al yield, once the (still uncertain) distance is determined with accuracy. Finally, the hotspots at $l \sim -14°$ and $-25°$ do not correspond to the spiral pattern revealed by HII regions, but they seem to have counterparts in both the >100 MeV γ-ray and FIR profiles. It is quite plausible that the spiral pattern of the inner Galaxy is poorly revealed by the HII map and that 1.8 MeV, FIR and >100 MeV γ-rays give a more accurate description. Alternatively, it may be that in the inner Galaxy important stellar activity takes place outside spiral arms, which do not probably extend to such small galactocentric distances.

The above conclusions result from a preliminary analysis of the COMPTEL data. More refined work is currently in progress, involving the convolution of theoretical sky maps (such as shown in Fig. 5.7) with the COMPTEL response function and a systematic comparison to observations through statistical tests [75]. This study will allow to probe more accurately the amount of ^{26}Al in various galactic locations and, perhaps, the scale height of the underlying source population; combined to more extensive investigations of the individual hot-spots it will provide the most accurate mapping of current nucleosynthetic activity in the Galaxy.

Further progress is expected from future missions with instruments of higher intrinsic spatial and energy resolution. This will allow more accurate measurements of the energy of the detected ^{26}Al line in various directions, providing information on the distances of the emitting regions: indeed, because of galactic rotation, the centroid of the 1.8 MeV line is expected to be displaced towards lower

or higher energies (depending on galactic location) by several tenths of a keV [145], a difference that next generation instruments should be able to measure. Also, a more precise localisation of the various hotspots already detected by COMPTEL will offer better chances of identification with counterparts observed in other wavelengths. The HIREGS balloon-borne instrument, launched in January 1995 for a two-week flight over Antarctica, exemplifies a new attempt to measure the line position and shape with adequate significance, more than 15 years after the HEAO-C pioneering and still best measurement of this type. It carries twelve state-of-the-art Ge detectors with 3 keV energy resolution and an effective area of $\sim$ 160 cm^2, but has no imaging capabilities within its 3.5° $\times$ 24° field-of-view. Future satellite missions with similar detectors but better angular resolution (due to the "coded mask" technique) will have greater sensitivity, with several years of observing time above the Earth atmosphere. Scheduled to fly the first year of the next century, ESA's INTEGRAL will have a sensitivity of $\sim 5 \times 10^{-6}$ cm^{-2} s^{-1} at 1.8 MeV and a spatial resolution of $\sim$ 12 arcmin. These capacities will allow it to perform a much more detailed mapping of the Galaxy in the light of 1.8 MeV photons, to measure the scale height of the underlying source distribution and, perhaps, the distances to the ^{26}Al hotspots. It is also expected to detect diffuse ^{60}Fe γ-ray lines at 1.2 and 1.3 MeV and give some hints as to their distribution in the Galaxy; if it is similar to the one of ^{26}Al, WR stars will have to be exluded as major ^{26}Al sources, since they are not expected to produce detectable ^{60}Fe amounts (see Sec. 3.2.2). Thus one may reasonably hope that, early in the next century, the "mystery" of interstellar ^{26}Al will have been solved, providing at the same time the most accurate information on current large scale nucleosynthetic activity in our Galaxy.

Acknowledgements

We gratefully acknowledge helpful discussions and criticism from: M. Arnould, A. Coc, J. Knödlseder, and R. Mochkovitch. We are also grateful to S. Woosley for many useful discussions and for the opportunity to use his ^{26}Al yields of massive stars, prior to publication.

References

[1] Anders E. and Zinner E. 1993, *Meteoritics*, **28**, 490
[2] Arnett D.W. 1969, *Ap. J.*, **157**, 1369
[3] Arnett D.W. 1977, *Ann. N.Y. Acad. Sci.*, **302**, 90
[4] Arnett D.W. 1994, *Ap. J.*, **427**, 932
[5] Arnett D.W., Wefel J.P. 1978, *Ap. J.*, **224**, L139
[6] Arnould M., Norgaard H., Thielemann F.-K., Hillebrandt W. 1980, *Ap. J.*, **237**, 931
[7] Aschenbach B. 1993, *Adv.Sp.Res.*, **13**, 12, 45-55
[8] Aschenbach B., Egger R., and Trümper J. 1995, *Nature*, **373**, 587
[9] Bartunov O., Makarova J., Tsvetkov D. 1992, *A.A.*, **264**, 428
[10] Bazan G., Brown L.E., Clayton D.D., El Eid M.F., Hartmann D.H., and Truran J.W. 1993, in *Compton Gamma-Ray Observatory*, eds. M. Friedlander, N. Gehrels and D. Macomb (AIP, New York) p. 47
[11] Becker W. 1995, Ph. Thesis, MPE Garching, Germany
[12] Blake J. and Dearborn D. 1989, *Ap. J.*, **338**, L17
[13] Bloemen H. et al. 1994, *A.A.*, **281**, L5
[14] Bronfmann L. 1992, in *The Center, Bulge and Disk of the Milky Way*, ed. L. Blitz (Kluwer, Netherlands) p. 131

[15] Braun H., and Langer N. 1994, in IAU Symp. 163, *WR stars: binaries, colliding winds, evolution*, eds. K. van der Hucht and P.M. Williams, in press
[16] Burbidge M., Burbidge G., Fowler W. and Hoyle F. 1957, *Rev. Mod. Phys.*, **29**, 547
[17] Burkert A., Truran J., and Hensler G. 1992, *Ap. J.*, **391**, 651
[18] Cameron A.G.W. 1984, *Icarus*, **60**, 416
[19] Cash W., et al. 1980, *Ap. J.*, **238**, L71
[20] Cassé M. 1986, *Adv. Sp. Res.*, **6**, 139
[21] Cassé M., Prantzos N. 1986, in *Nucleosynthesis and its implications on Nuclear and Particle Physics*, eds. J. Audouze and N. Mathieu, (Reidel, Dordrecht) p. 339
[22] Cassé M., Prantzos N. 1993, in *Origin and Evolution of the Elements*, eds. N. Prantzos, E. Vangioni-Flam and M. Cassé (Cambridge, CUP), p. 349
[23] Caughlan G.R., Fowler W.A. 1988, *At. Data Nucl. Data Tables*, **40**, 238
[24] Champagne A.E., Brown B.A., Sherr R. 1993, *Nucl. Phys.*, **A556**, 123
[25] Chen W., Gehrels N. and Diehl R. 1995, *ApJ*, **440**, L57
[26] Chiosi C., Maeder A. 1986, *A.R.A.A.*, **24**, 329
[27] Clayton D.D. 1984, *Ap. J.*, **280**, 144
[28] Clayton D.D. 1975, *Nature*, **257**, 36
[29] Clayton D.D. 1994, *Nature*, **368**, 222
[30] Clayton D.D. and Craddock W. 1965, *Ap. J.*, **142**, 189
[31] Clayton D.D., Leising M.D. 1987 *Phys. Rep.*, **144**, 1
[32] Clayton D.D., Colgate S. and Fishman G., 1969, *Ap. J.*, **155**, 755
[33] Clayton D.D., Cox D.P. and Michel F.C. 1986, in *The Galaxy and the Solar System*, eds. R. Smoluchowski, J. Bahcall and M. Mathews (The Universtity of Arizona Press), p. 129
[34] Clayton D.D., Hartmann D.H, Leising M.D. 1993, *Ap. J.*, **415**, L25
[35] Coc A., Mochkovitch R., Oberto Y., Thibaud J.P., Vangioni-Flam E. 1995, *A.A.*, **299**, 479
[36] Conti P.S. and Vacca W.D. 1990, *Astr.J.*, **100**, 2, 431
[37] Dame T.M., Ungerechts H., Cohen R.S., deGeus E.J., Grenier I.A., May J., Murphy D.JC., Nyman L.-A., and Thaddeus P. 1987, *Ap. J.*, **322**, 706
[38] Dearborn D.S.P., Blake J.B. 1984, *Ap. J.*, **277**, 783
[39] Dearborn D.S.P., Blake J.B. 1985, *Ap. J.*, **288**, L21
[40] Della Valle M. and Livio M. 1995, *A.A.*, in press
[41] Della Valle M., Rosino L., Bianchini A. and Livio M. 1995, *A.A.*, in press
[42] de Boer H., Bennett K., Bloemen H., den Herder J.W., Hermsen W., Klumper A., Lichti G., McConnell M., Ryan J., Schönfelder V., Strong A.W., and de Vries C., 1992, in: *Data Analysis in Astronomy IV*, eds. V. diGesu et al. (Plenum Press, New York) p. 241-249
[43] del Rio E., Diehl R., Oberlack U., Schönfelder V., and von Ballmoos P. , 1994, in: *Proc. of 2nd Compton Symposium, University of Maryland, College Park, MD* 1993, AIP Conf. Proc. 304, eds. C.E. Fichtel, N. Gehrels, J.P. Norris (AIP Press, New York) p. 171-175
[44] Delbourgo-Salvador P., Mochkovitch R., Vangioni-Flam E. 1985, *Proceedings of the ESA Workshop: Recent results on Cataclysmic Variables*, Bamberg, p. 229
[45] Diehl R., Aarts H., Bennett K., Collmar W., de Boer H., Deerenberg A., den Herder J.W., de Vries C., Hermsen W., Kippen M., Knödlseder J., Kuiper L., Lichti G., Lockwood J., Macri J., McConnell M., Much R., Morris D., Ryan J., Schönfelder V., Simpson G., Steinle H., Strong A.W., Swanenburg B.N., van Sant T., Webber W.R., and Winkler C. 1992, In: Data Analysis in Astronomy IV, eds. V. diGesu et al. (Plenum Press, New York) p. 201-216
[46] Diehl R., Bennett K., Bloemen H., deBoer H., Busetta M., Collmar W., Connors A., den Herder J.W., deVries C., Hermsen W., Knödlseder J., Kuiper L., Lichti G.G., Lockwood J., Macri J., McConnell M., Morris D., Much R., Ryan J., Schönfelder V., Simpson G., Stacy J.G., Steinle H., Strong A.W., Swanenburg B.N., Varendorff M., von Ballmoos P., Webber W., and Winkler C., 1993, *A&A Suppl.*, Vol. 97 No.1, p. 181-184
[47] Diehl R., Collmar W., Lichti G., Schönfelder V., Strong A., Bloemen H., Dupraz C., de Vries C., Hermsen W., Swanenburg B.N., Morris D., Varendorff M., and Winkler C. 1993, in: *Proc. of 1st Compton Symposium, St. Louis*, eds. M. Friedlander, N. Gehrels & D.J. Macomb, AIP Conf. Proc. 280, p. 40-46

[48] Diehl R., Dupraz C., Bennett K., Bloemen H., de Boer H., Hermsen W., Lichti G.G., McConnell M., Morris D., Ryan J., Schönfelder V., Steinle H., Strong A.W., Swanenburg B.N., Varendorff M., and Winkler C. 1994, *Ap .J. Suppl.*, **92** 429
[49] Diehl R., Knödlseder J., Lichti G., Schönfelder V., Steinle H., Strong A., Dupraz C., Bloemen H., Hermsen W., Swanenburg B., Morris D., Ryan J., Stacy G., Bennett K., and Winkler C. 1994, in: *Proc. of 2nd Compton Symposium*, University of Maryland, College Park, MD, AIP Conf. Proc. 304, eds. C.E. Fichtel, N. Gehrels, J.P. Norris (AIP Press, New York) p. 147-155
[50] Diehl R., Dupraz C., Bennett K., Bloemen H., Hermsen W., Knödlseder J., Lichti G., Morris D., Ryan J., Schönfelder V., Stacy G., Steinle H., Strong A., Swanenburg B., Varendorff M., and Winkler C. 1995, *A&A*, **298**, 445
[51] Diehl R., Knödlseder J., Lichti G.G., Oberlack U., Schönfelder V., Steinle H., Strong A.W., Varendorff M., Dupraz C., Hermsen W., Bloemen H., Morris D., Ryan J., Stacy G., Bennett K., and Winkler C. 1995, *Adv. Sp. Res.*, 15, 5, 123
[52] Diehl R., et al. 1995, *A.A.*, **298**, L25
[53] Durouchoux Ph., Wallyn P., Chapuis C., Matteson J., Bowman B., Pelling M., Peterson L., Vedrenne G., von Ballmoos P., Malet I., Niel M., Lin R., Feffer P., Smith D. and Hurley K. 1993, *A.A. Sup.* **97**, 185
[54] Forestini M., Paulus G., Arnould M. 1991, *A.A.*, **252**, 597
[55] Fowler W.A. 1984, *Rev. Mod. Phys.*, **56**, 149
[56] Frantsman Yu. 1989, *Sov. Astr.*, **33**, 565
[57] Gehrels N., Chipman E., and Kniffen D.A. 1993, *Astr.& Astroph.*, **97**, 5-10
[58] Genzel R., Hollenbach D., and Townes C.H. 1994, *Rep. Prog. Phys.*, **57**, 417-479
[59] Gehrz R., Truran J. and Williams R. 1993, in *Protostars and Planets III*, eds. E. Levy and J. Lunine (The University of Arizona Press) p. 75
[60] Georgelin Y.M. and Georgelin Y.P. 1976, *A.A.*, **49**, 57
[61] Güsten R. 1989, in *The Center of the Galaxy*, ed. M. Morris (IAU Symposium), p. 89
[62] Harding A. 1981, *Ap. J.*, **247**, 639
[63] Hartmann D.H. 1994, in: *Second Compton Symposium*, eds. C.E. Fichtel, N. Gherels, and J. Norris (AIP, New York) p. 176
[64] Higdon J.C. 1995, submitted to *Ap. J.*
[65] Higdon J.C., Lingenfelter R.E. 1976, *Ap. J.*, **208**, L107
[66] Higdon J.C., Fowler W.A. 1987, *Ap. J.*, **317**, 750
[67] Higdon J.C., Fowler W.A. 1989, *Ap. J.*, **339**, 956
[68] Hillebrandt W., Thielemann F.-K. 1982, *Ap. J.*, **255**, 657
[69] Hillebrandt W., Thielemann F.-K. and Langer N. 1987, *Ap. J.*, **321**, 761
[70] Hoffman R., Woosley S., Weaver T., Timmes F., Eastman R., Hartmann D. 1995, in: *The Gamma-Ray Sky with GRO and SIGMA*, eds. M. Signore, P. Salati, and G. Vedrenne, ASI Series C, **461**, 267
[71] Iliadis Ch. *et al.* 1990, *Nucl. Phys.*, **A512**, 509
[72] Iben I., Truran J. 1978, *Ap. J.*, **220**, 980
[73] Kent 1992, *Ap. J.*, **387**, 181
[74] Knödlseder J. 1994, Diploma Thesis, MPE Garching, Germany
[75] Knödlseder J., Prantzos N., and Diehl R. 1995, 3rd Compton Symposium (A.A. Suppl.), in press
[76] Kroupa P., Tout C. and Gilmore G. 1993, *M.N.R.A.S.*, **262**, 545
[77] Lambert D., 1989, in *Evolution of Peculiar Red Giants*, IAU Colloqu. 106, eds. H. Johnson and B. Zuckerman (CUP), p. 101
[78] Langer N., Braun H., Fliegner J. 1994, in *Circumstellar Matter*, eds. G. Watt and P. Williams (Kluwer), in press
[79] Lattanzio J. 1992, *Proc. Astr. Soc. Australia*, **10**, 120
[80] Lazareff B, Audouze J., Starrfield S., Truran J. 1979, *Ap. J.*, **228**, 875
[81] Law W. and Ritter P. 1983, *A.A.*, **63**, 265
[82] Lee T., Papanastassiou D. and Wasserburg G. 1977, *Ap. J.*, **211**, L107
[83] Lee Y.W. 1992, *Astr. J.*, **104**, 1780
[84] Leising M.D. 1991, in *Gamma-Ray Line Astrophysics*, eds. Ph. Durouchoux and N. Prantzos (AIP, New York) p. 173
[85] Leising M.D. 1993, *A.A. Sup.* , **97**, 299

[86] Leising M.D., Clayton D.D. 1985, *Ap. J.*, **294**, 591
[87] Leising M.D., et al. 1995, 3rd Compton Symposium (A.A. Suppl.), in press
[88] Li Z., Wheeler J.C., Bash F., Jefferys W.H. 1991, *Ap. J.*, **378**, 93
[89] Livio M. and Truran J. 1994, *Ap. J.*, **425**, 797
[90] McCallum C.J., Huters A.F., Stang P.D., Leventhal M. 1987, *Ap. J.*, **317**, 877
[91] McDonald J. 1983, *Ap. J.*, **267**, 732
[92] Maeder A. and Meynet G. 1994, *A.A.*, **287**, 803
[93] Mahoney W.A., Ling J.C., Jacobson A.S., Lingenfelter R. 1982, *Ap. J.*, **262**, 742
[94] Mahoney W.A., Ling J.C., Wheaton W.A., Jacobson A.S. 1984, *Ap. J.*, **286**, 578
[95] Mahoney W.A., Higdon J.C., Ling J.C., Wheaton W.A., Jacobson A.S. 1985, *Proceedings of the 19th ICRC*, La Jolla, USA, OG 3.2-3 (p. 357)
[96] Malet I., Neil N., Vedrenne G., von Ballmoos P., Bowman B., Briggs M., Gruber D., Matteson J., Pelling M., Peterson L., Feffer P., Hurley K., Lin R., Smith D., Cork C., Landis D., Luke P., Madden N., Malone D., Pehl R., Pollard M., Chapuis C., and Durouchoux P. 1991, in *Gamma-Ray Line Astrophysics*, eds. Ph. Durouchoux and N. Prantzos (AIP, New York) p. 123
[97] Malet I., Montmerle T. and von Ballmoos P. 1993, *A.A. Sup.*, **97**, 137
[98] Mayer-Hasselwander et al. 1982, *9th Texas Symp. Relat. Ap.*, 211
[99] Meynet G. 1994, *Ap. J. Suppl.*, **92**, 441
[100] Meynet G. 1994, private communication
[101] Meynet G. and Arnould M. 1993, in *Origin and Evolution of the Elements*, eds. N. Prantzos, E. Vangioni-Flam and M. Cassé (CUP, Cambridge) p. 539
[102] Meynet G. and Arnould M. 1993, in *Nuclei in the Cosmos*, eds. F. Kappeler and K. Wisshak (IOP) p. 503
[103] Mezger P. 1995, in: *The Gamma-Ray Sky with GRO and SIGMA*, eds. M. Signore, P. Salati, and G. Vedrenne, ASI Series C, **461**, 415
[104] Milne D.K., 1968, *Austr. J. Phys.*, **21**, 201
[105] Morfill G. and Hartquist G. 1985, *Ap. J.*, **297**, 194
[106] Morgan J.A. 1980, *Ap. J.*, **238**, 674
[107] Myra E.S., Burrows A. 1990, *Ap. J.*, **364**, 222
[108] Norgaard H. 1980, *Ap. J.*, **236**, 95
[109] Nofar I, Shaviv G. and Starrfield S. 1991, *Ap. J.*, **369**, 440
[110] Oberlack U., Diehl R., Montmerle T., Prantzos N., and von Ballmoos P. 1994, *Ap. J. Suppl.*, **92**, 443
[111] Patterson 1984, *Ap. J. Suppl.*, **54**, 443
[112] Paulus G., and Forestini M. 1991, in *Gamma-Ray Line Astrophysics*, eds. Ph. Durouchoux and N. Prantzos, (AIP, New York), 183
[113] Paulus G. and Meynet G. 1994, private communication
[114] Prantzos N. 1987, in *Nuclear Astrophysics*, eds. W. Hillebrandt, R. Kuhfuss, E. Müller, J. Truran (Springer, Berlin) p. 250
[115] Prantzos N. 1991, in *Gamma-Ray Line Astrophysics*, eds. Ph. Durouchoux and N. Prantzos (AIP, New York) p. 129
[116] Prantzos N. 1993a, *A.A. Sup.*, **97**, 119
[117] Prantzos N. 1993b, *Ap J*, **405**, L55
[118] Prantzos N. 1993c, in *Compton Gamma-Ray Observatory*, eds. M. Friedlander, N. Gehrels and D. Macomb (AIP, New York) p. 52
[119] Prantzos N. 1995, in *Nuclei in the Cosmos*, eds. M. Busso et al. (AIP, New York) p. 553
[120] Prantzos N., Cassé M. 1986 *Ap J.*, **307**, 324
[121] Prantzos N., and Diehl R. 1995 *COSPAR Proceedings, Adv. In Sp. Res.*, in press
[122] Prantzos N., Arnould M., Arcoragi J.P. 1987, *Ap J.*, **315**, 209
[123] Prantzos N, Cassé M., Arnould M. 1987, *Proceedings of the 20th ICRC*, Moscow, OG:2.3-4 (**2**, 152)
[124] Purcell W.R., Ulmer M.P., Share G.H., and Kinzer R.L., 1989, in: *Proc. of the Gamma-Ray Observatory Science Workshop*, ed. N. Johnson, 4-327
[125] Rana N., 1991, *A.R.A.A*, **29**, 129
[126] Ramaty R., Lingenfelter R.E. 1977, *Ap J*, **213**, L5
[127] Ramaty R. and Prantzos N. 1991, *Comments on Astrophysics*, XV, 301

[128] Ramaty R., Kozlovsky B., and Lingenfelter R.E. 1995, *Ap. J.*, **438**, L21
[129] del Rio E. et al. 1995, preprint
[130] Rollefson A.A. et al. 1990, *Nucl. Phys.*, **A507**, 413
[131] Rolfs C. and Rodney W. 1988, *Cauldrons in the Cosmos* (Univ. of Chicago Press)
[132] Ruiz J., Porras E., Ferrero J., Reglero V., Sanchez F., Lei F., Bird A., Carter T. and Dean A., 1994, *Ap. J.S.*, **92**, 683
[133] Schönfelder V. , Hirner A., Schneider K., 1973, *Nucl. Instr. & Meth.*, **107**, 385-394
[134] Schönfelder V., Aarts H., Bennett K., de Boer H., Clear J., Collmar W., Connors A., Deerenberg A., Diehl R., v. Dordrecht A., den Herder J.W., Hermsen W., Kippen M., Kuiper L., Lichti G., Lockwood J., Macri J., McConnell M., Morris D., Much R., Ryan J., Simpson G., Snelling M., Stacy G., Steinle H., Strong A., Swanenburg B.N., Taylor B., de Vries C., and Winkler C., 1993, *Ap. J. Suppl.*, **86**, 657-692,
[135] Schönfelder V. and Varendorff M. 1991, in *Gamma-Ray Line Astrophysics*, eds. Ph. Durouchoux and N. Prantzos (AIP, New York) p. 101
[136] Scoville N.Z., Sanders D.B. 1987, in *Interstellar Processes*, eds. H. Thronson and D. Hollenbach (Reidel) p. 21
[137] Shara M. 1994, *Astr. J.*, **107**, 1546
[138] Shara M. and Prialnik D. 1994, *Astr. J.*, **107**, 1542
[139] Share G.H., Kinzer R.L., Kurfess J.D., Forrest J.D., Chupp F.L., Rieger E. 1985, *Ap. J.*, **292**, L61
[140] Share G.H., Kinzer R.L., Kurfess J.D., Forrest J.D., Chupp F.L., Rieger E. 1985, in *Proceedings of the 19th ICRC*, La Jolla, USA, OG:3.2-1, 353
[141] Sharov A.S. 1971, *Astr. Zh.*, **48**, 1258
[142] Shaver P.A., Mc Gee R.X., Newton L.M., Danks A.C., Pottasch S.R. 1983, *M.N.R.A.S.*, **204**, 53
[143] Signore M., Dupraz C. 1990, *A.A.*, **234**, L15
[144] Signore M., Dupraz C. 1993, *A.A. Suppl.*, **97**, 141
[145] Skibo J and Ramaty R. 1991, in *Gamma-Ray Line Astrophysics*, eds. Ph. Durouchoux and N. Prantzos (AIP, New York) p. 168
[146] Strong A.W., Cabeza-Orcel P., Bennett K., Collmar W., Diehl R., den Herder J.W., Hermsen W., Lichti G., McConnell M., Ryan J., Steinle H., Schönfelder V., and Winkler C., 1992, in: Data Analysis in Astronomy IV, eds. V. diGesu et al. (Plenum Press, New York) p. 251-260
[147] Starrfield S., Truran J.W., Sparks K. 1978, *Ap. J.*, **226**, 186
[148] Starrfield S., Sparks W., Truran J.W. 1986, *Ap. J.*, **303**, L5
[149] Starrfield S., Truran J., Sparks W., Politano M., Nofar I., Shaviv G. 1993, in *Origin and Evolution of the Elements*, eds. N. Prantzos, E. Vangioni-Flam and M. Cassé (CUP, Cambridge) p. 337
[150] Stecker F., 1993, in *Currents in Astrophysics and Cosmology*, eds. G. Fazio and R. Silberberg (CUP) p. 85
[151] Tammann G., Loffler W., Schröder A. 1994, *Ap. J. Suppl.*, **92**, 487
[152] Taylor J.H. and Cordes J.M. 1993, *Ap. J.*, **411**, 674
[153] Teegarden B., *et al.* 1991, in *Gamma-Ray Line Astrophysics*, eds. Ph. Durouchoux and N. Prantzos (AIP, New York) p. 116
[154] Teegarden B., Barthelmy S., Gehrels N., Tueller J., Leventhal M. and MacCallum C. 1991, *Ap. J.*, **375**, L9
[155] Thielemann F.-K., Hashimoto M., Nomoto K. 1990, *Ap. J.*, **349**, 222
[156] Thielemann F.-K., Hashimoto M., Nomoto K. 1994, in *Les Houches Ecole d'Ete de Physique Theorique*, p. 629
[157] Timmermann R., Becker H.W., Rolfs C., Schroder U. and Trautevetter H.P. 1988, *Nucl. Phys.*, **A477**, 105
[158] Timmes F., Woosley S., Weaver T. 1995, *Ap. J. Suppl.*, **98**, 617
[159] Trautvetter H.P. 1986, in *Nucleosynthesis and its implications on Nuclear and Particle Physics*, eds. J. Audouze and N. Mathieu (Reidel, Dordrecht) p. 347
[160] Trimble V., 1991, *A.A. Rev.*, **3**, 1
[161] Truran J.W., Cameron A.G.W. 1978, *Ap. J.*, **219**, 236
[162] van der Hucht K., 1992, *A.A. Rev.*, **4**, 123
[163] van der Hucht K., Hidayat B., Admiranto A., Supelli K., Doom C. 1988, *A.A.*, **199**, 217
[164] Varendorff M. and Schönfelder V. 1992, *Ap. J.*, **395**, 158
[165] von Ballmoos P., Diehl R., Schönfelder V. 1987, *Ap. J.*, **318**, 654
[166] von Ballmoos P. 1991, in *Gamma-Ray Line Astrophysics*, eds. Ph. Durouchoux and N. Prantzos (AIP, New York) p. 149
[167] Walter R., Maeder A. 1989, *A.A.*, **218**, 123

[168] Ward R.A., Fowler W.A. 1980, *Ap. J.*, **238**, 266
[169] Weaver T. and Woosley S. 1993, *Phys. Rep.*, **227**, 65
[170] Webber W.R., Schönfelder V., Diehl R. 1986, *Nature*, **323**, 692
[171] Weiss A., Truran J.W. 1990, *A.A.*, **238**, 178
[172] Wiescher M., Görres, J., Thielemann, F.-K., Ritter, H. 1986, *A.A.*, **160**, 56
[173] Wolf M.T., Leising M.D. 1988, in *Gamma-Ray Spectroscopy in Astrophysics*, eds. N. Gehrels and G. Share (AIP) p. 136
[174] Woosley S.E. 1986, in *Saas-Fe Lectures : Nucleosynthesis and Chemical Evolution*, eds. B. Hauck, A. Maeder and G. Meynet (Geneva Observatory) p. 78
[175] Woosley S.E., Weaver T.A. 1980, *Ap. J.*, **238**, 1017
[176] Woosley S.E., Langer N., Weaver T.A. 1993, *Ap. J.*, **411**, 823
[177] Woosley S.E., Langer N., Weaver T.A. 1995, *Ap. J.*, **448**, 315
[178] Woosley S.E., Hartmann D.H., Hoffman R.D., Haxton W.C. 1990, *Ap. J.*, **356**, 272
[179] Woosley S.E. 1991, in *Gamma-Ray Line Astrophysics*, eds. Ph. Durouchoux and N. Prantzos (AIP, New York) p. 270
[180] Woosley S.E., et al. 1994, *Ap. J.*, **433**, 229